

UNCLASSIFIED

AD NUMBER

ADB013389

LIMITATION CHANGES

TO:

Approved for public release; distribution is unlimited.

FROM:

Distribution authorized to U.S. Gov't. agencies only; Test and Evaluation; SEP 1978. Other requests shall be referred to Space and Missile Systems Organization, Los Angeles, CA 90009.

AUTHORITY

SAMSO ltr 14 Dec 1976

THIS PAGE IS UNCLASSIFIED

cy.2



**AERODYNAMIC FORCES AND PRESSURE DISTRIBUTIONS  
ON THE MINUTEMAN INSTRUMENTED PAYLOAD  
DELIVERY SYSTEM AT MACH NUMBERS FROM 0.5 TO 1.3**

**PROPULSION WIND TUNNEL FACILITY  
ARNOLD ENGINEERING DEVELOPMENT CENTER  
AIR FORCE SYSTEMS COMMAND  
ARNOLD AIR FORCE STATION, TENNESSEE 37389**

**September 1976**

**Final Report for Period March 30 - April 2, 1976**

Distribution limited to U.S. Government agencies only; this report contains information on test and evaluation of military hardware; September 1976; other requests for this document must be referred to Space and Missile Systems Organization (RSTB), P.O. Box 92960, Worldway Postal Center, Los Angeles, California 90009.

Property of U.S. Air Force  
RSTB LIBRARY  
742000 75 0-0001

Prepared for

**SPACE AND MISSILE SYSTEMS ORGANIZATION (RSTB)  
P.O. BOX 92960, WORLDWAY POSTAL CENTER  
LOS ANGELES, CALIFORNIA 90009**

## NOTICES

When U. S. Government drawings specifications, or other data are used for any purpose other than a definitely related Government procurement operation, the Government thereby incurs no responsibility nor any obligation whatsoever, and the fact that the Government may have formulated, furnished, or in any way supplied the said drawings, specifications, or other data, is not to be regarded by implication or otherwise, or in any manner licensing the holder or any other person or corporation, or conveying any rights or permission to manufacture, use, or sell any patented invention that may in any way be related thereto.

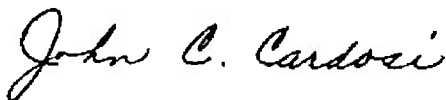
Qualified users may obtain copies of this report from the Defense Documentation Center.

References to named commercial products in this report are not to be considered in any sense as an endorsement of the product by the United States Air Force or the Government.

## APPROVAL STATEMENT

This technical report has been reviewed and is approved for publication.

FOR THE COMMANDER



JOHN C. CARDOSI  
Lt Colonel, USAF  
Chief Air Force Test Director, PWT  
Directorate of Test



ALAN L. DEVEREAUX  
Colonel, USAF  
Director of Test

# UNCLASSIFIED

REPORT DOCUMENTATION PAGE		READ INSTRUCTIONS BEFORE COMPLETING FORM
1 REPORT NUMBER <b>AEDC-TR-76-124</b>	2 GOVT ACCESSION NO.	3 RECIPIENT'S CATALOG NUMBER
4 TITLE (and Subtitle) <b>AERODYNAMIC FORCES AND PRESSURE DISTRIBUTIONS ON THE MINUTEMAN INSTRUMENTED PAYLOAD DELIVERY SYSTEM AT MACH NUMBERS FROM 0.5 TO 1.3</b>	5 TYPE OF REPORT & PERIOD COVERED <b>Final Report - March 30 - April 2, 1976</b>	
	6 PERFORMING ORG REPORT NUMBER	
7 AUTHOR(s)  <b>David M. Cahill, ARO, Inc.</b>		8 CONTRACT OR GRANT NUMBER(s)
9 PERFORMING ORGANIZATION NAME AND ADDRESS <b>Arnold Engineering Development Center (XO) Air Force Systems Command Arnold Air Force Station, Tennessee 37389</b>		10 PROGRAM ELEMENT, PROJECT, TASK AREA & WORK UNIT NUMBERS <b>Program Element 63311F System 627A, Task 01</b>
11 CONTROLLING OFFICE NAME AND ADDRESS <b>Space and Missile Systems Organization (RSTB), P.O.Box 92960, Worldway Postal Center, Los Angeles, California 90009</b>		12 REPORT DATE <b>September 1976</b>
		13 NUMBER OF PAGES <b>100</b>
14 MONITORING AGENCY NAME & ADDRESS (if different from Controlling Office)		15 SECURITY CLASS. (of this report)  <b>UNCLASSIFIED</b>
		15a DECLASSIFICATION/DOWNGRADING SCHEDULE <b>N/A</b>
16 DISTRIBUTION STATEMENT (of this Report) <b>Distribution limited to U.S. Government agencies only; this report contains information on test and evaluation of military hardware; September 1976; other requests for this document must be referred to Space and Missile Systems Organization (RSTB), P.O. Box 92960, Worldway Postal Center, Los Angeles, California 90009.</b>		
17 DISTRIBUTION STATEMENT (of the abstract entered in Block 20, if different from Report)		
18 SUPPLEMENTARY NOTES  <b>Available in DDC</b>		
19 KEY WORDS (Continue on reverse side if necessary and identify by block number)		
<b>aerodynamic force (mechanics) distribution pressure</b>	<b>Minuteman instrumented payload delivery vehicles</b>	<b>Mach numbers angles of attack</b>
20 ABSTRACT (Continue on reverse side if necessary and identify by block number)  <b>Wind tunnel tests were conducted in the Arnold Engineering Development Center (AEDC) Aerodynamic Wind Tunnel (4T) on a 0.06-scale model of the Minuteman Instrumented Payload Delivery System (MIPDS). Pressure distributions and force and moment data were obtained over a Mach number range from 0.5 to 1.3, at angles of attack from -6 to 24 deg, and at angles of roll from -180 to 165 deg.</b>		

# UNCLASSIFIED

## PREFACE

The work reported herein was conducted by the Arnold Engineering Development Center (AEDC), Air Force Systems Command (AFSC), at the request of the Space and Missile Systems Organization (SAMSO/RSTB) under Program Element 63311F, System 627A, Task 01. The results of these tests were obtained by ARO, Inc. (a subsidiary of Sverdrup & Parcel and Associates, Inc.), contract operator of AEDC, AFSC, Arnold Air Force Station, Tennessee under ARO Project No. P41C-C8A. The author of this report was David M. Cahill, ARO, Inc. The data analysis was completed on May 17, 1976, and the manuscript (ARO Control No. ARO-PWT-TR-76-73) was submitted for publication on July 14, 1976.

## CONTENTS

	<u>Page</u>
1.0 INTRODUCTION . . . . .	7
2.0 TEST APPARATUS	
2.1 Test Facility . . . . .	7
2.2 Test Article . . . . .	8
2.3 Instrumentation . . . . .	9
3.0 TEST DESCRIPTION	
3.1 Test Conditions, Procedures, and Program . . . . .	9
3.2 Data Reduction and Corrections . . . . .	10
3.3 Uncertainty of Measurements . . . . .	10
4.0 RESULTS AND DISCUSSION	
4.1 Nose Forces and Moments . . . . .	11
4.2 Total Missile Forces and Moments . . . . .	12
4.3 Pressure Data . . . . .	14
5.0 SUMMARY OF RESULTS . . . . .	14
REFERENCES . . . . .	15

## ILLUSTRATIONS

Figure

1. Schematic of the Tunnel Test Section Showing Model Installation . . . . .	17
2. Details and Dimensions of the Test Article . . . . .	18
3. Pressure Orifice Locations on Missile Body . . . . .	19
4. Pressure Orifice Locations on Missile Nose . . . . .	20
5. Installation of the Pressure Model in the Test Section. . . . .	21
6. Typical Variation of the Nose Aerodynamic Coef- ficients with Angle of Attack, $M_\infty = 1.1$ . . . . .	23
7. Variation of the Nose Normal-Force Coefficient with Model Roll Angle . . . . .	28

<u>Figure</u>	<u>Page</u>
8. Variation of the Nose Pitching-Moment Coefficient with Model Roll Angle . . . . .	32
9. Variation of the Nose Side-Force Coefficient with Model Roll Angle . . . . .	36
10. Variation of the Nose Yawing-Moment Coefficient with Model Roll Angle . . . . .	40
11. Variation of the Nose Rolling-Moment Coefficient with Model Roll Angle . . . . .	44
12. Variation of the Nose Forebody-Axial-Force Coefficient with Angle of Attack and Mach Number, $\phi_a = 0$ . . . . .	48
13. Typical Variations of the Missile Aerodynamic Coefficients with Angle of Attack, $M_\infty = 1.1$ . . . . .	49
14. Variation of the Missile Normal-Force Coefficient with Model Roll Angle . . . . .	54
15. Variation of the Missile Pitching-Moment Coefficient with Model Roll Angle . . . . .	58
16. Variation of the Missile Side-Force Coefficient with Model Roll Angle . . . . .	62
17. Variation of the Missile Yawing-Moment Coefficient with Model Roll Angle . . . . .	66
18. Variation of the Missile Rolling-Moment Coefficient with Model Roll Angle . . . . .	70
19. Variation of the Missile Forebody-Axial-Force Coefficient with Angle of Attack and Mach Number, $\phi_a = 0$ . . . . .	74
20. Comparison of Free-Flight and Test Model Base Pressure Coefficients . . . . .	75
21. Missile Pressure Distributions, $M_\infty = 0.5$ . . . . .	76
22. Missile Pressure Distributions, $M_\infty = 0.8$ . . . . .	80
23. Missile Pressure Distributions, $M_\infty = 0.95$ . . . . .	83
24. Missile Pressure Distributions, $M_\infty = 1.1$ . . . . .	87

<u>Figure</u>		<u>Page</u>
25.	Missile Pressure Distributions, $M_\infty = 1.3$ . . . . .	91

### TABLES

1.	Model Surface Pressure Orifices . . . . .	94
2.	Summary of Nominal Test Conditions . . . . .	96
3.	Summary of Pressure Data Uncertainty . . . . .	96
4.	Summary of Force Data Uncertainty . . . . .	97
	NOMENCLATURE . . . . .	98

## 1.0 INTRODUCTION

Wind tunnel tests were conducted to determine the aerodynamic forces and the pressure distributions on the Minuteman Instrumented Payload Delivery System (MIPDS) nose section and total vehicle. The tests were conducted in the Aerodynamic Wind Tunnel (4T) of the AEDC Propulsion Wind Tunnel Facility (PWT) utilizing a 0.06-scale MIPDS model. The test objectives were to verify the aerodynamic characteristics of the proposed MIPDS design and to provide aerodynamic data for trajectory calculations, control systems design, and structural design. The test was conducted in two phases, a pressure phase and a force phase. Because of the large volume of data obtained during both phases of this test, only selected force and pressure data are presented herein. The force data presented were obtained with the raceway on the missile and with no seal in the metric break. The pressure data were obtained with the raceway off and with a hard seal in the metric break. Data, for both phases, were obtained at Mach numbers ranging from 0.5 to 1.3 (limited force data obtained at Mach number 1.3) at a Reynolds number per foot of  $4.0 \times 10^6$ . The model angle of attack was varied from -6 to 24 deg at various roll angles. Roll sweeps from -180 to 165 deg in 15-deg increments were made at several angles of attack.

## 2.0 APPARATUS

### 2.1 TEST FACILITY

The Aerodynamic Wind Tunnel (4T) is a closed-loop, continuous flow, variable density tunnel in which the Mach number can be varied from 0.1 to 1.3. At all Mach numbers, the stagnation pressure can be varied from 300 to 3,700 psfa. The test section is 4 ft square and 12.5 ft long with perforated, variable porosity (0.5- to 10-percent open) walls. It is completely enclosed in a plenum chamber from which the air can be evacuated, allowing part of the tunnel airflow to be removed through

the perforated walls of the test section. A more thorough description of the tunnel may be found in Ref. 1. A sketch of the test section wall details and the installation of the model in the test section is shown in Fig. 1.

## 2.2 TEST ARTICLE

The test article was a 0.06-scale model of the MIPDS. Details and dimensions of the model are shown in Fig. 2. The booster section, defined as those components downstream of model station (MS) 15.445 (metric break location on the force model) consisted of a centerbody (MS 15.445 to 31.534), booster afterbody (MS 31.534 to 47.052), removeable raceway (MS 15.510 to 45.094), and a base plate with four nozzles. The booster section had a total of 40 surface and four base pressure orifices. All of the booster section components were common to both phases of this test. The payload or nose section, defined as that section forward of MS 15.445, consisted of separate pressure and force noses with two nose fairings. The nose fairings were located in the vertical plane ( $\phi_\alpha = 0$ ) from MS 10.525 to 12.325. The nose section was axisymmetric from the nosetip to MS 9.038 and downstream of MS 12.352. From MS 9.038 to 12.325, the nose section was not axisymmetric.

The location and identification of the pressure orifices for the booster and nose sections are shown in Figs. 3 and 4, respectively, and are listed in Table 1.

The force nose was mounted such that there was a metric break between the force nose and the booster centerbody. The metric break allowed the use of a separate nose balance to measure the aerodynamic forces on the nose section while the booster balance measured the aerodynamic forces on the entire missile. Three seal arrangements were employed in the metric break. One arrangement employed a flexible foam seal to prevent flow circulation through the gap. The second arrangement employed a ring

adapter which eliminated the gap and provided for the hard mounting of the nose section to the booster centerbody. The pressure nose was hard mounted to the centerbody through the use of the ring adapter. The third arrangement was with no seal in the metric break. Most of the data on the force phase was obtained with no seal in the metric break. Photographs of the pressure model installed in the wind tunnel are shown in Fig. 5.

## 2.3 INSTRUMENTATION

The aerodynamic forces on the total missile were measured with a six-component, internal strain-gage balance. A second six-component, internal strain-gage balance was used to measure the aerodynamic forces on the nose section. Four base, two booster cavity, and two nose cavity pressures were measured during the force phase of this test. Ninety-one surface and four base pressures were measured during the pressure phase.

The pressure data, for both phases, were measured using the 4T pressure system. This system consists of fifty 15-psid pressure transducers which are maintained in a constant temperature environment. Each transducer is connected to two pressure orifices by utilizing a two-way valve. For each cycle of the two-way valves, a computer monitors the pressure settling rate. The computer initiates the data acquisition when the pressure settling rate has reached a preselected value. Electrical signals from the balances, pressure transducers, and standard 4T tunnel instrumentation are processed by the PWT data acquisition system and digital computer for online data reduction.

## 3.0 TEST DESCRIPTION

### 3.1 TEST CONDITIONS, PROCEDURES, AND PROGRAM

The test was conducted in a pressure phase and a force phase. Data for both phases were obtained for Mach numbers ranging from 0.5 to 1.3

(limited force data were obtained at Mach number 1.3) and at a Reynolds number per foot of  $4.0 \times 10^6$ . The nominal test conditions are presented in Table 2.

The tunnel conditions were held constant at the prescribed Mach number, Reynolds number, and angle of attack, whereas the model roll angle was varied from -180 to 165 deg and from -150 to 90 deg for the pressure and force phases, respectively. For each angle of attack, data were recorded at 15-deg intervals of the model roll angle. In addition, for the force phase only, the model roll angle was held constant, whereas the angle of attack was varied from -6 to 24 deg.

### 3.2 DATA REDUCTION AND CORRECTIONS

Wind tunnel force and moment data were reduced to coefficient form in the aeroballistic axis system. The base and booster cavity pressures were measured and were used to calculate the forebody coefficients for the missile. The nose cavity pressure was also measured and was used to calculate the forebody coefficients for the MIPDS nose. The angle of attack and roll angle were corrected for sting and balance deflections caused by the aerodynamic loads. The model was tested both at 0 and 180 deg of roll to provide the data to correct the angle of attack for tunnel flow angularity and model misalignment. Corrections for the components of model weight, normally termed static tares, were also applied to the data.

### 3.3 UNCERTAINTY OF MEASUREMENTS

The balance and pressure transducer uncertainties, based on a 95-percent confidence level, were combined with the uncertainties in the tunnel parameters, assuming a Taylor series error propagation, to estimate the uncertainty of the pressure and aerodynamic coefficients. The maximum uncertainties determined are given in Tables 3 and 4 for the pressure and force data, respectively. The uncertainty in setting and

maintaining a specific Mach number was  $\pm 0.005$ . The Mach number variation in the test section occupied by the model was no greater than  $\pm 0.005$  for Mach numbers up to 0.95 and  $\pm 0.01$  for Mach numbers greater than 1.0. The uncertainty in setting the angle of attack was  $\pm 0.05$  deg and in setting the roll angle was  $\pm 0.3$  deg.

## 4.0 RESULTS AND DISCUSSION

Because of the large volume of data obtained during both phases of the test, only selected force and pressure data are presented herein. The force data presented were obtained with the raceway on the missile and no seal in the metric break. The pressure data presented were obtained with the raceway off and the hard seal in the metric break. Since limited data at Mach number 1.3 were obtained on the force phase, no force data at Mach number 1.3 are presented.

### 4.1 NOSE FORCES AND MOMENTS

Shown in Fig. 6 are typical variations of the nose aerodynamic coefficients (excluding axial-force) with angle of attack for roll angles of 0, 90, and -135 deg. These data were presented to show how the nose aerodynamic characteristics typically varied with angle of attack. A more detailed study of the effect of model roll angle is considered in the remainder of this section.

The variations of the nose normal-force and pitching-moment coefficients with roll angle are presented in Figs. 7 and 8, respectively, at several angles of attack. As expected, the data show that these coefficients generally had a maximum value when the nose was at roll angles of  $\pm 90$  deg (nose fairings normal to the pitch plane of the model). Correspondingly, the minimum value for these coefficients generally occurred when the nose was at roll angles of 0 or 180 deg (nose fairings in the pitch plane of the model). The effect of the nose fairings orientation increased as both the angle of attack and Mach number were increased.

Presented in Figs. 9 and 10 are the variations of the nose side-force and yawing-moment coefficients, respectively, with roll angle at various angles of attack. The side-force coefficient had a maximum positive value at a roll angle of approximately  $-45$  deg and maximum negative values at roll angles of approximately  $45$  and  $-135$  deg. The yawing-moment coefficient had a maximum positive value at a roll angle of approximately  $-60$  deg and maximum negative values at approximately  $60$  and  $-120$  deg roll angles. The effect of the nose fairings orientation on these coefficients also increased as both the angle of attack and Mach number were increased.

The variation in the nose rolling-moment coefficient with roll angle at several angles of attack is presented in Fig. 11. The data show that the maximum positive rolling-moment coefficients were produced at roll angles of approximately  $45$  and  $-135$  deg and the maximum negative rolling-moment coefficient occurred at approximately a  $-45$ -deg roll angle. The rolling-moment coefficient was zero when the nose fairings were either normal to or in the pitch plane of the model (i.e., roll angles of  $\pm 90$ ,  $0$ , and  $180$  deg). The rolling-moment coefficient increased as the angle of attack was increased but did not vary significantly as the Mach number was varied.

The forebody-axial-force coefficient of the nose decreased as the angle of attack was increased as shown by the data in Fig. 12.

## 4.2 TOTAL MISSILE FORCES AND MOMENTS

Shown in Fig. 13 are some typical variations of the missile aerodynamic coefficients (excluding axial-force) with angle of attack for roll angles of  $0$ ,  $90$ , and  $-135$  deg. These data were presented to show how the missile aerodynamic characteristics typically varied with angle of attack. A more detailed study of the effects of model roll angle is considered in the remainder of this section.

The variation of the missile normal-force coefficient with roll angle at several angles of attack is presented in Fig. 14. The data show that the normal-force coefficient generally had maximum values when the raceway was in a position normal to the airflow, that is at roll angles of 60 and -120 deg. The normal-force coefficient variations with roll angle increased as both the angle of attack and Mach number were increased.

The pitching-moment coefficient variation with roll angle at various angles of attack is shown in Fig. 15. Generally, the variation in the pitching-moment coefficient was small compared to that of the normal-force coefficient, and the maximum values occurred at roll angles of approximately -120 and 75 deg.

The variation of the side-force and yawing-moment coefficients with roll angle at several angles of attack are shown in Figs. 16 and 17, respectively. For angles of attack less than 8 deg, the side-force coefficient was very small. However, for angles of attack greater than about 8 deg the side-force coefficient became almost as large as the normal-force coefficient and varied widely with roll angle. Large variations in the yawing moment were not observed until the angle of attack was increased to about 16 deg.

Presented in Fig. 18 is the variation of rolling-moment coefficient with roll angle. The data show that the rolling-moment coefficient had maximum positive and negative values at roll angles of approximately 15 and -75 deg, respectively. The rolling-moment coefficient variation increased as the angle of attack was increased but did not vary significantly as the Mach number was varied.

The variation of the forebody-axial-force coefficient with angle of attack and Mach number is shown in Fig. 19. Shown in Fig. 20 is a comparison between the base pressure coefficients of the model and an

ogive cylinder in free flight (Ref. 2). The data indicate that the base pressure coefficients for this model were only slightly affected by the presence of the sting.

### 4.3 PRESSURE DATA

The only pressure data presented herein are for the 45 pressure orifices along the 90-deg ray of the missile. These pressure coefficients are plotted against length ratio for several angles of attack and are presented in Figs. 21 through 25.

The pressure distributions presented were obtained at model roll angles of 0, 90, 180, and -90 deg and at Mach numbers of 0.5, 0.8, 0.95, 1.1, and 1.3.

## 5.0 SUMMARY OF RESULTS

Wind tunnel tests were conducted on a 0.06-scale model of the Minuteman Instrumented Payload Delivery System. These tests were conducted to determine the aerodynamic characteristics of the model as a function of roll angle and angle of attack. Aerodynamic coefficients for the model nose section were also measured. A summary of the results of this test is as follows:

1. The maximum values of the normal-force and pitching-moment coefficients for the model nose section were noted at model roll angles of approximately  $\pm 90$  deg, whereas, for the total missile, the maximum values for the normal-force coefficient occurred at roll angles of approximately -120 and 60 deg while the pitching-moment coefficient had maximum values at -120- and 75-deg angles of roll.

2. The side-force coefficients for the total missile showed small variations with roll angle for angles of attack up to 8 deg, but for angles of attack greater than 8 deg, the side-force coefficient varied widely with roll angle and at certain roll angles became almost as large as the normal-force coefficient.
3. The variation of the missile yawing-moment coefficient with roll angle was similar to the variation in the missile side-force coefficient except that the wide variations did not begin until the angle of attack was 16 deg.
4. Maximum value of the rolling-moment coefficient for the nose section was noted at model roll angles of approximately 45, -45, and -135 deg, whereas, for the total missile the maximum values for the rolling-moment coefficient occurred at roll angles of approximately 15 and -75 deg.

#### REFERENCES

1. Test Facilities Handbook (Tenth Edition). "Propulsion Wind Tunnel Facility, Vol. 4." Arnold Engineering Development Center, May 1974.
2. Hart, Roger G. "Effects of Stabilizing Fins and a Rear-Support Sting on the Base Pressures of a Body of Revolution in Free Flight at Mach Numbers from 0.7 to 1.3." NACA RM L52E06, September 1952.

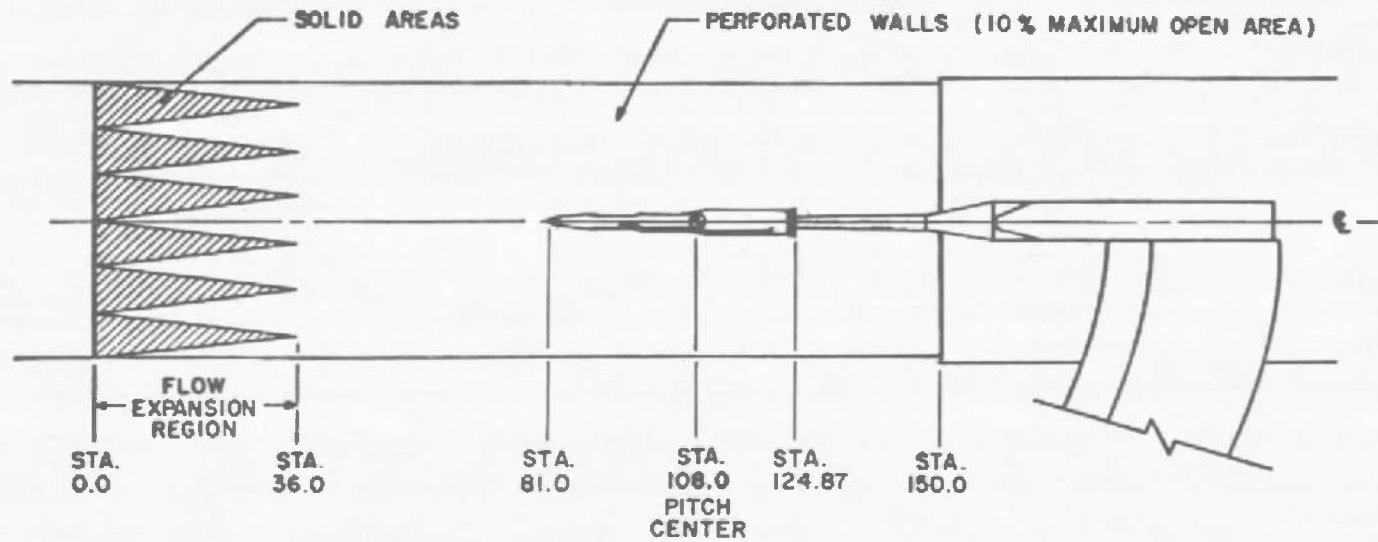
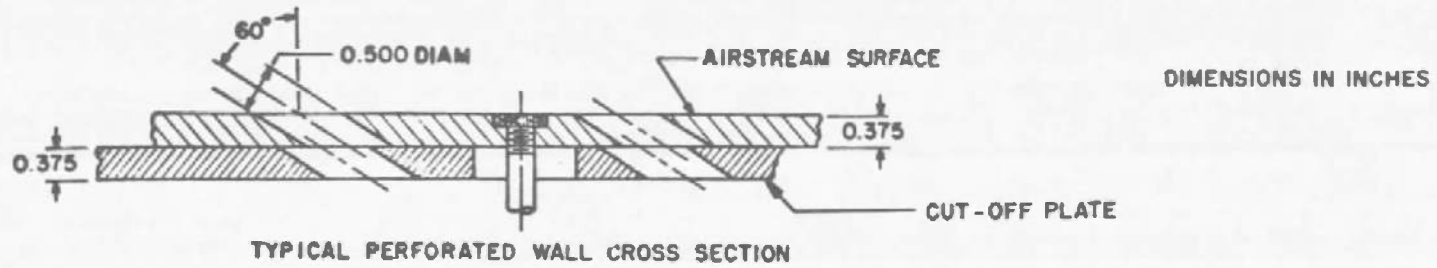


Figure 1. Schematic of the tunnel test section showing model installation.

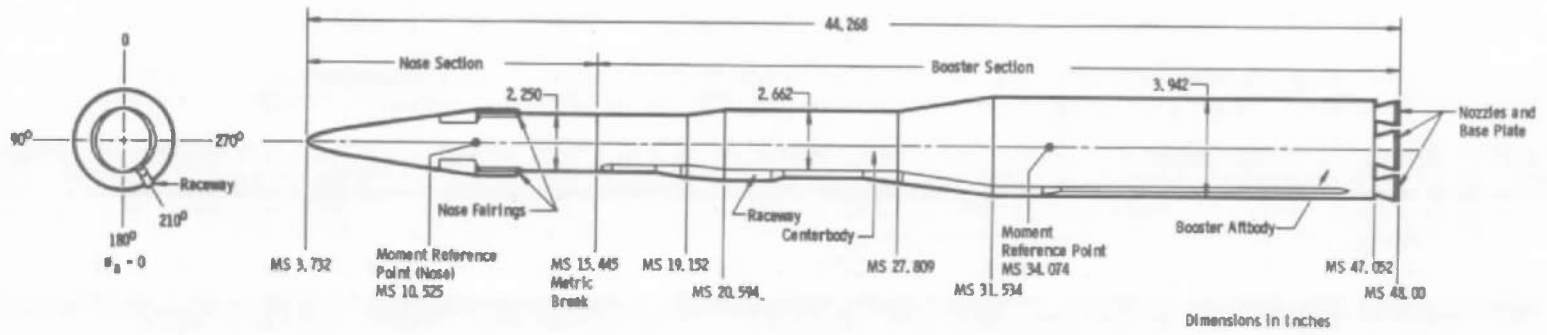


Figure 2. Details and dimensions of the test article.

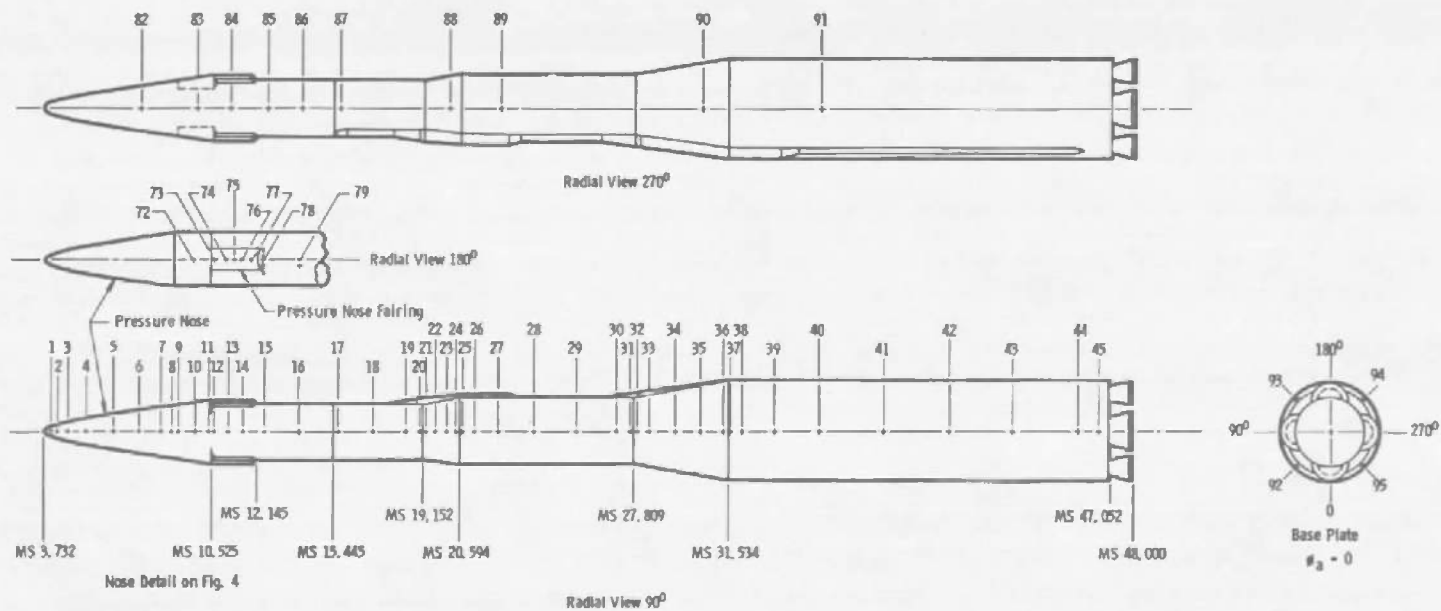


Figure 3. Pressure orifice locations on missile body.

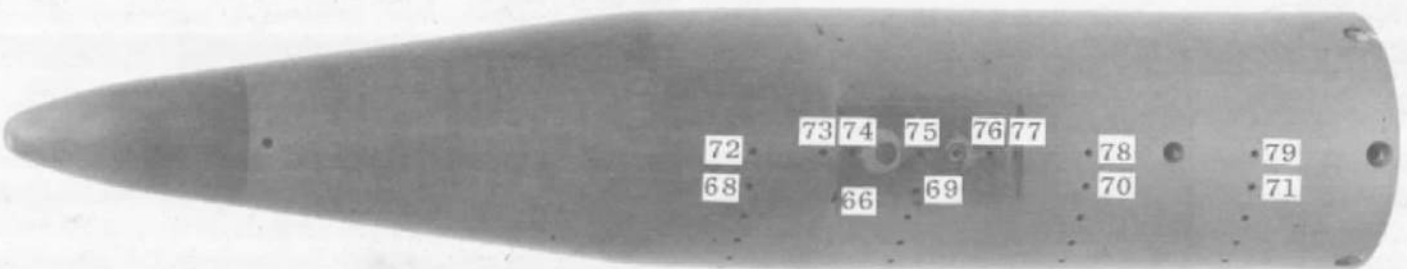
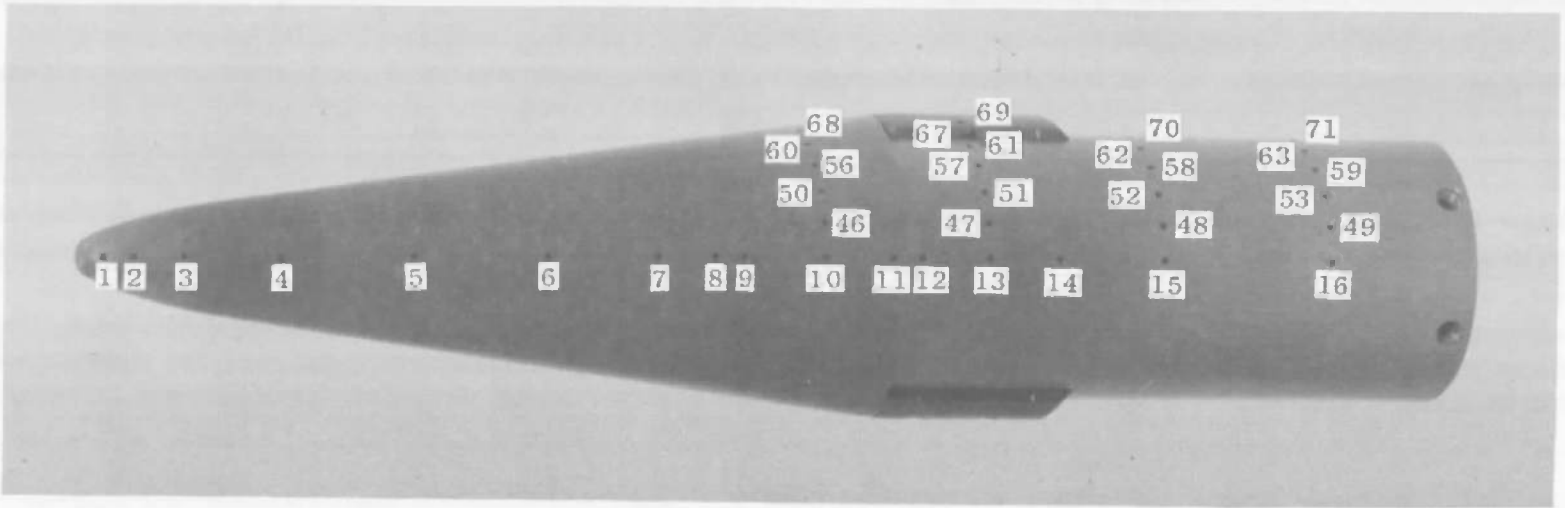
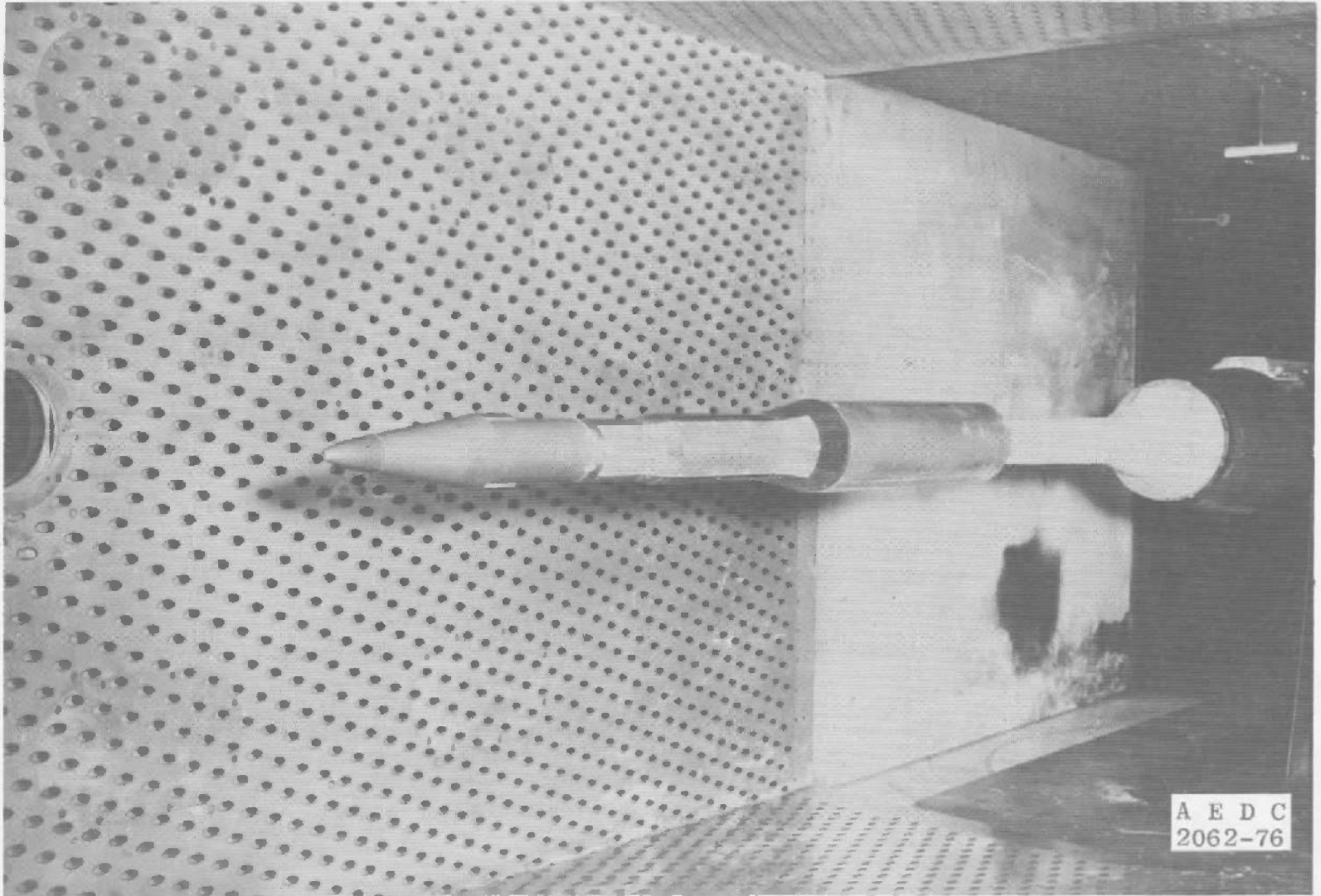
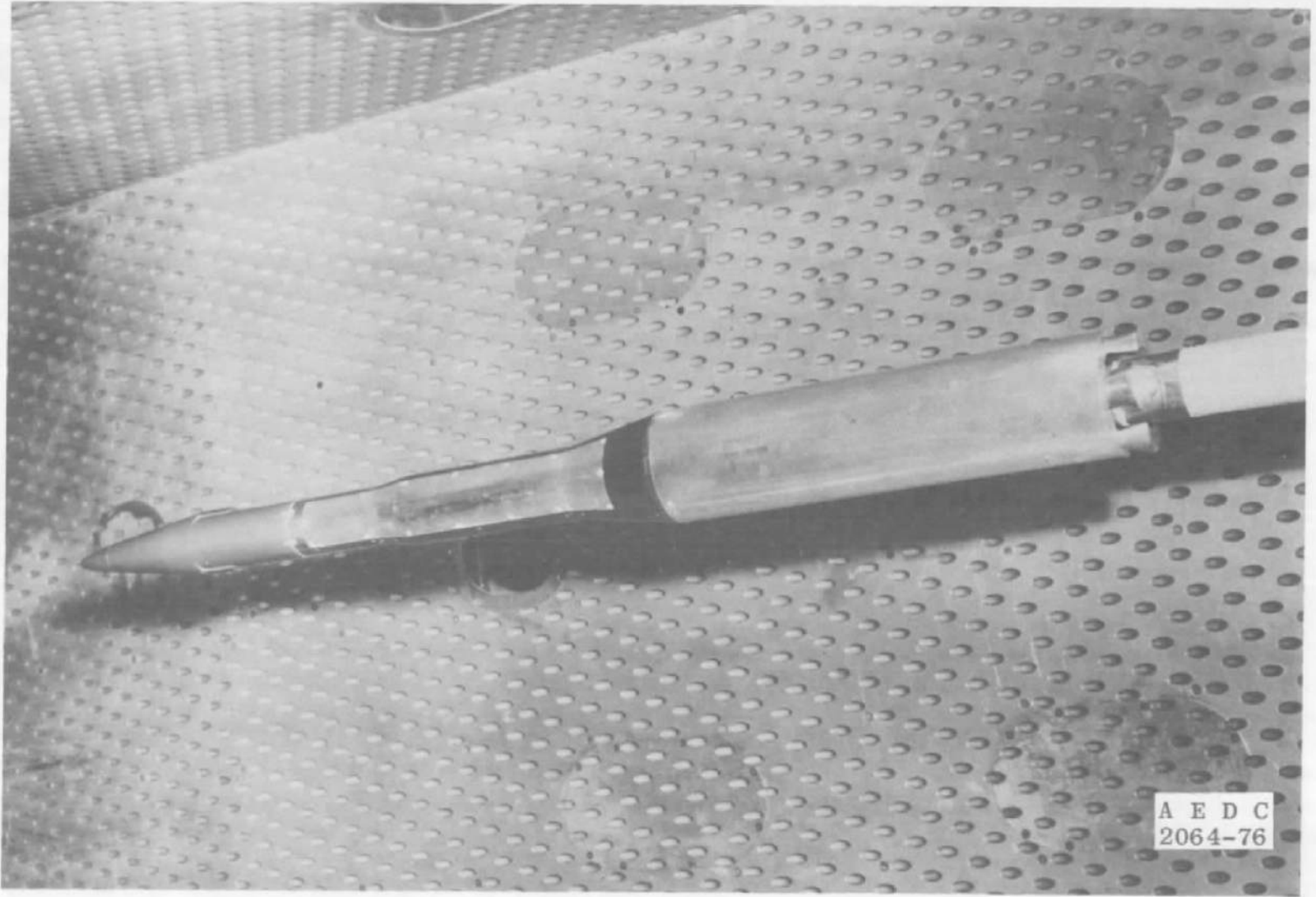


Figure 4. Pressure orifice locations on missile nose.

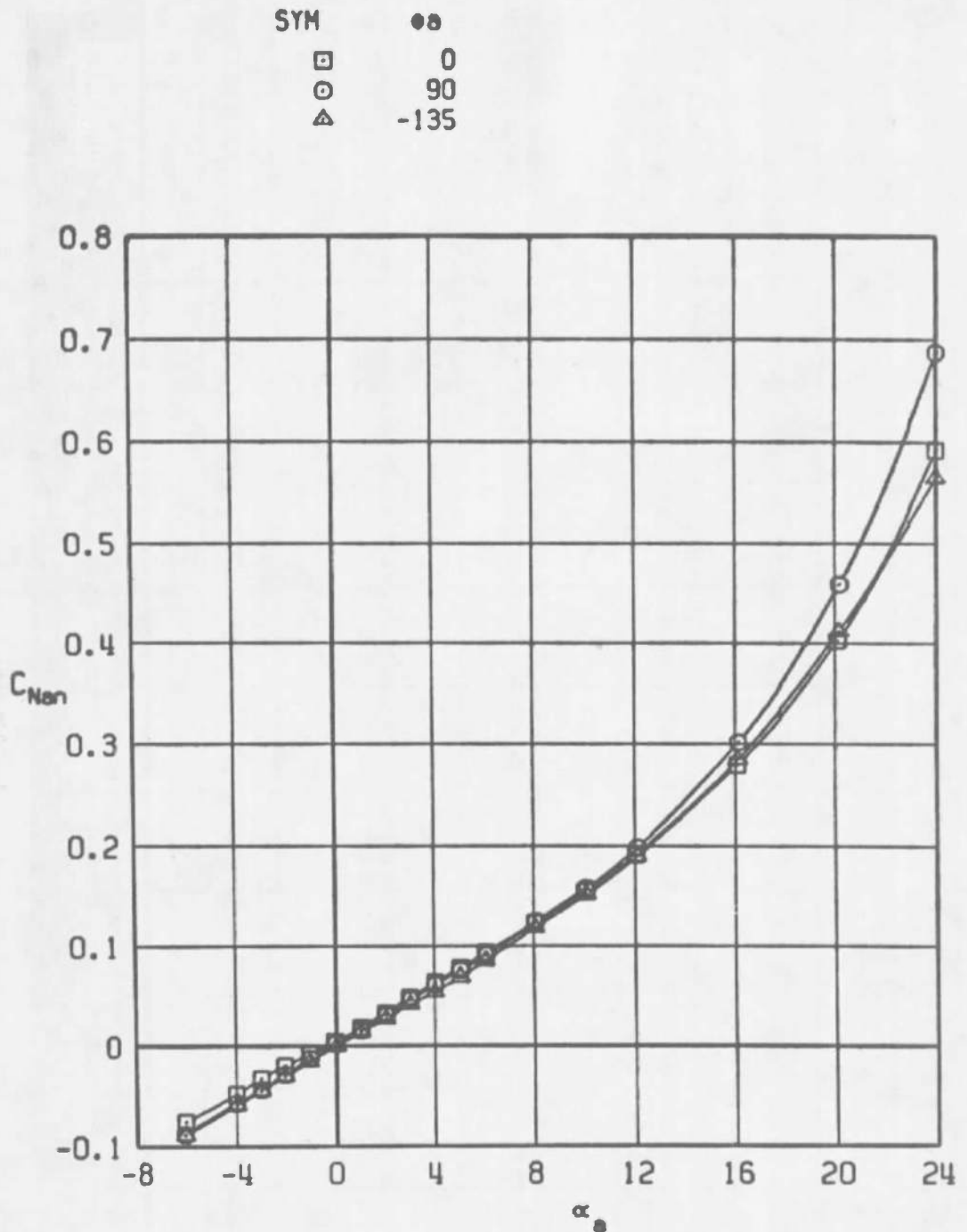


a. Front view

Figure 5. Installation of the pressure model in the test section.



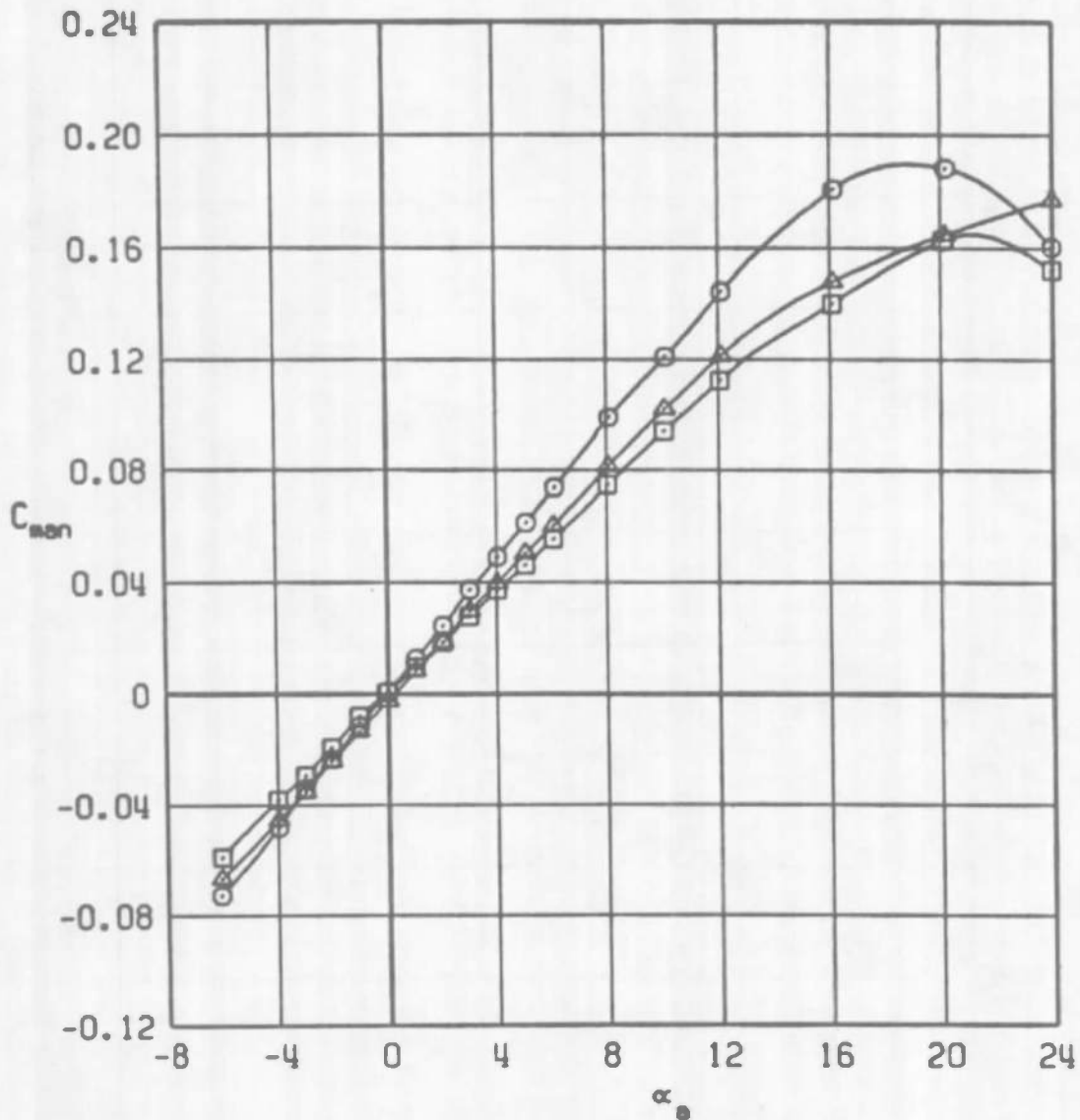
b. Aft view  
Figure 5. Concluded.



a. Normal-force coefficient

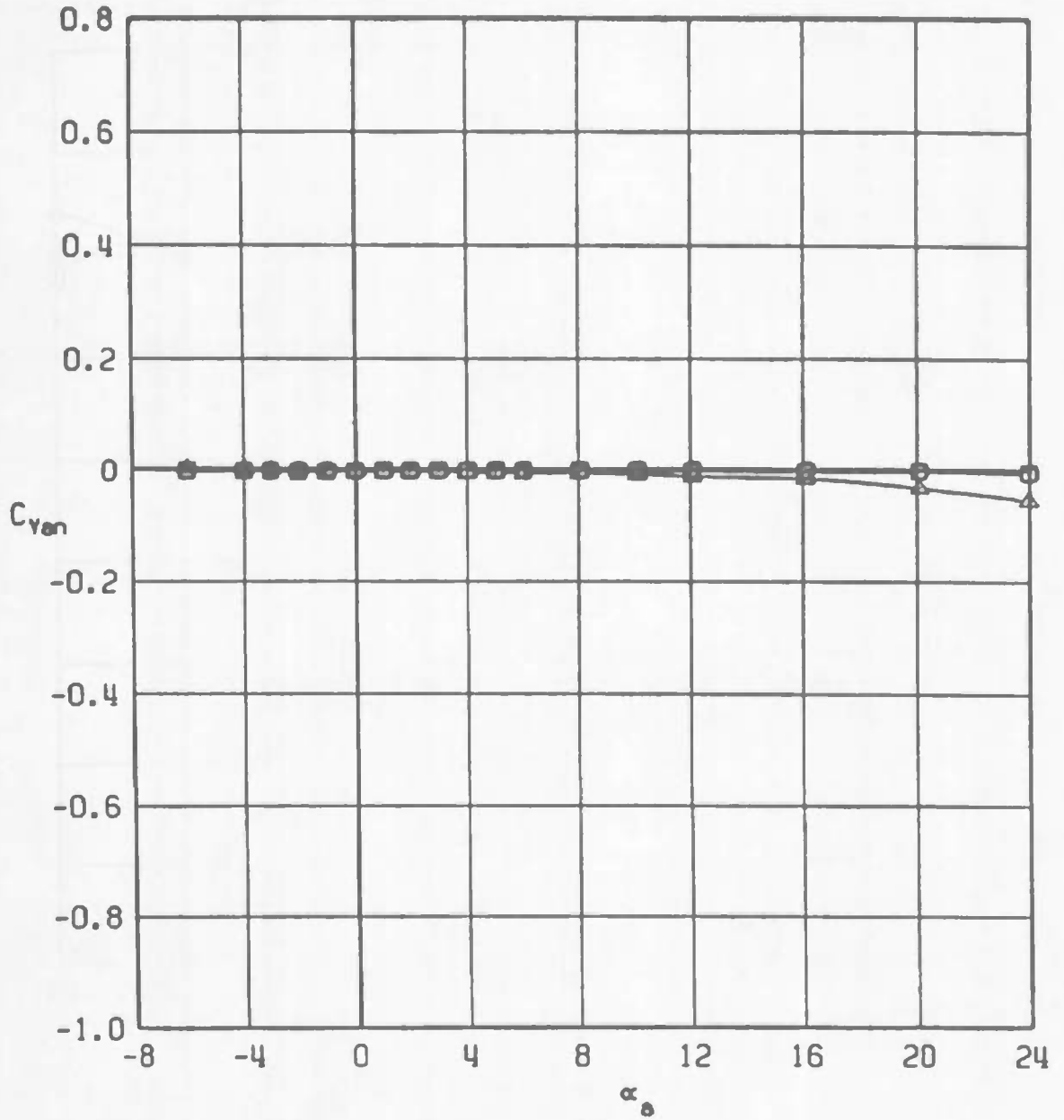
Figure 6. Typical variation of the nose aerodynamic coefficients with angle of attack,  $M_\infty = 1.1$ .

SYM      ●●  
           □      0  
           ○      90  
           △      -135



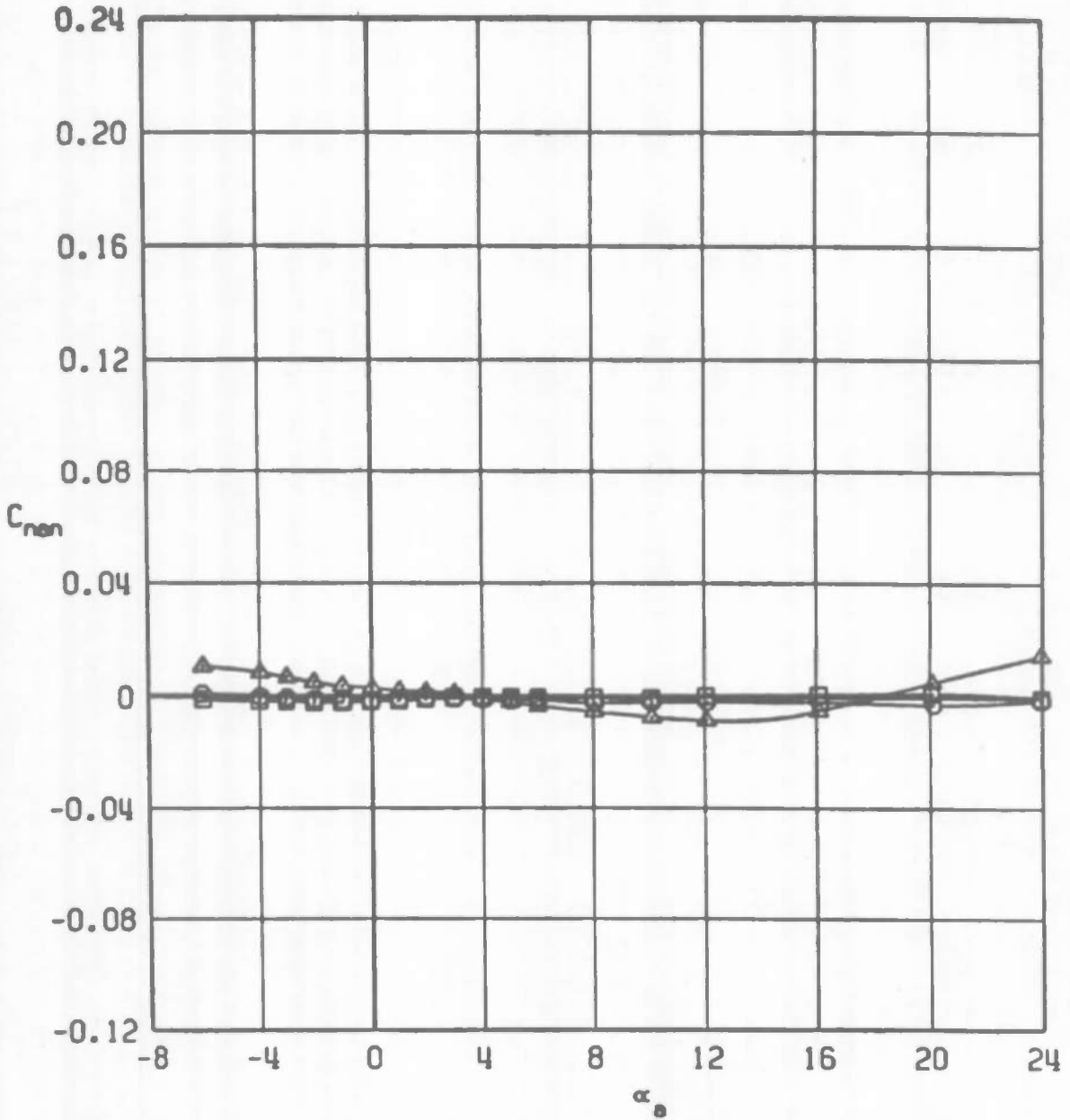
b. Pitching-moment coefficient  
 Figure 6. Continued.

SYM      ●●  
 □        0  
 ○        90  
 ▲        -135

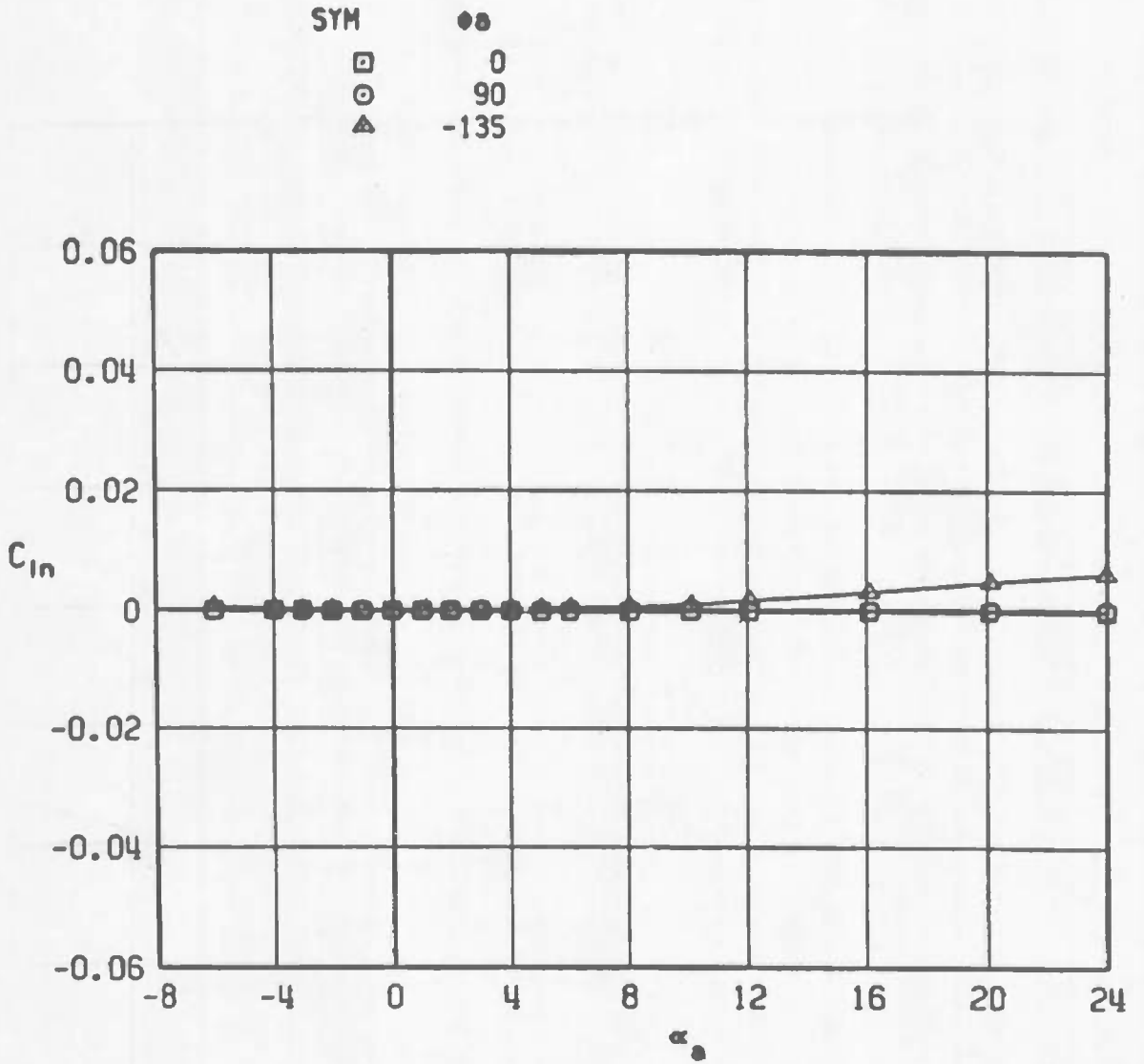


c. Side-force coefficient  
 Figure 6. Continued.

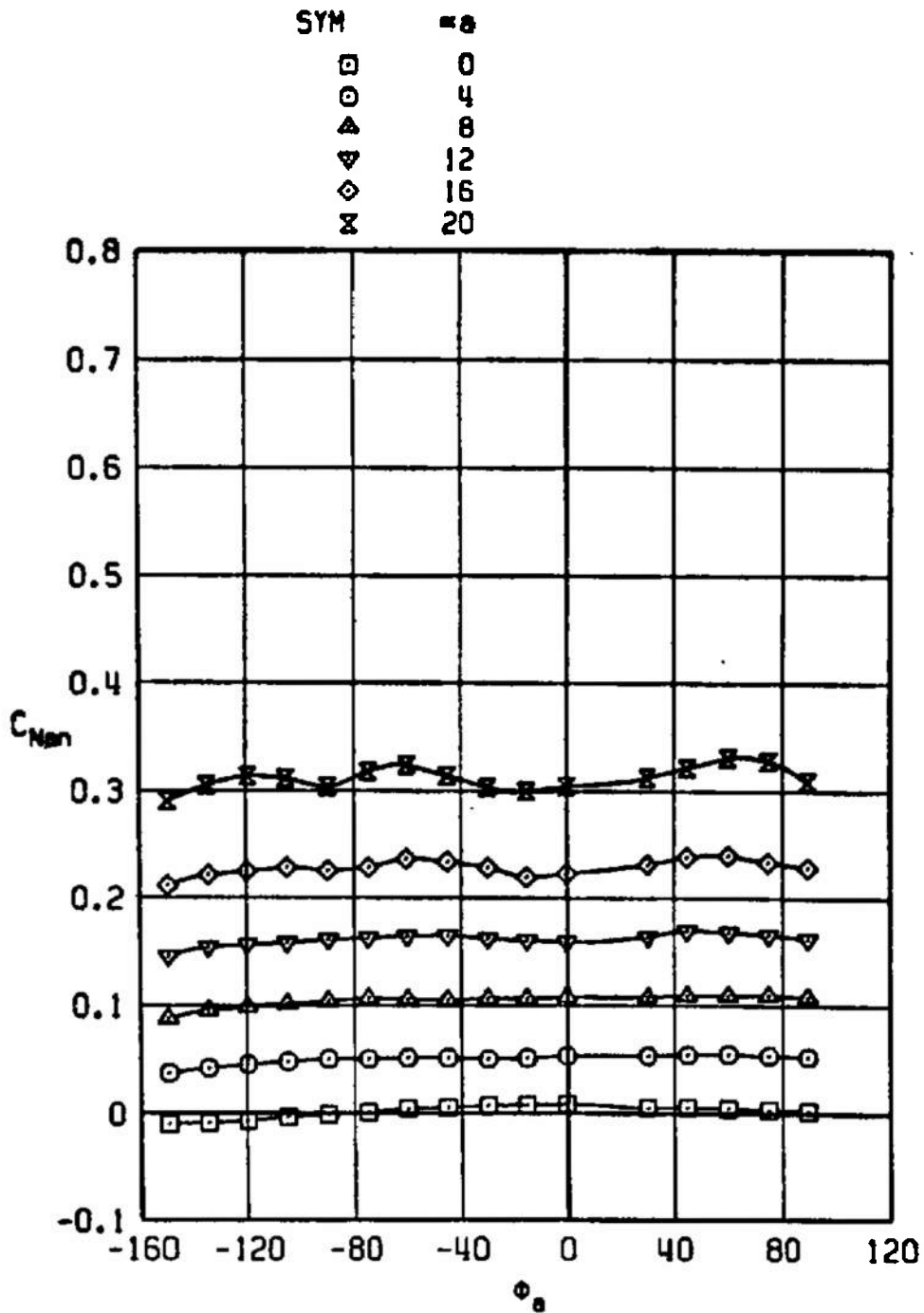
SYM      ● a  
           □ 0  
           ○ 90  
           ▲ -135



d. Yawing-moment coefficient  
 Figure 6. Continued.

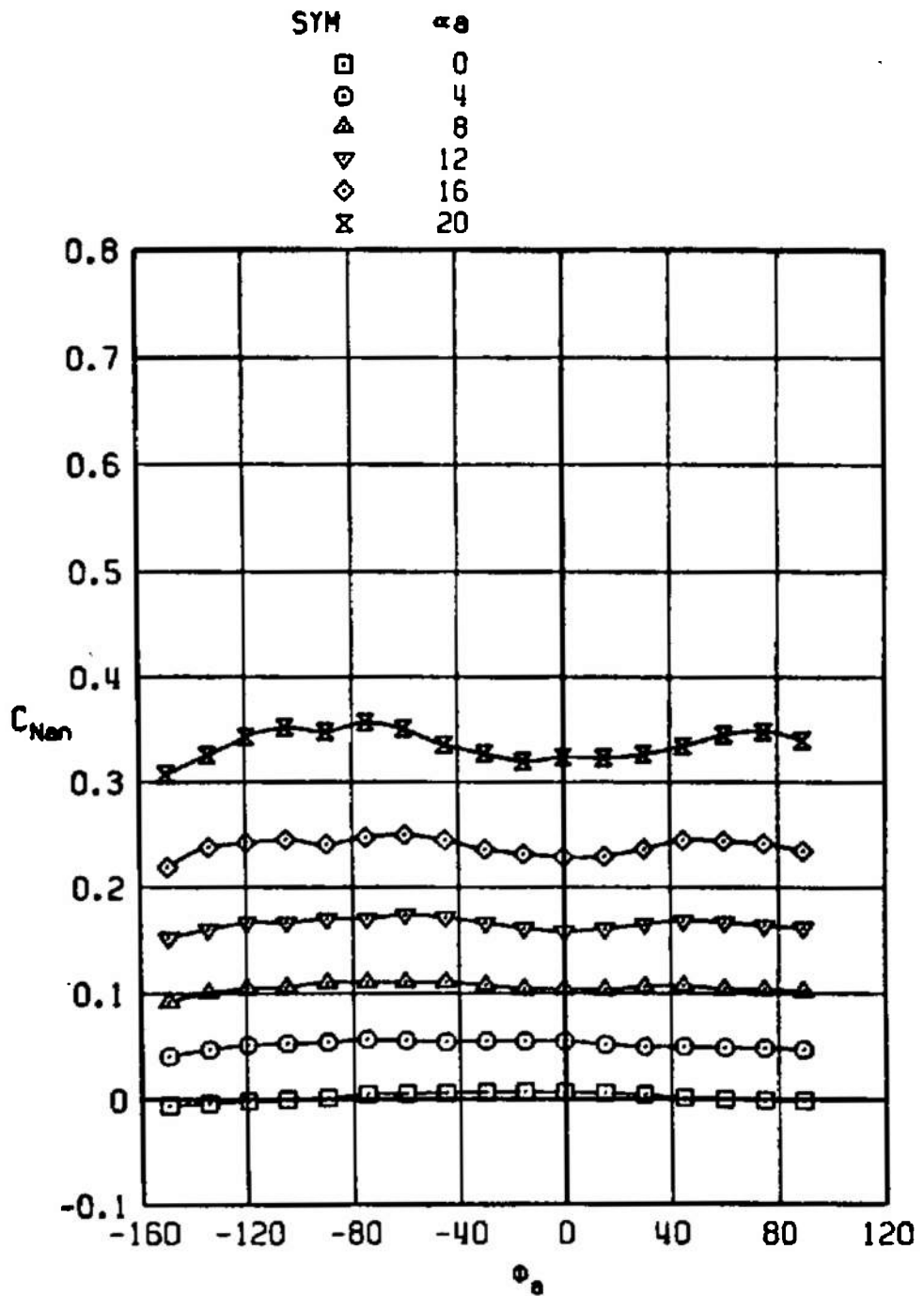


e. Rolling-moment coefficient  
Figure 6. Concluded.

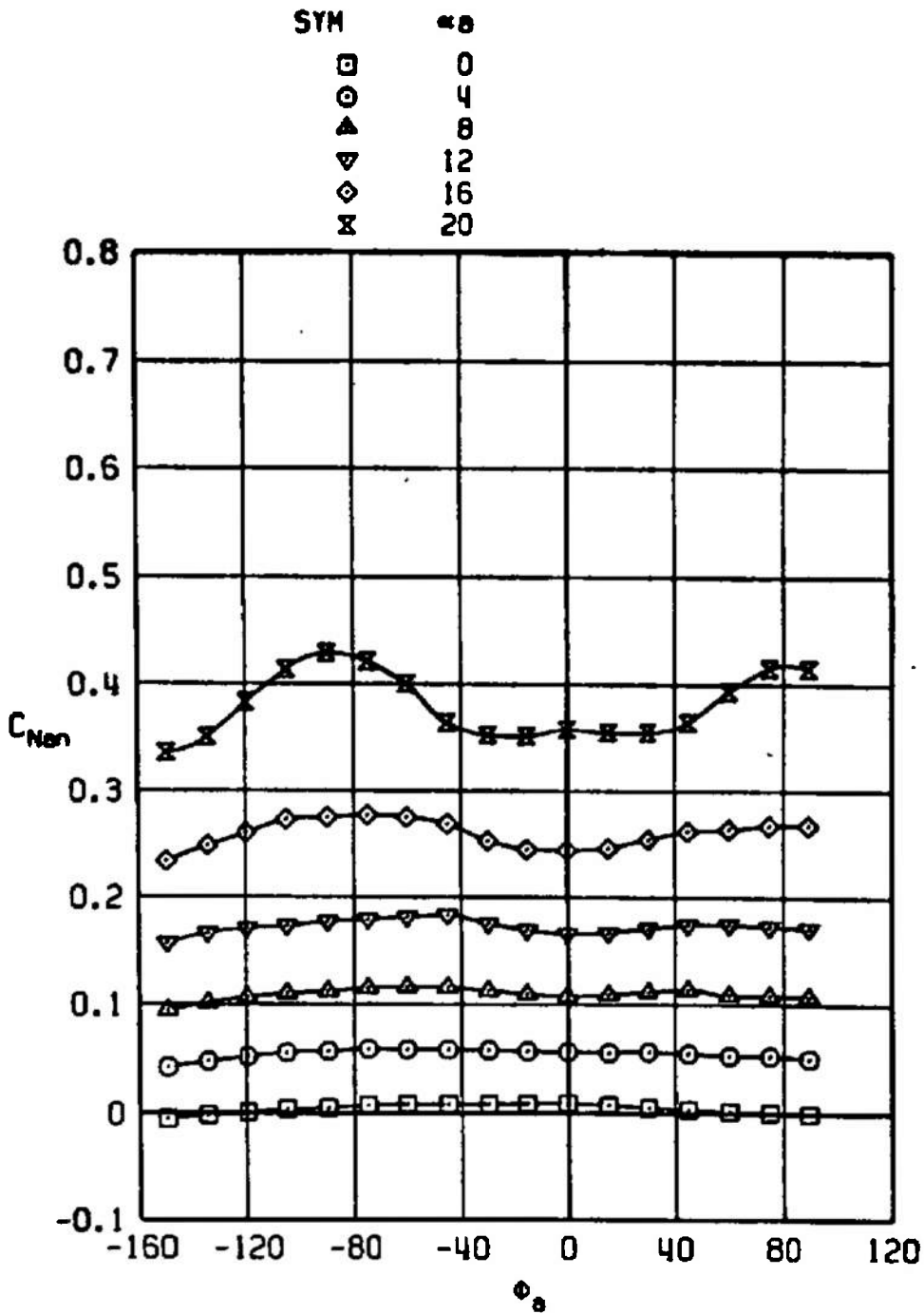


a.  $M_\infty = 0.50$

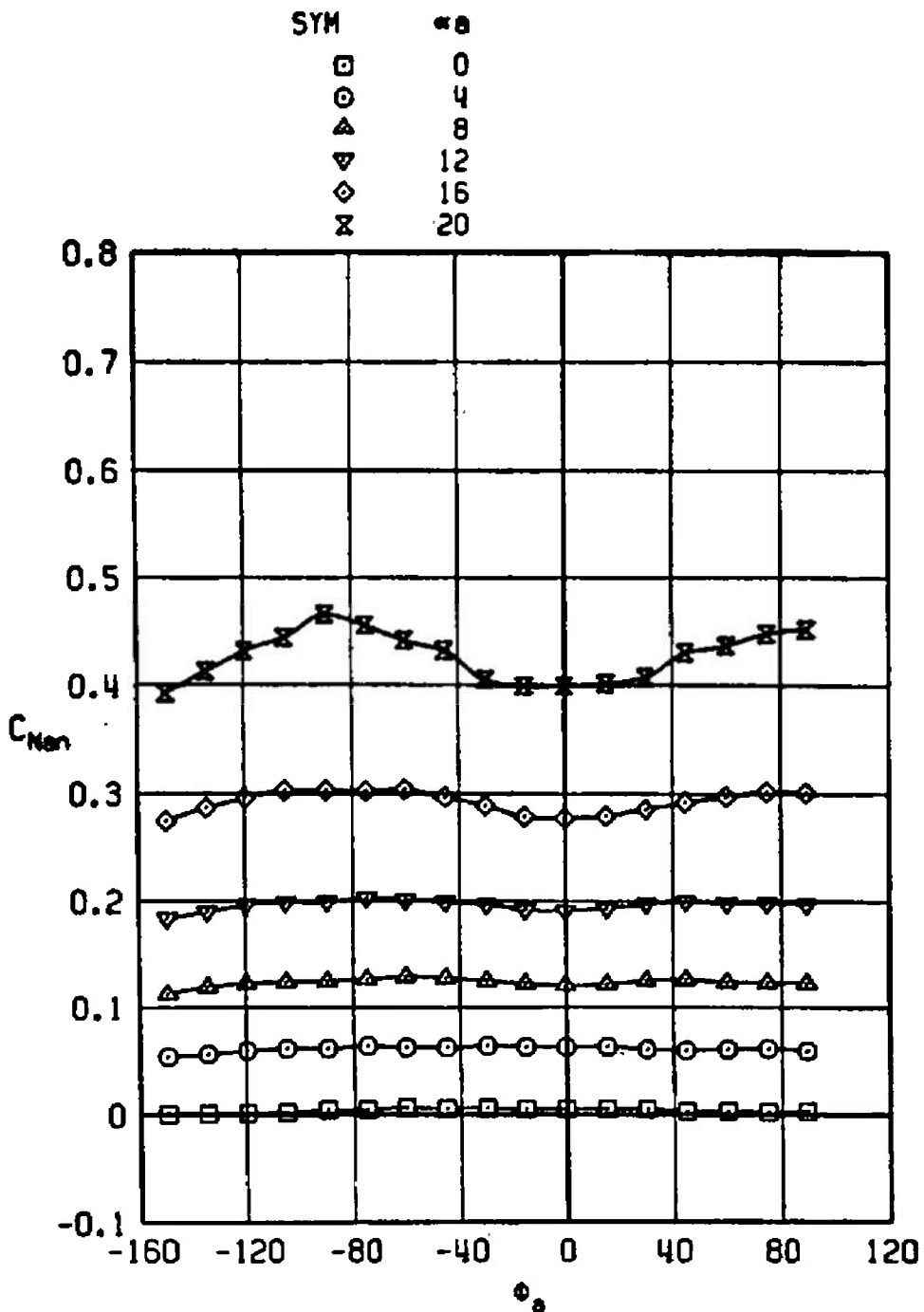
Figure 7. Variation of the nose normal-force coefficient with model roll angle.



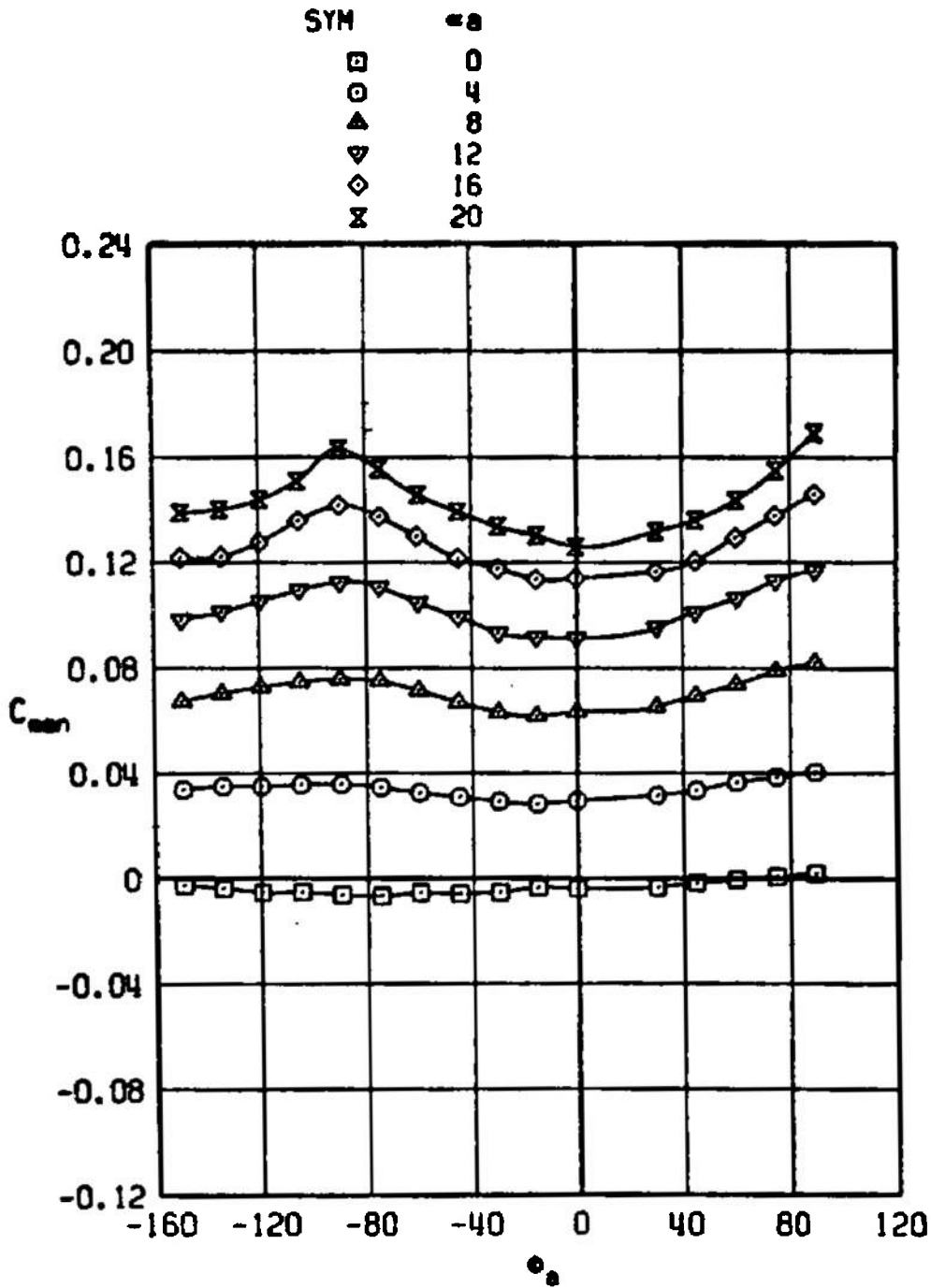
b.  $M_\infty = 0.80$   
 Figure 7. Continued.



c.  $M_\infty = 0.95$   
 Figure 7. Continued.

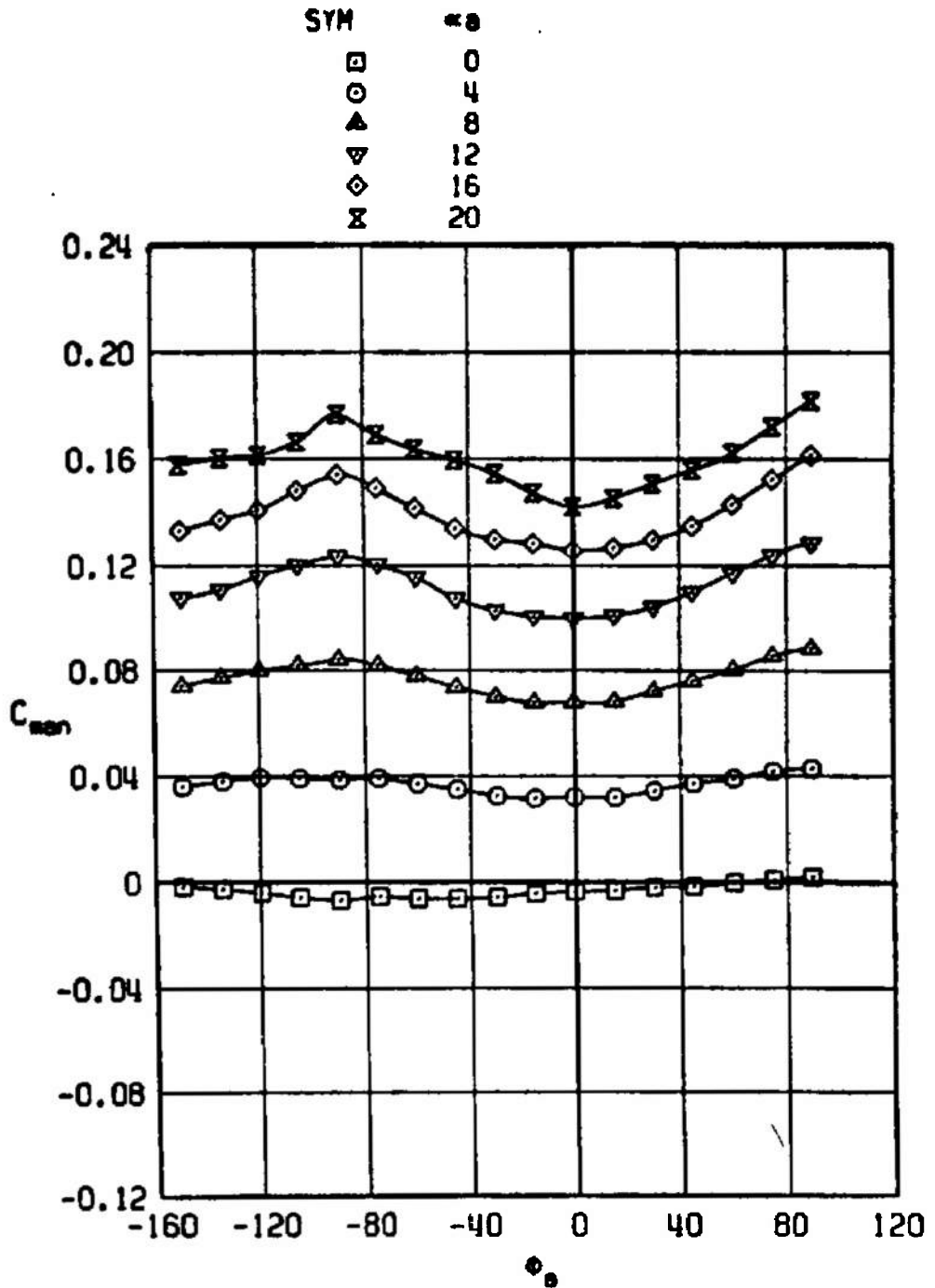


d.  $M_\infty = 1.10$   
 Figure 7. Concluded.

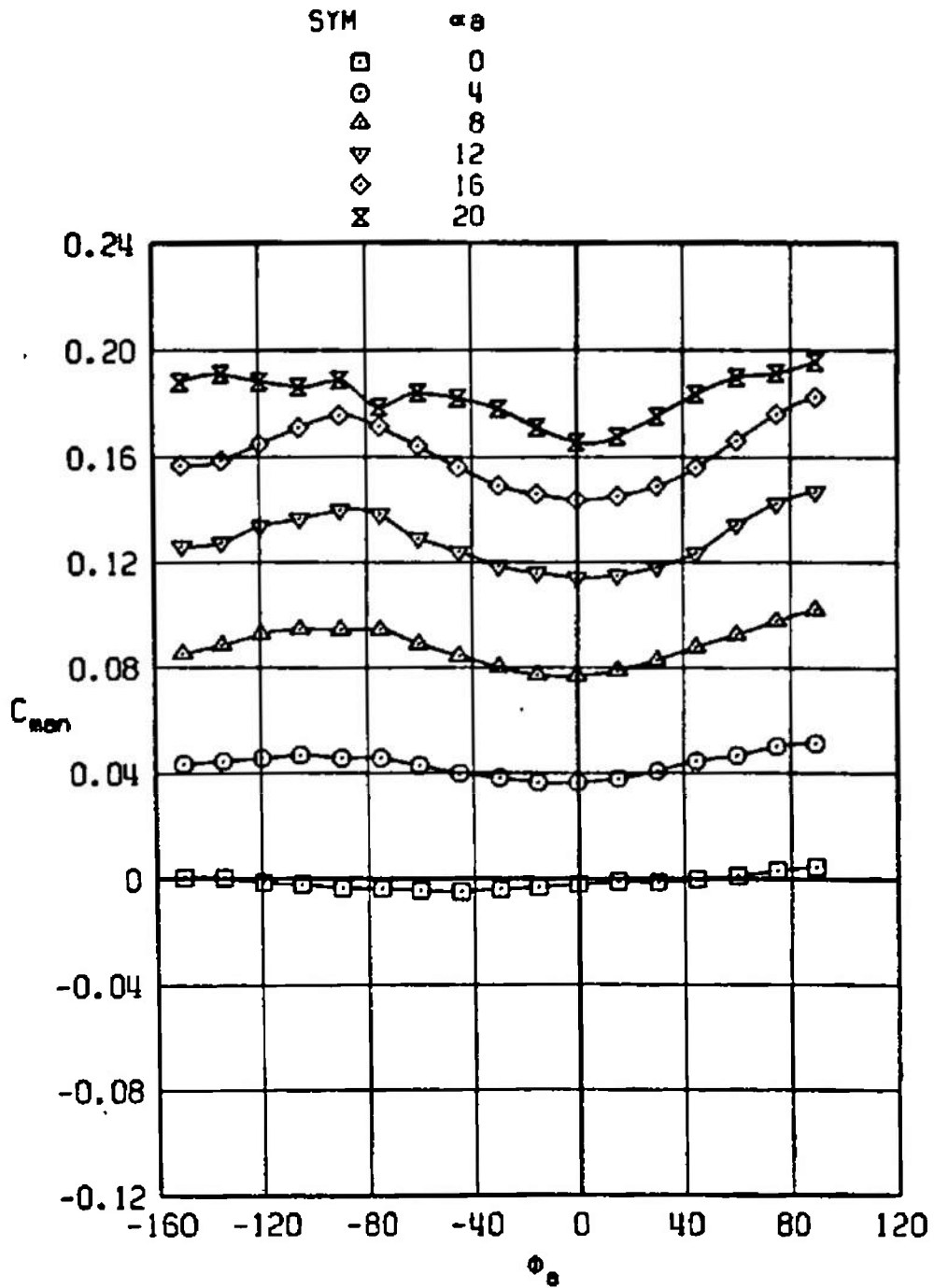


a.  $M_\infty = 0.50$

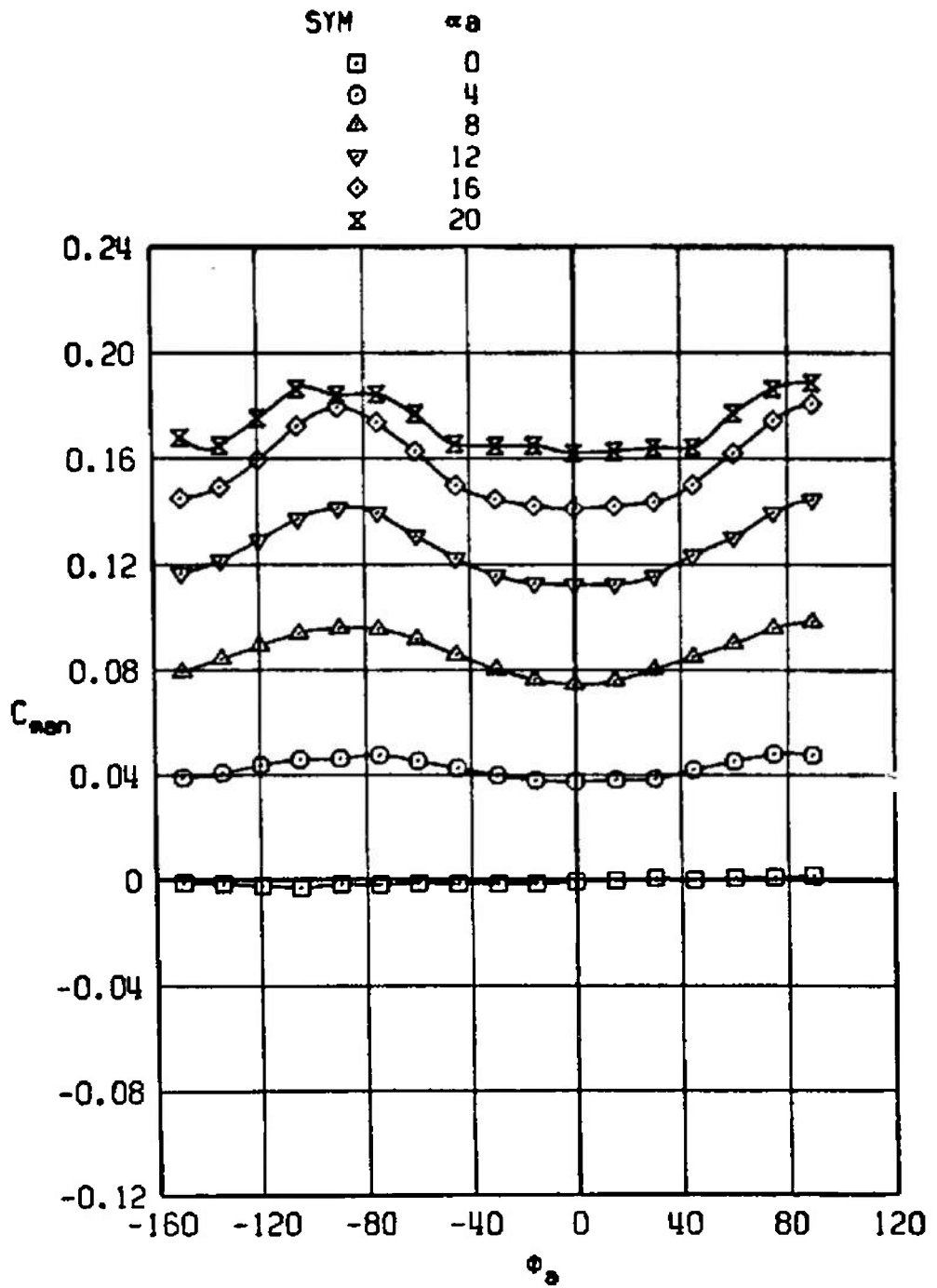
Figure 8. Variation of the nose pitching-moment coefficient with model roll angle.



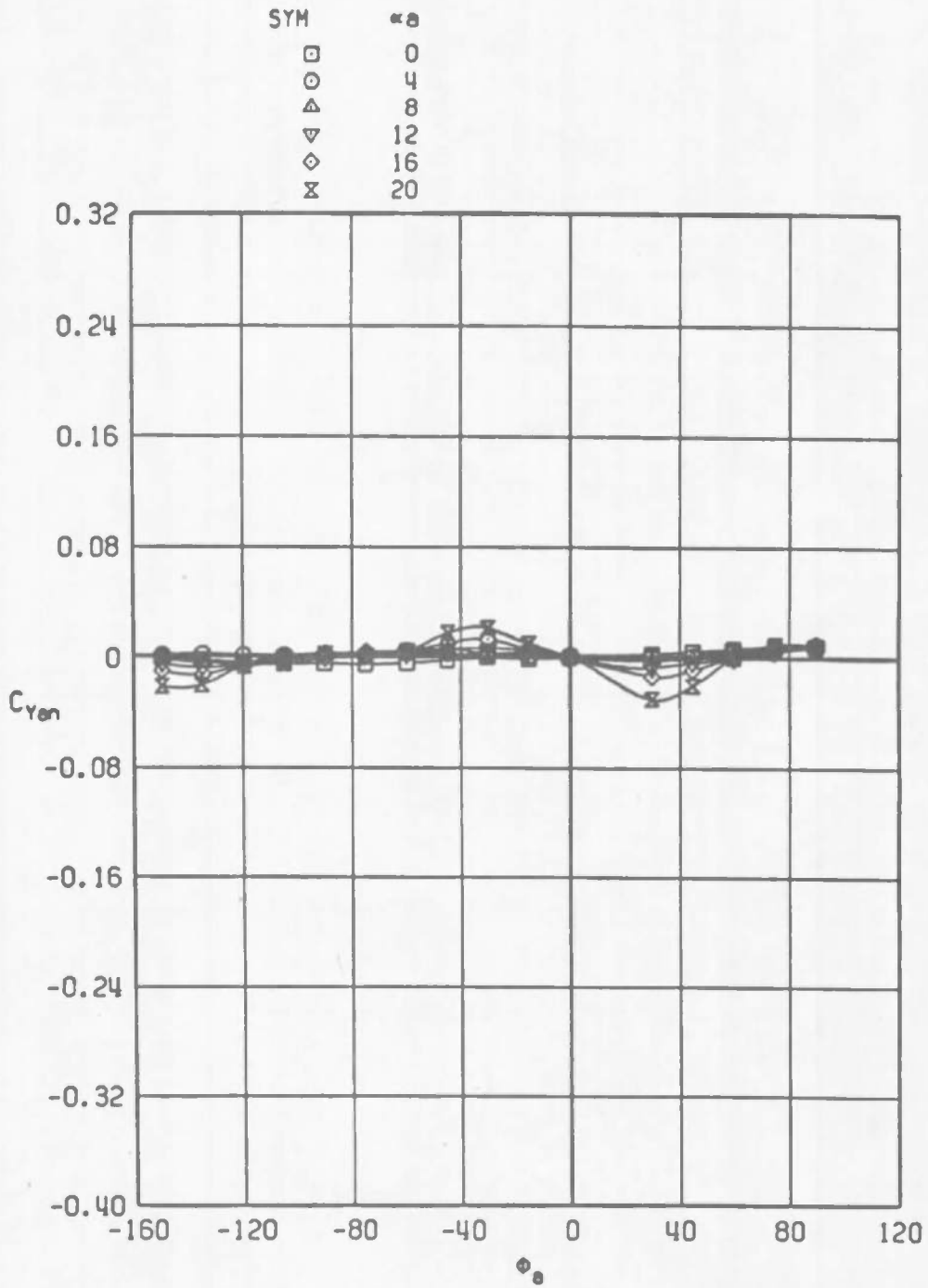
b.  $M_\infty = 0.80$   
Figure 8. Continued.



c.  $M_\infty = 0.95$   
 Figure 8. Continued.

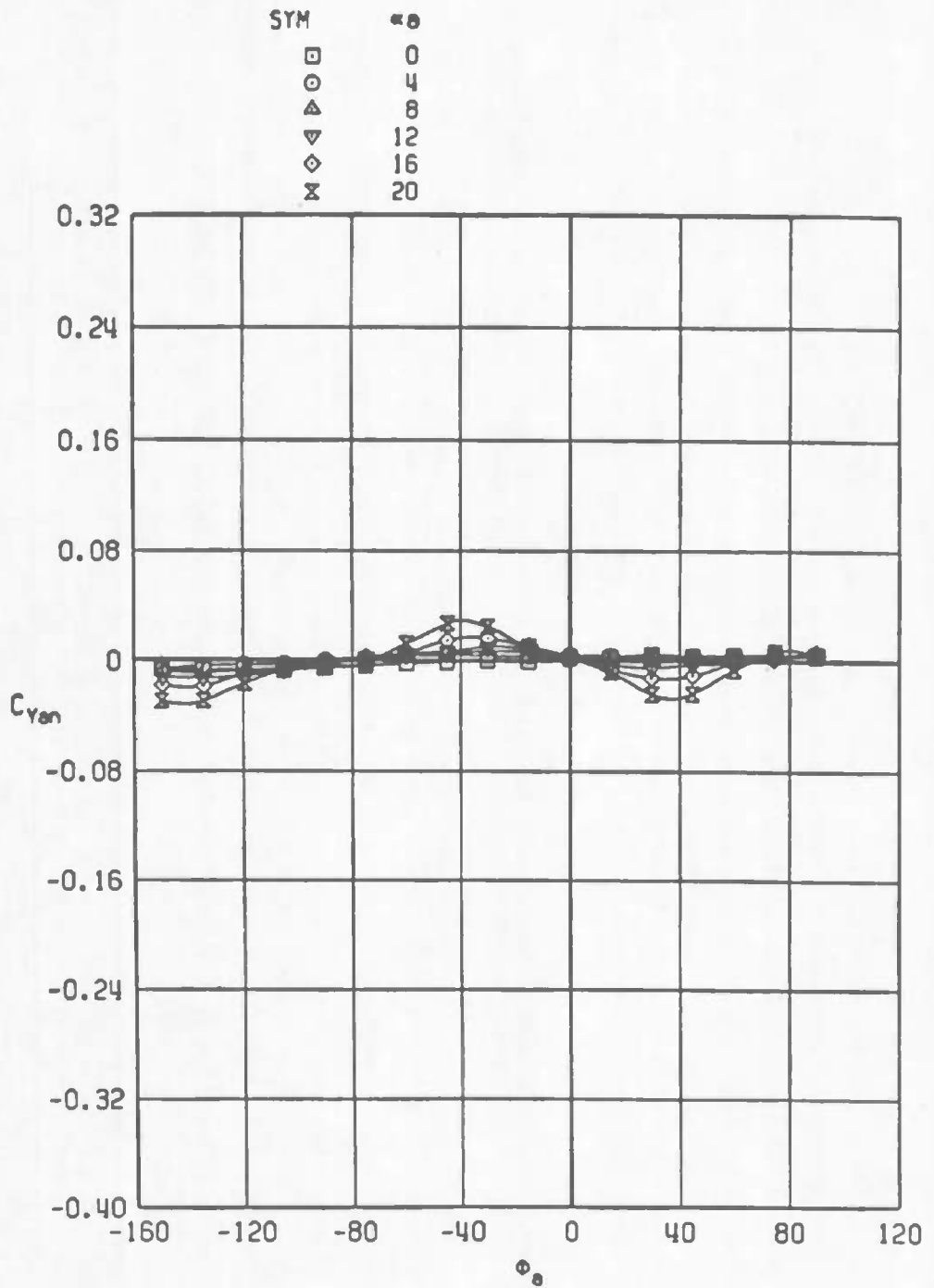


d.  $M_\infty = 1.10$   
 Figure 8. Concluded.

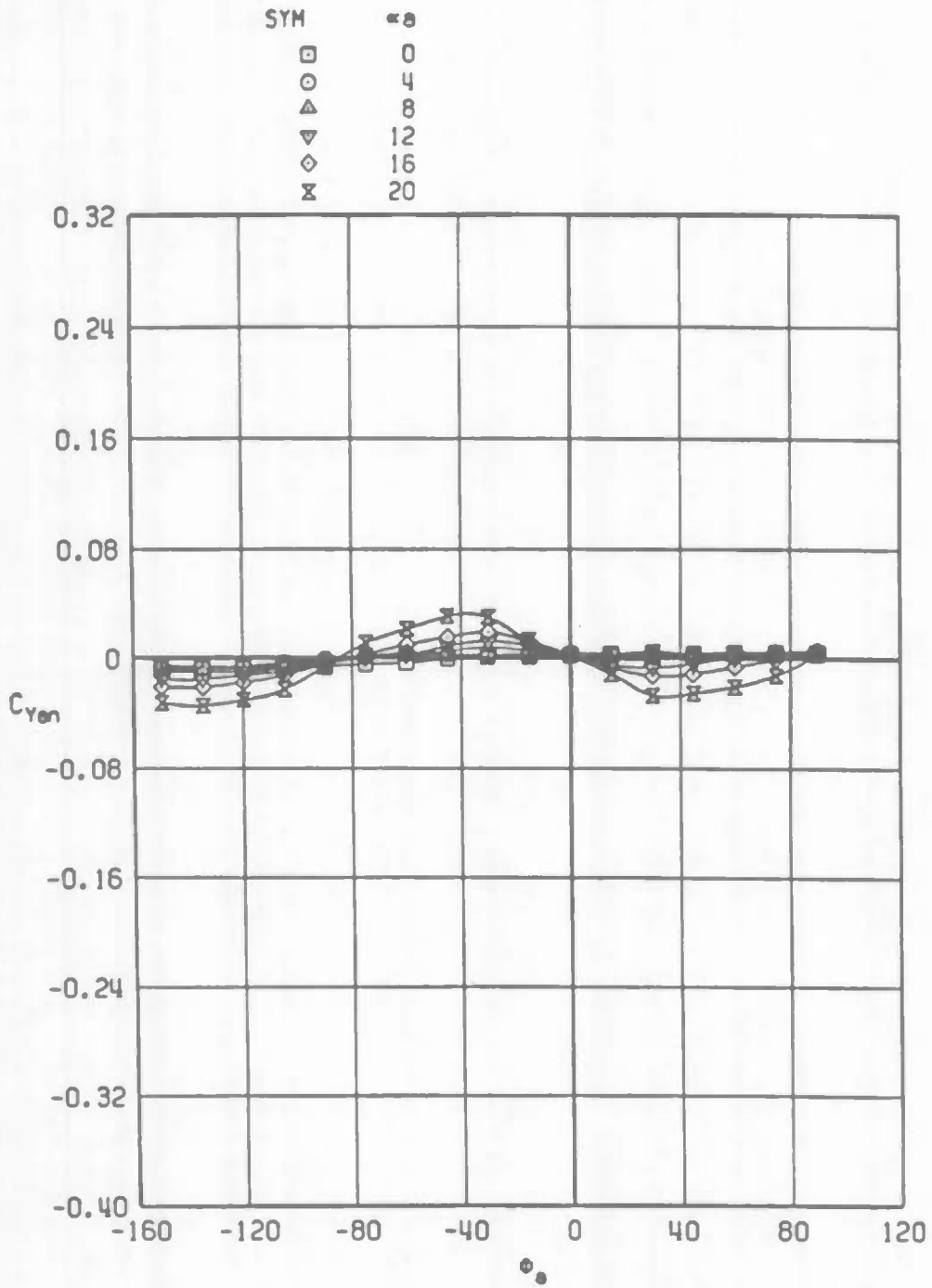


a.  $M_{\infty} = 0.50$

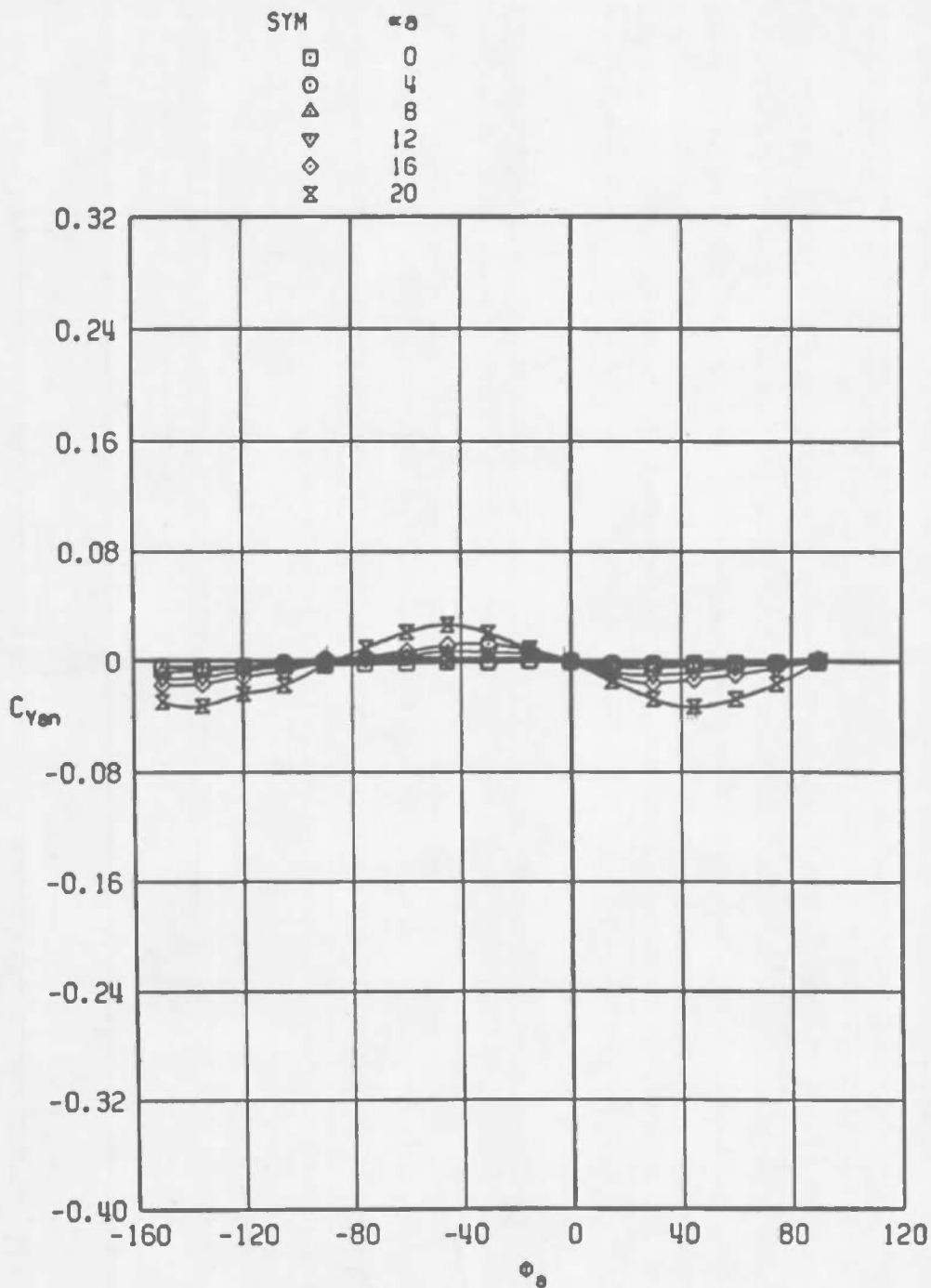
Figure 9. Variation of the nose side-force coefficient with model roll angle.



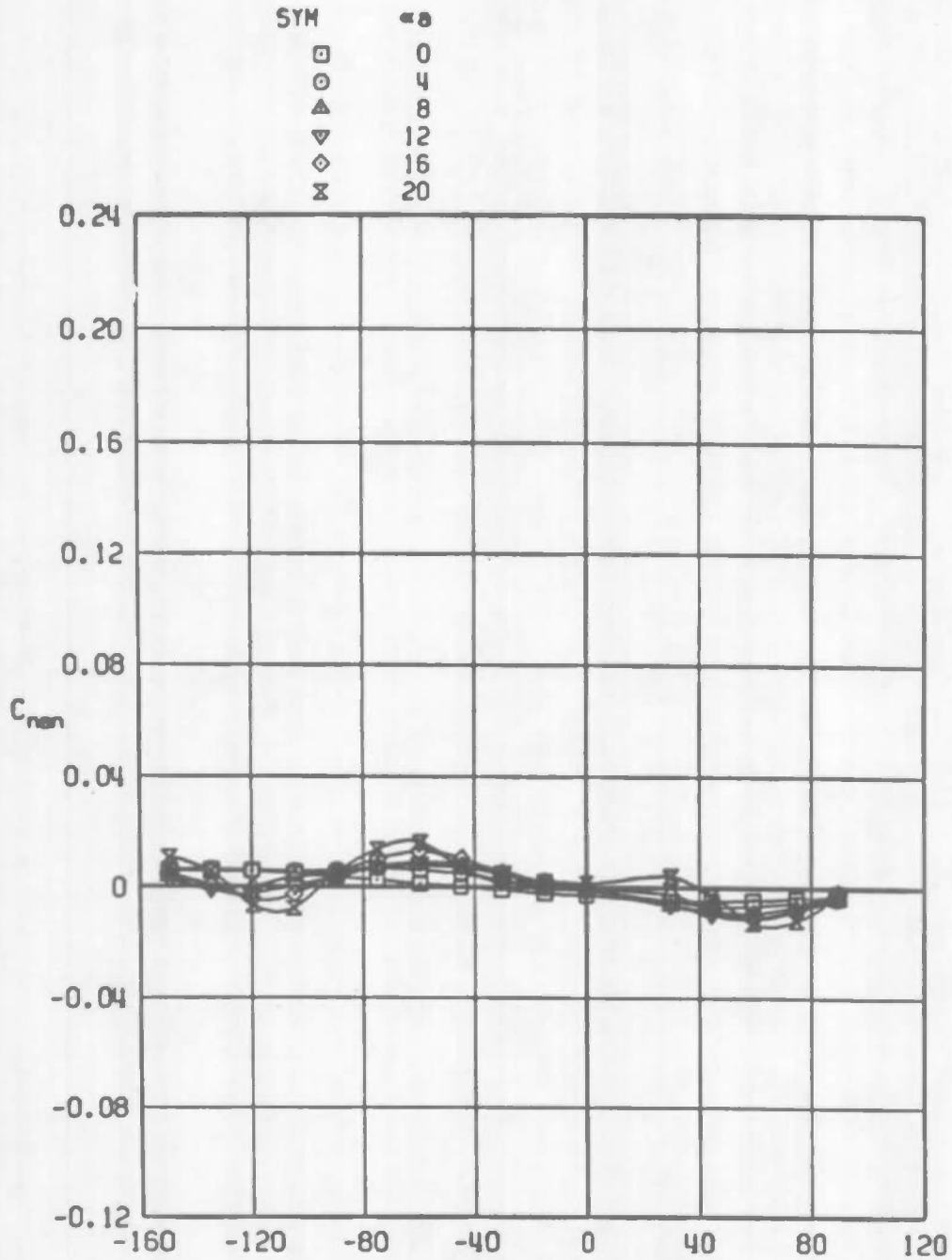
b.  $M_\infty = 0.80$   
 Figure 9. Continued.



c.  $M_\infty = 0.95$   
 Figure 9. Continued.

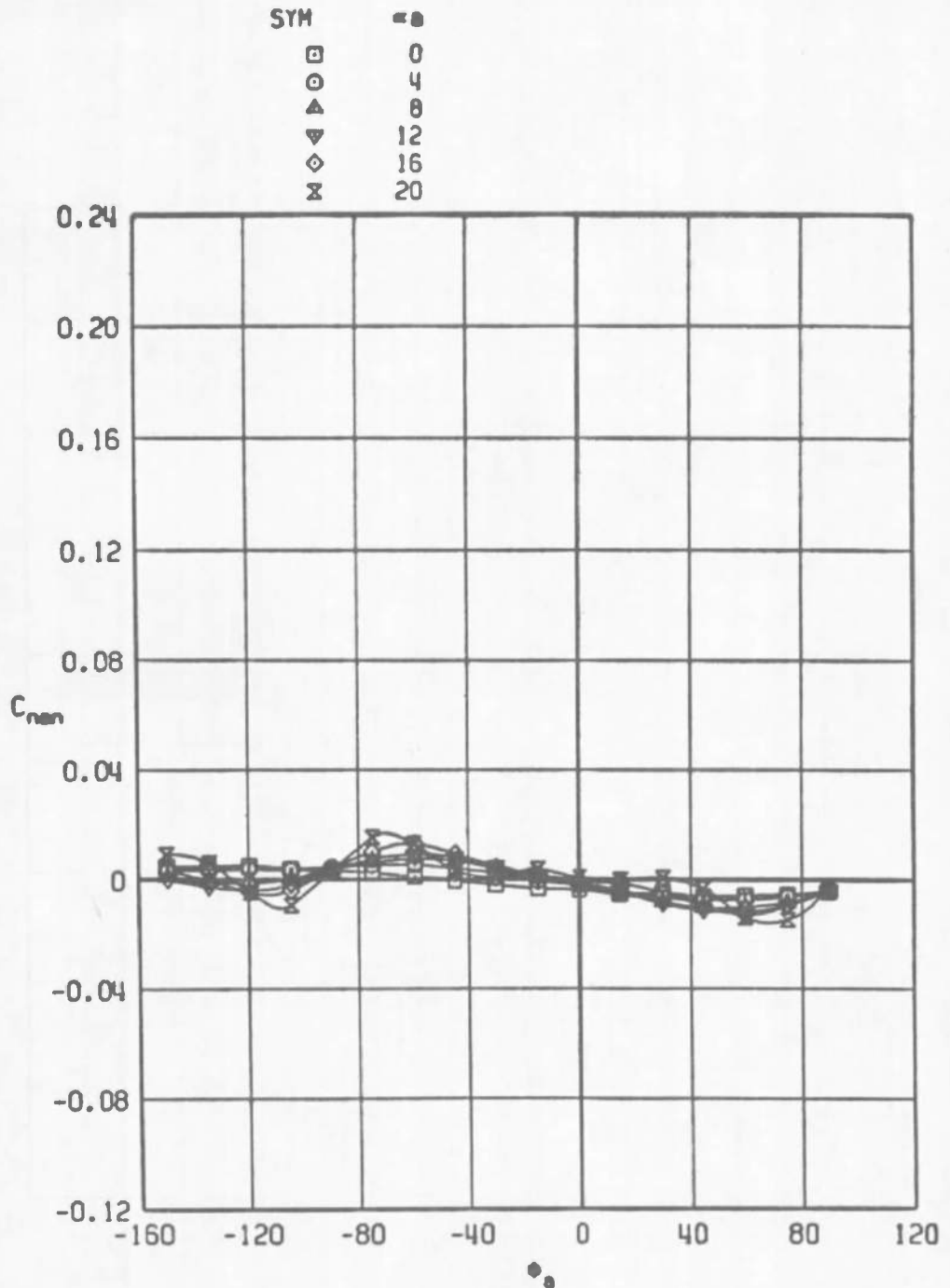


d.  $M_\infty = 1.10$   
 Figure 9. Concluded.

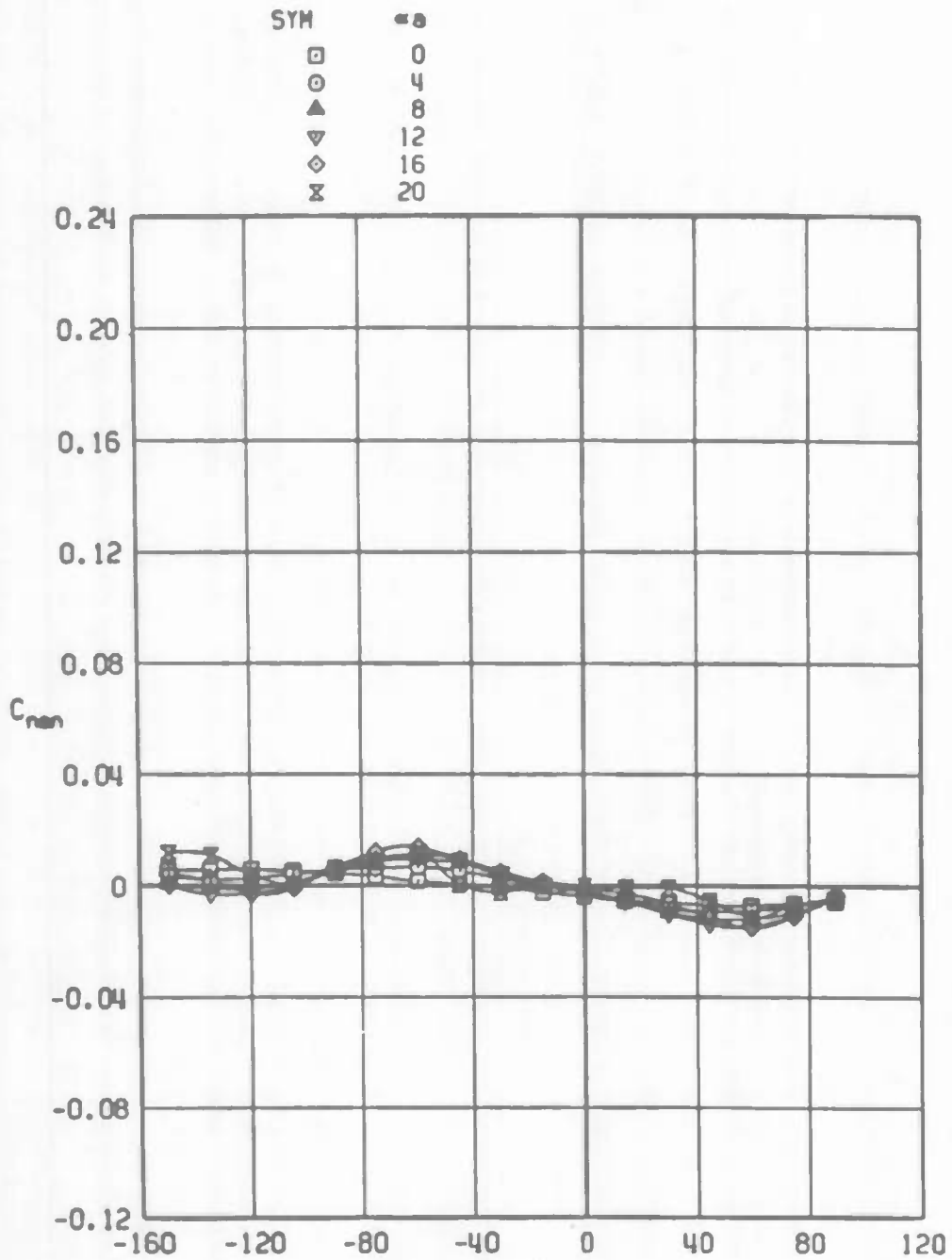


a.  $M_\infty = 0.50$

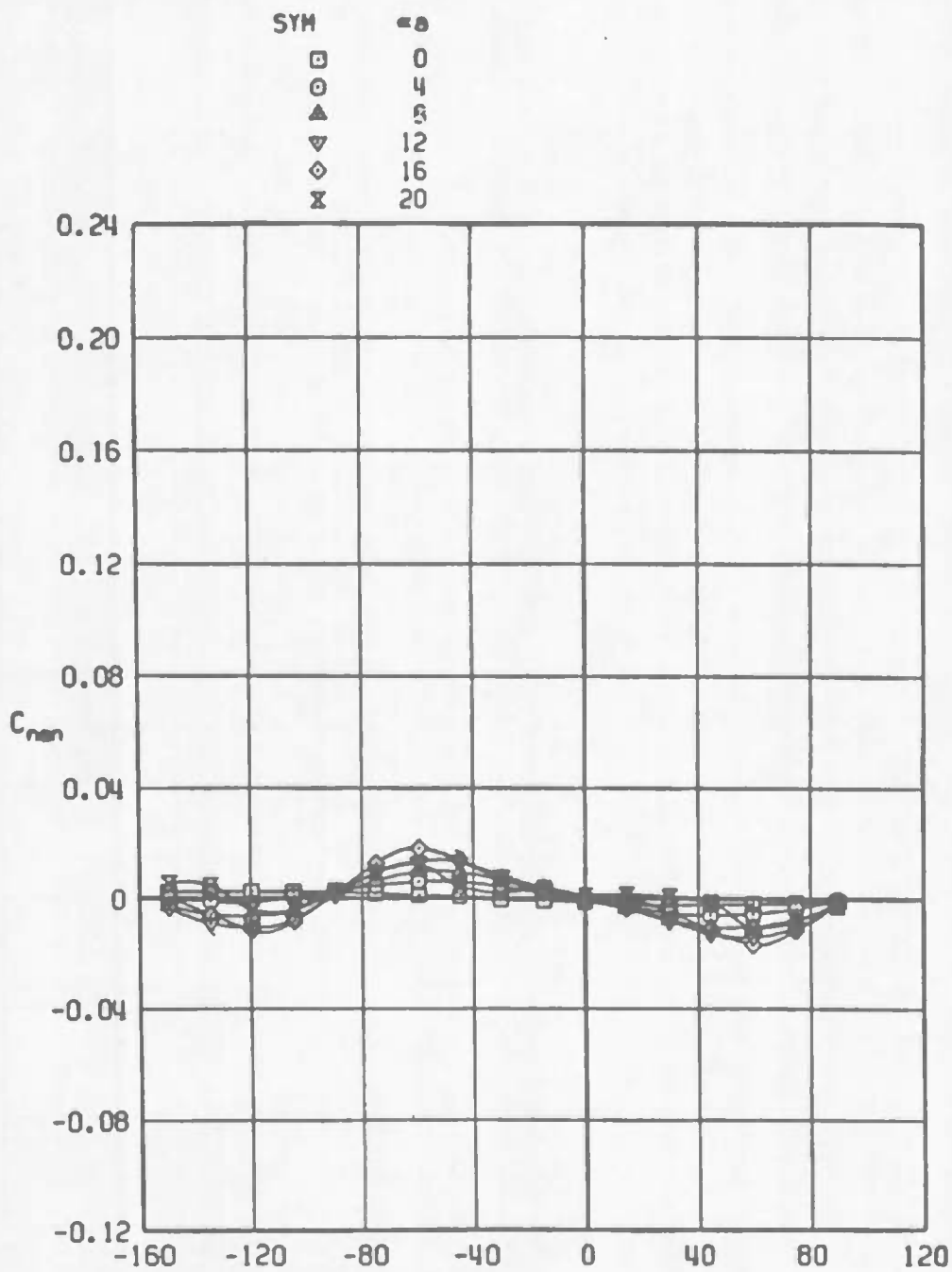
Figure 10. Variation of the nose yawing-moment coefficient with model roll angle.



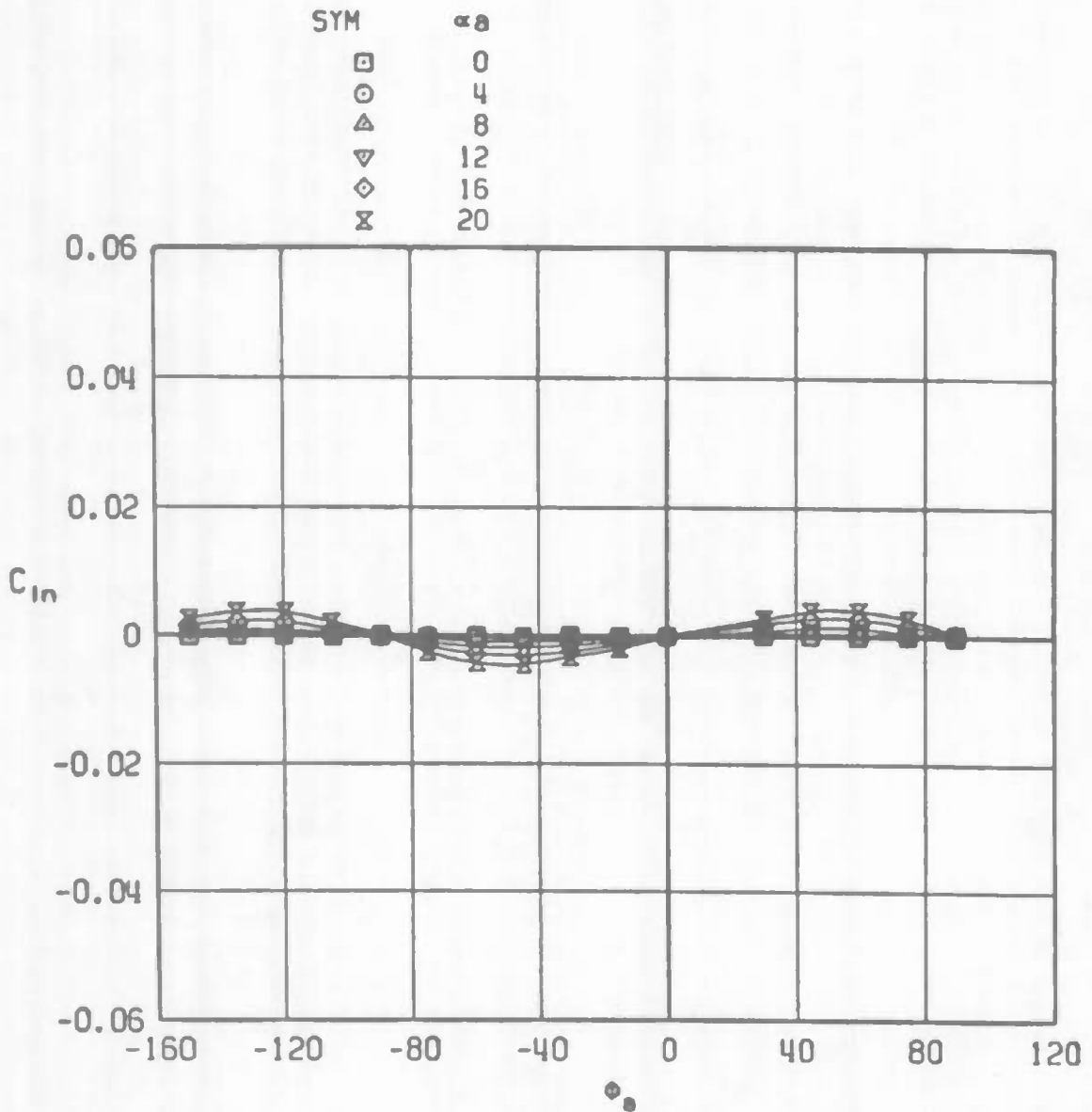
b.  $M_\infty = 0.80$   
 Figure 10. Continued.



c.  $M_\infty = 0.95$   
 Figure 10. Continued.

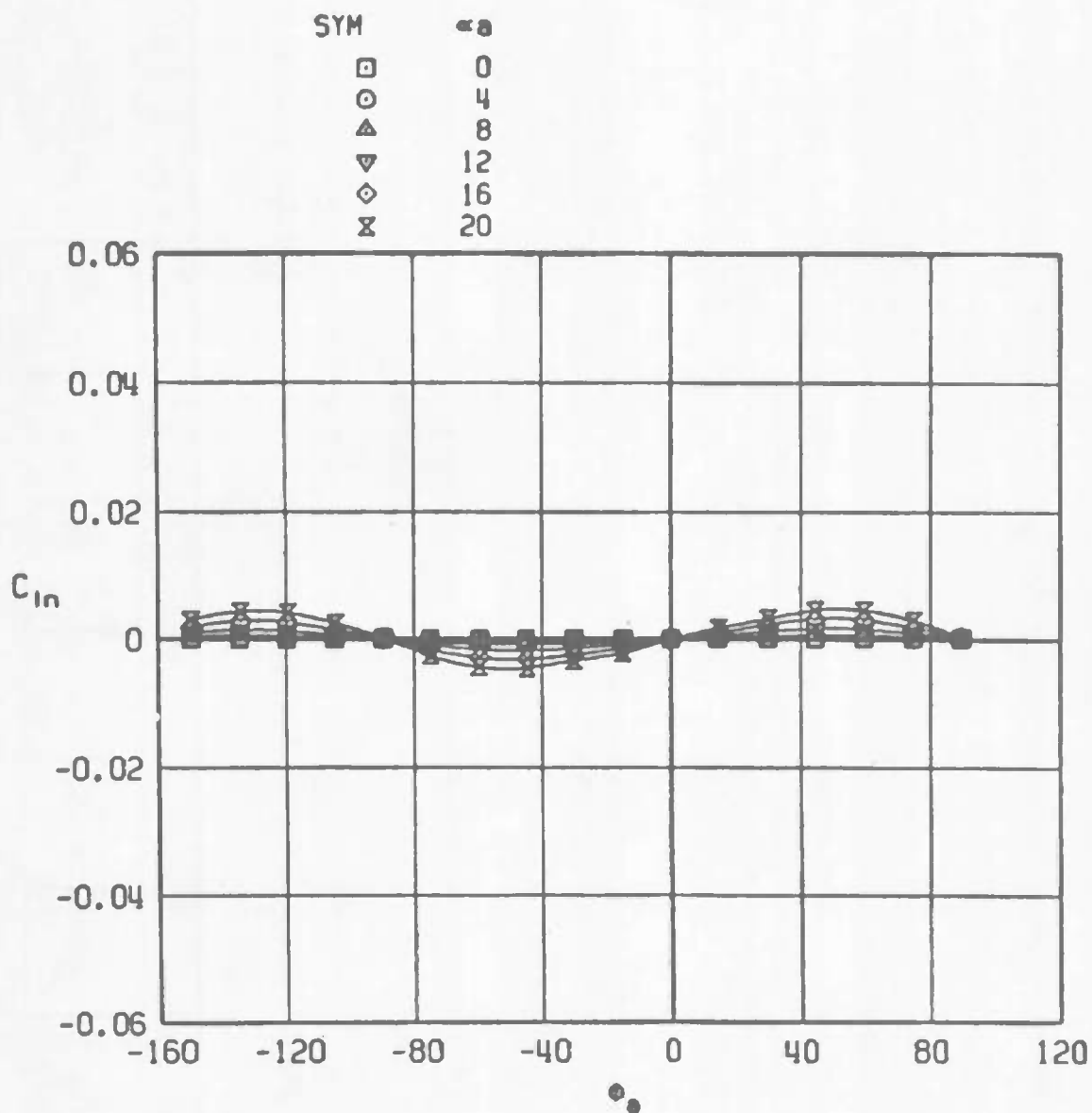


d.  $M_\infty = 1.10$   
 Figure 10. Concluded.

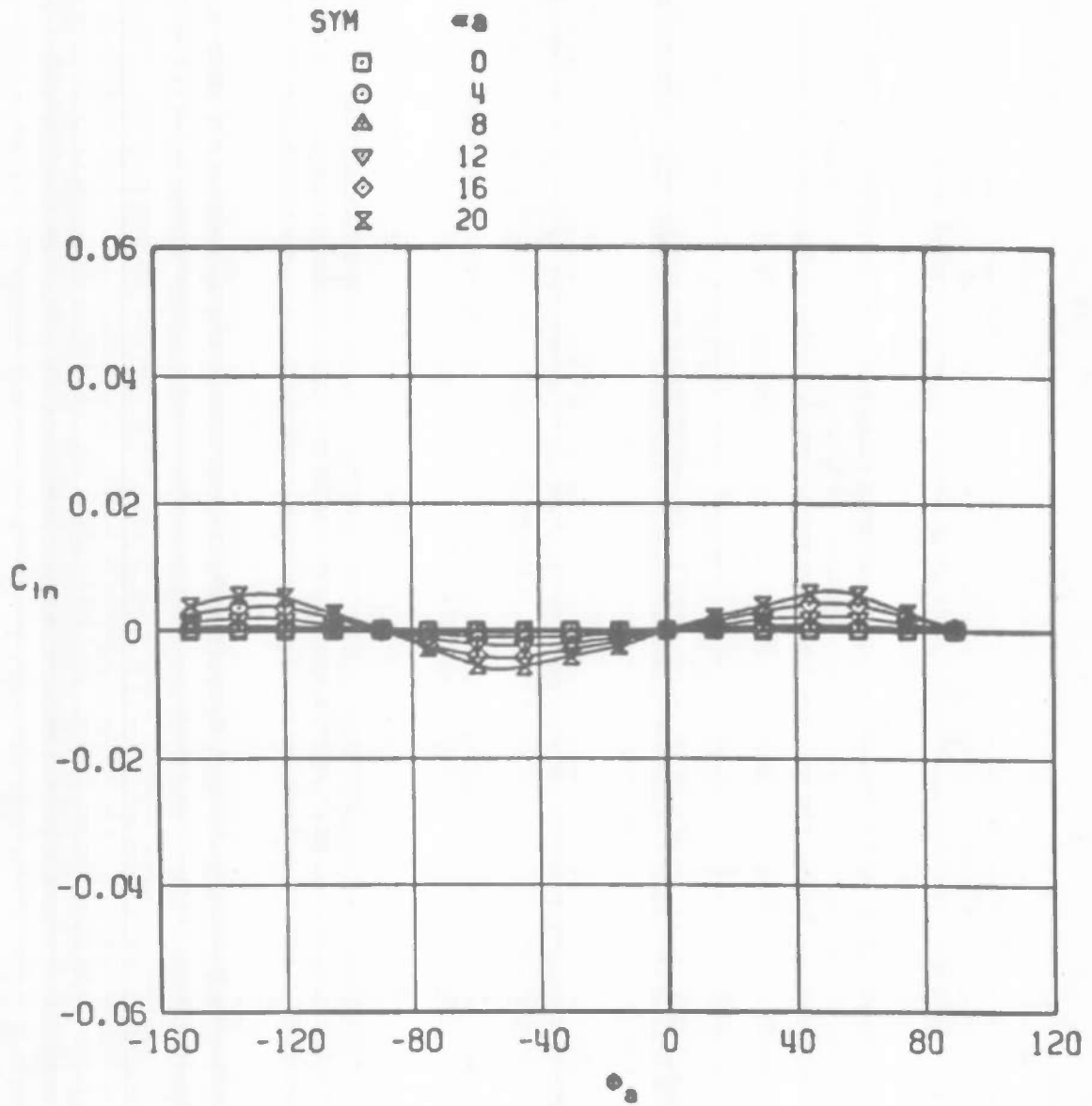


a.  $M_\infty = 0.50$

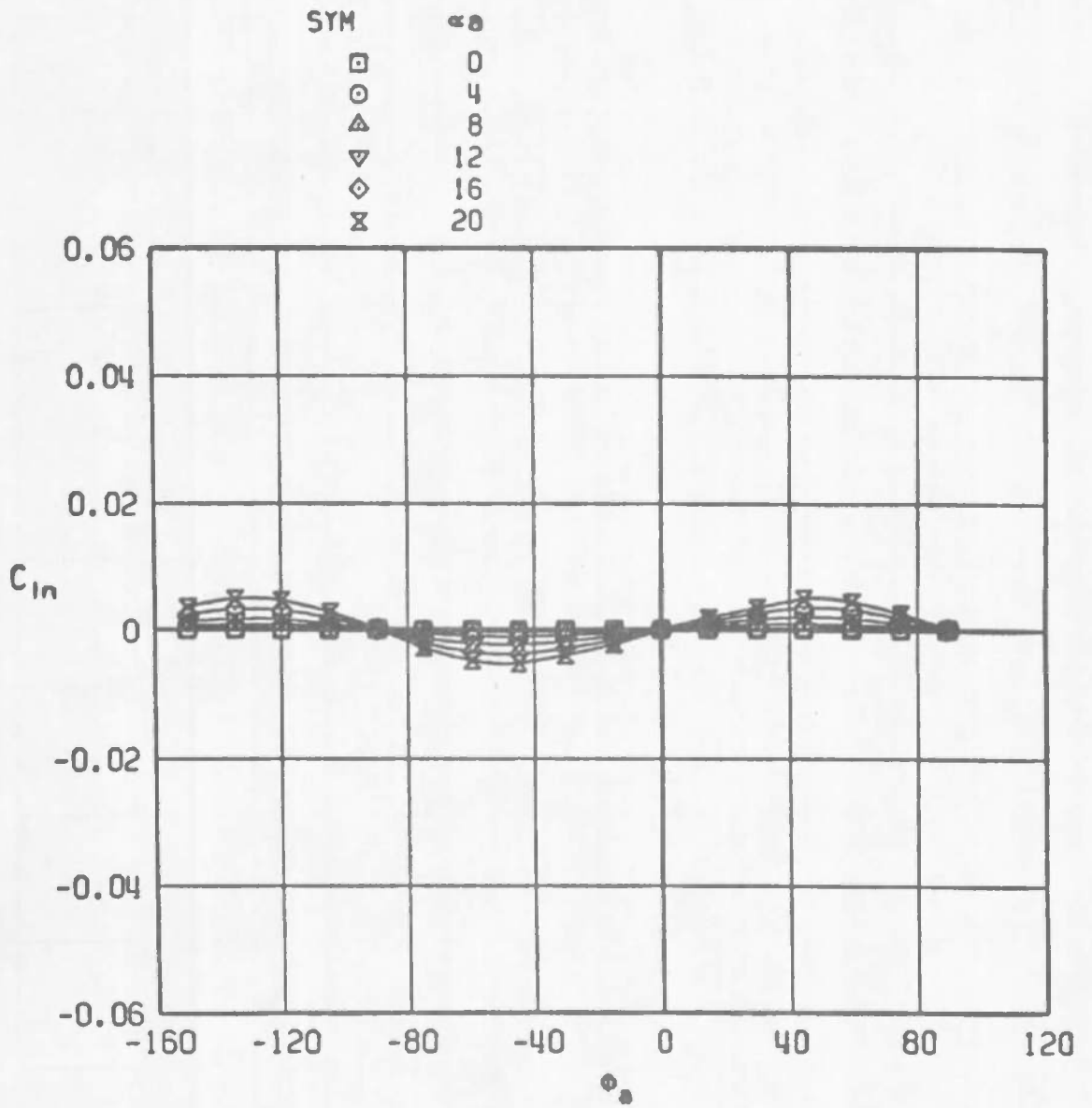
Figure 11. Variation of the nose rolling-moment coefficient with model roll angle.



b.  $M_\infty = 0.80$   
 Figure 11. Continued.



c.  $M_\infty = 0.95$   
 Figure 11. Continued.



d.  $M_\infty = 1.10$   
 Figure 11. Concluded.

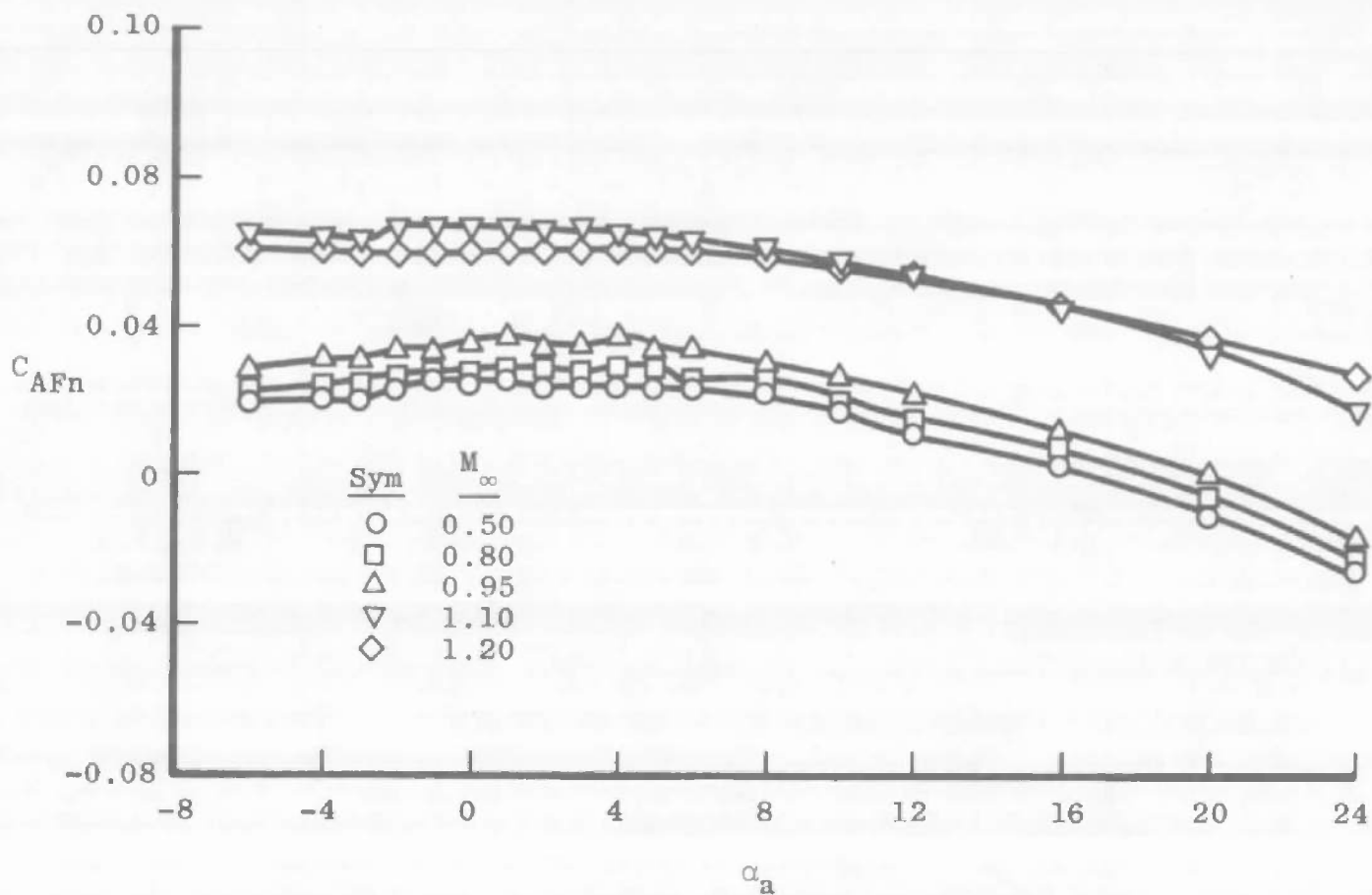
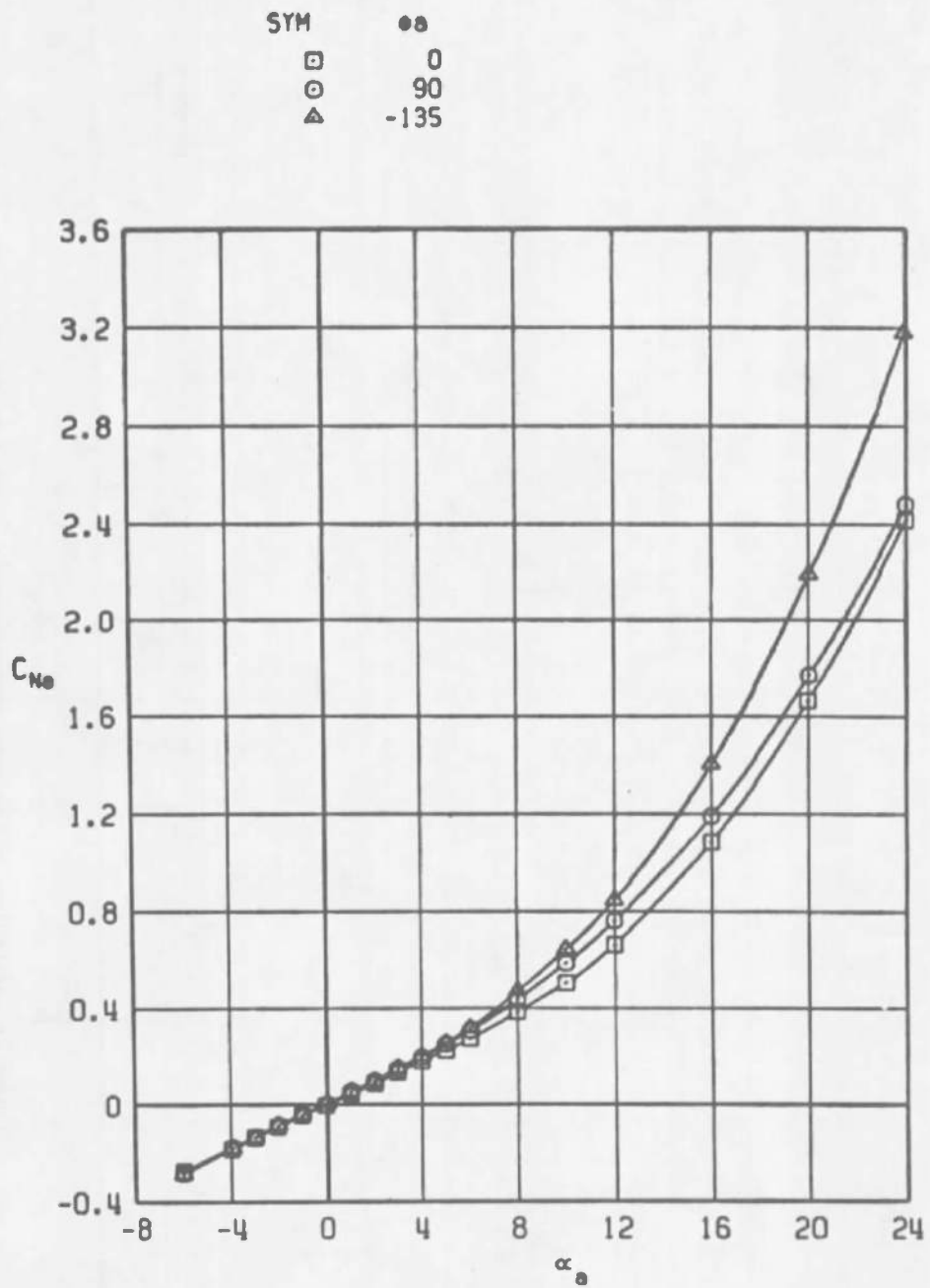
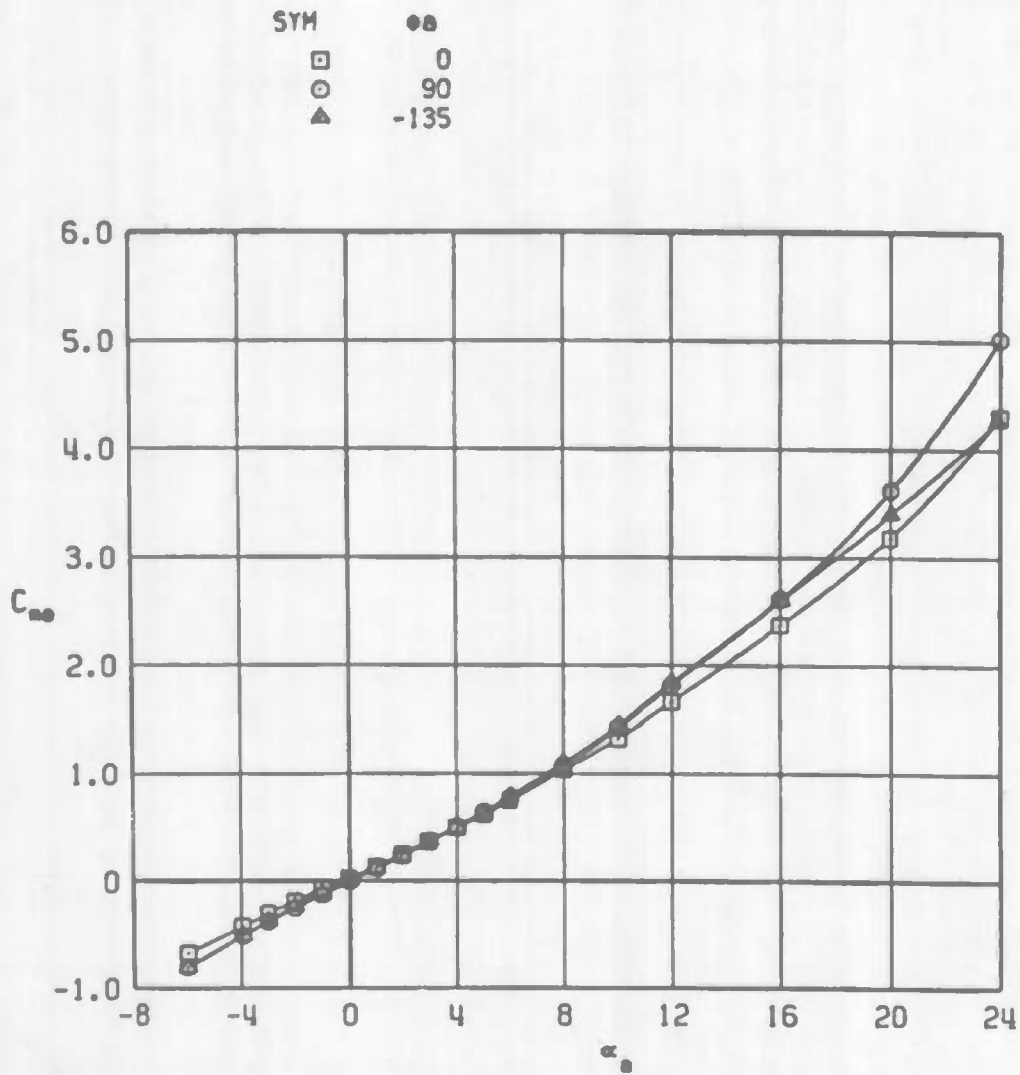


Figure 12. Variation of the nose forebody-axial-force coefficient with angle of attack and Mach number,  $\phi_a = 0$ .

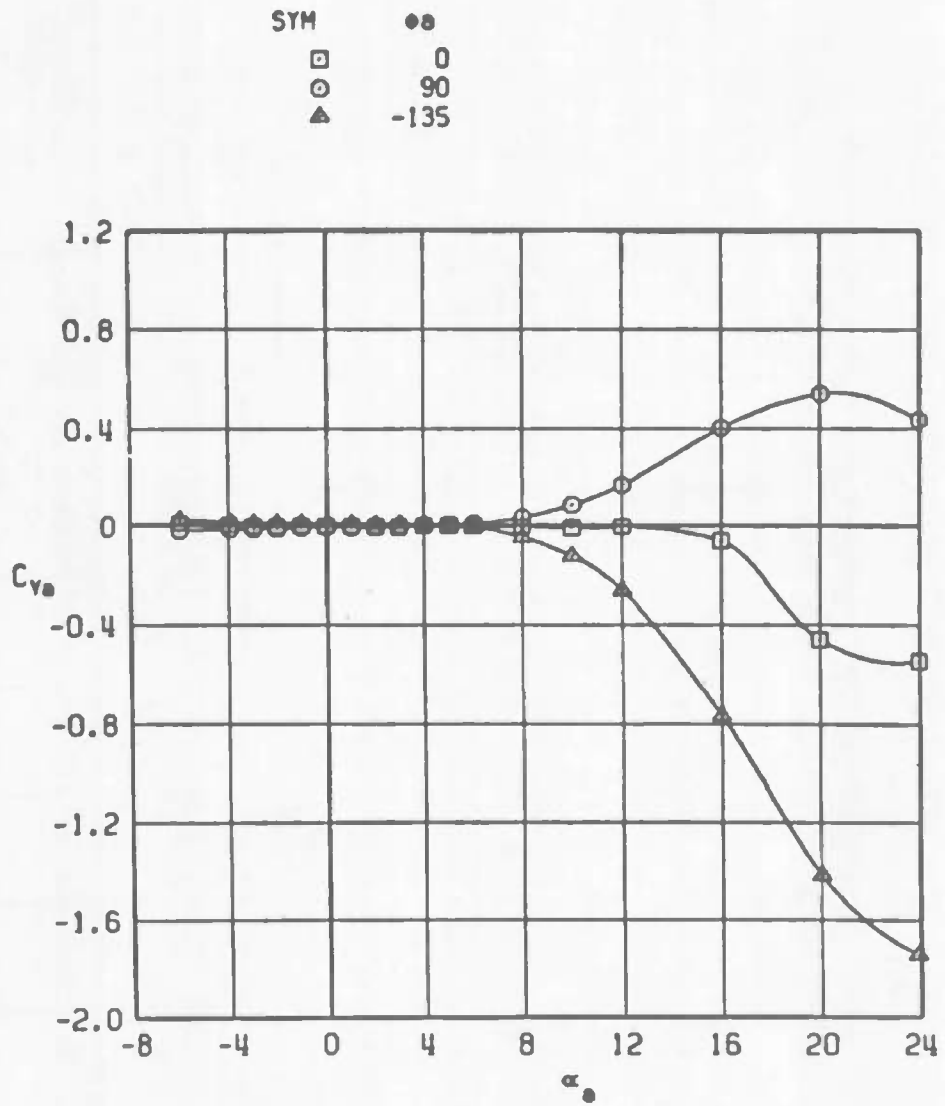


a. Normal-force coefficient

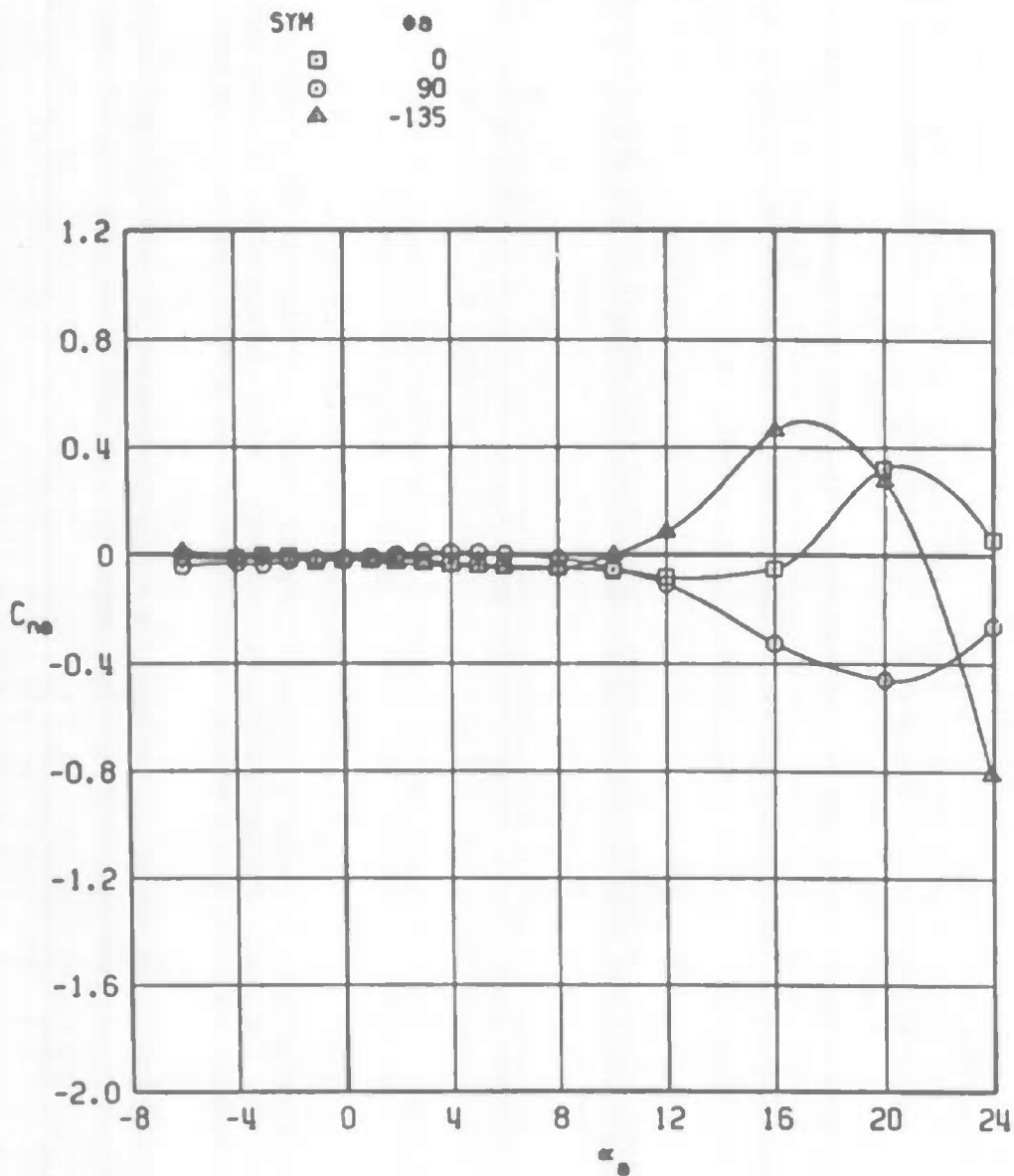
Figure 13. Typical variations of the missile aerodynamic coefficients with angle of attack,  $M_\infty = 1.1$ .



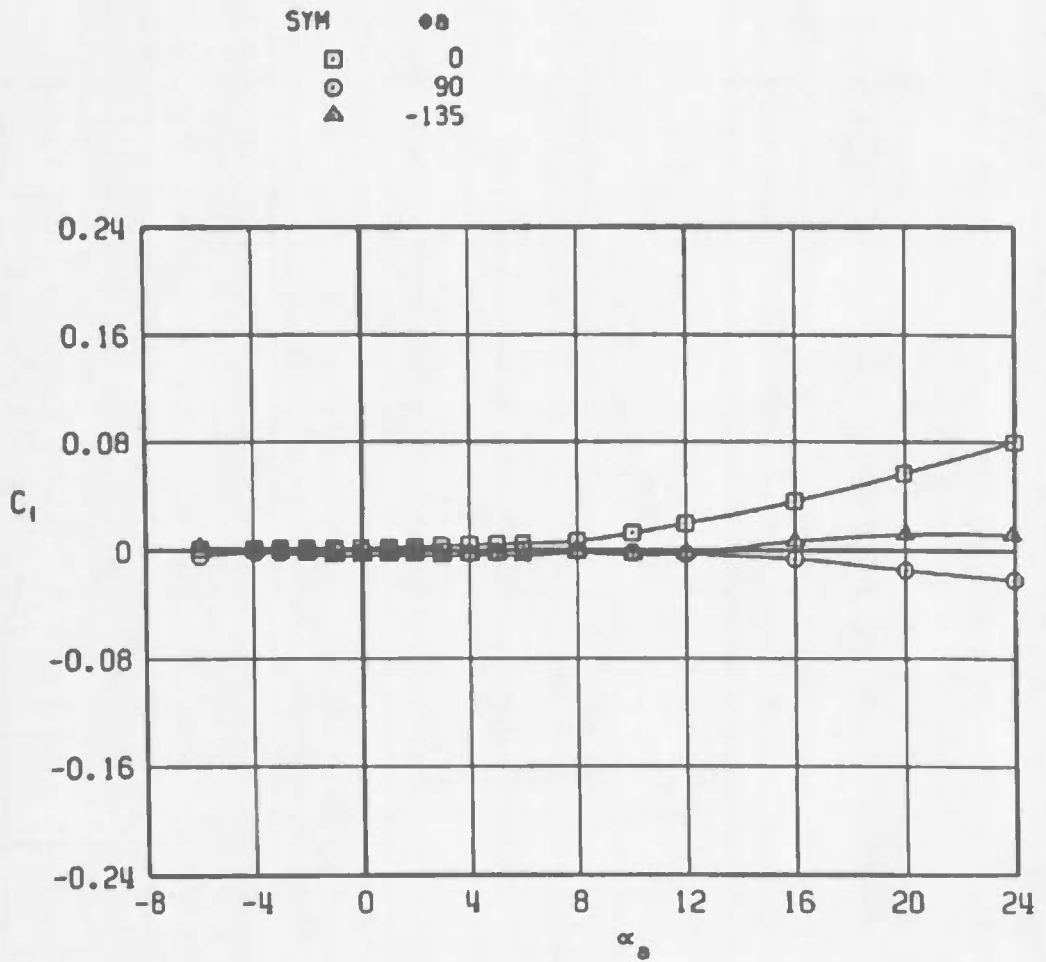
b. Pitching-moment coefficient  
Figure 13. Continued.



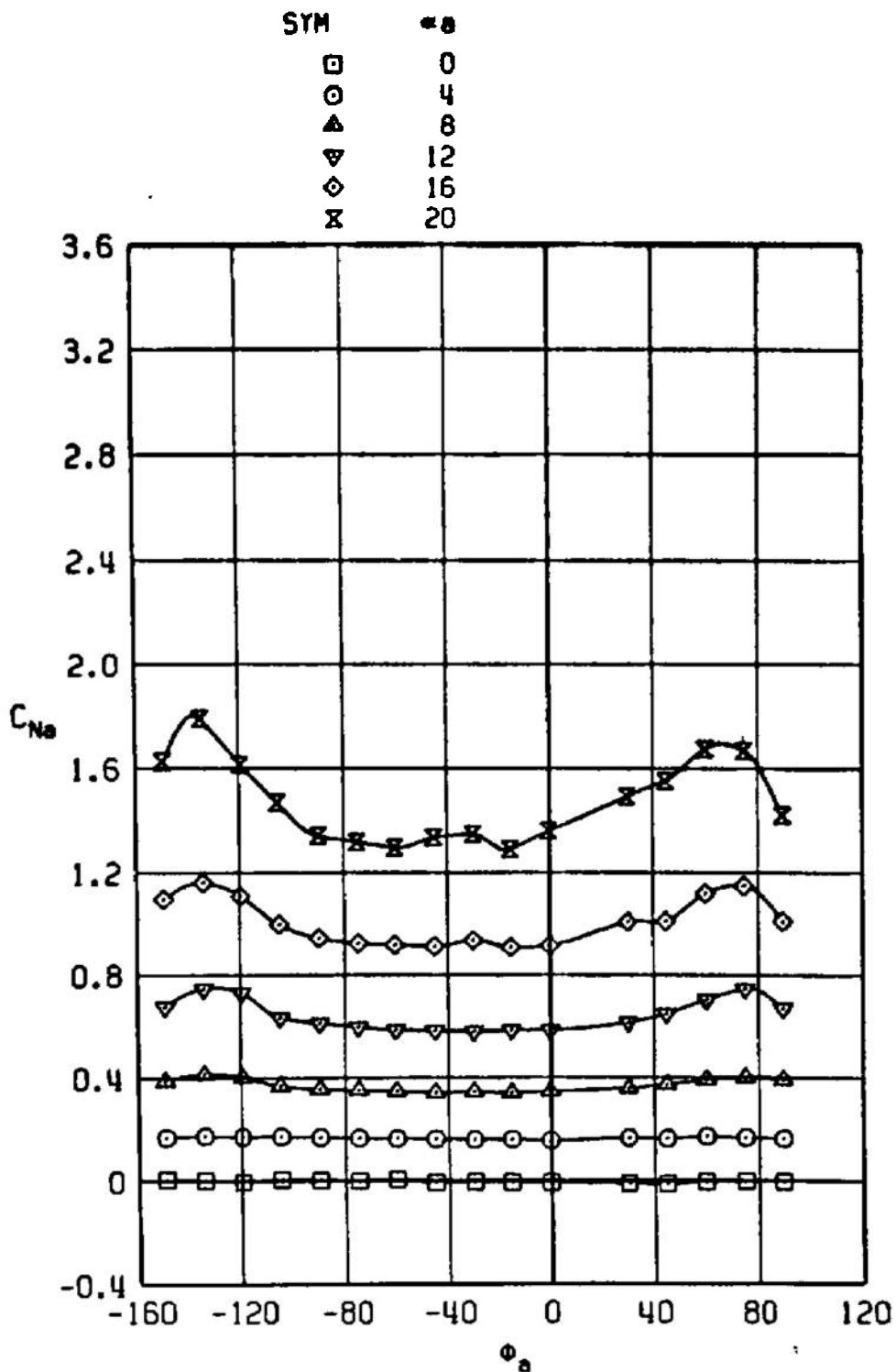
c. Side-force coefficient  
Figure 13. Continued.



d. Yawing-moment coefficient  
Figure 13. Continued.

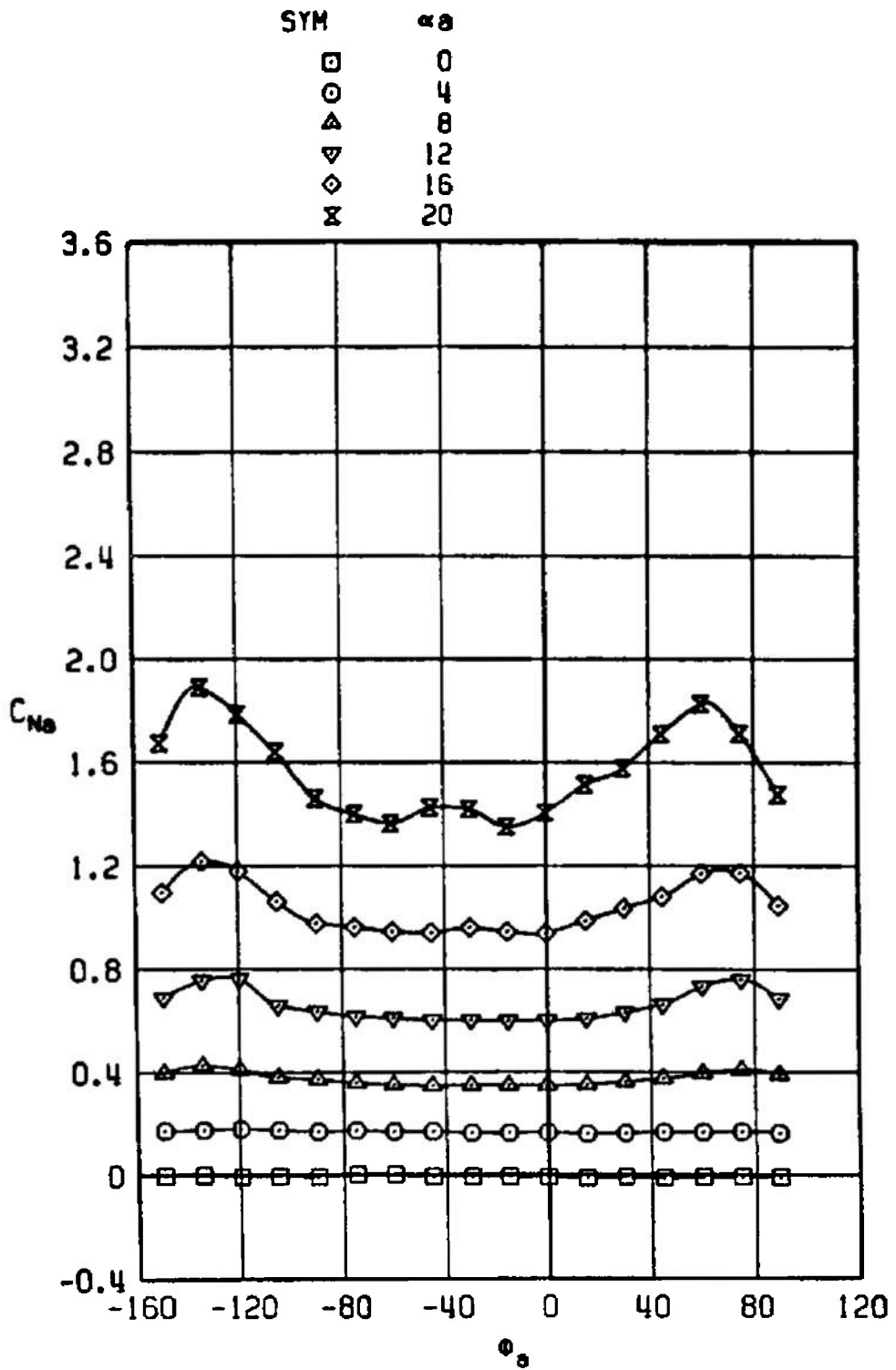


e. Rolling-moment coefficient  
Figure 13. Concluded.



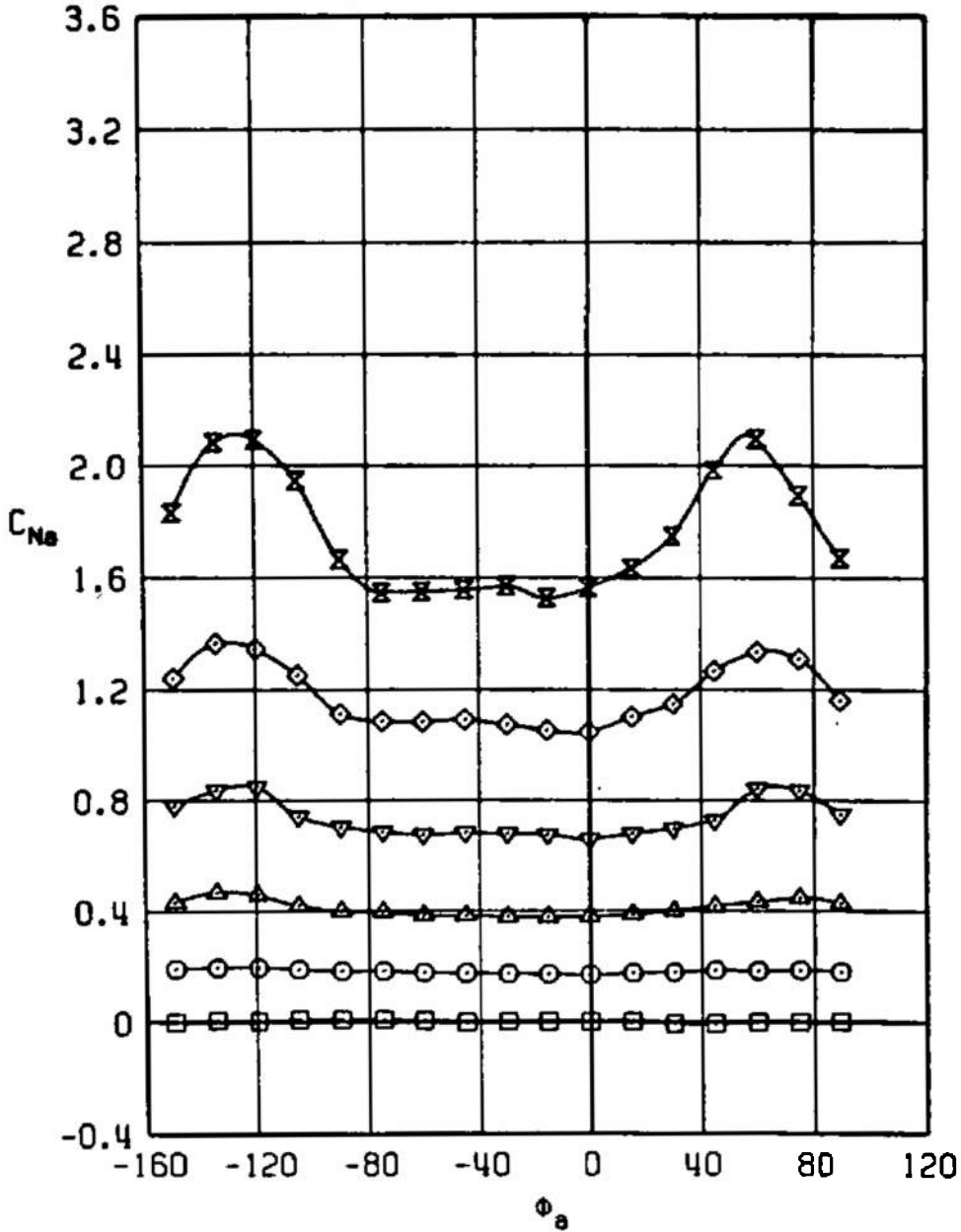
a.  $M_\infty = 0.50$

Figure 14. Variation of the missile normal-force coefficient with model roll angle.

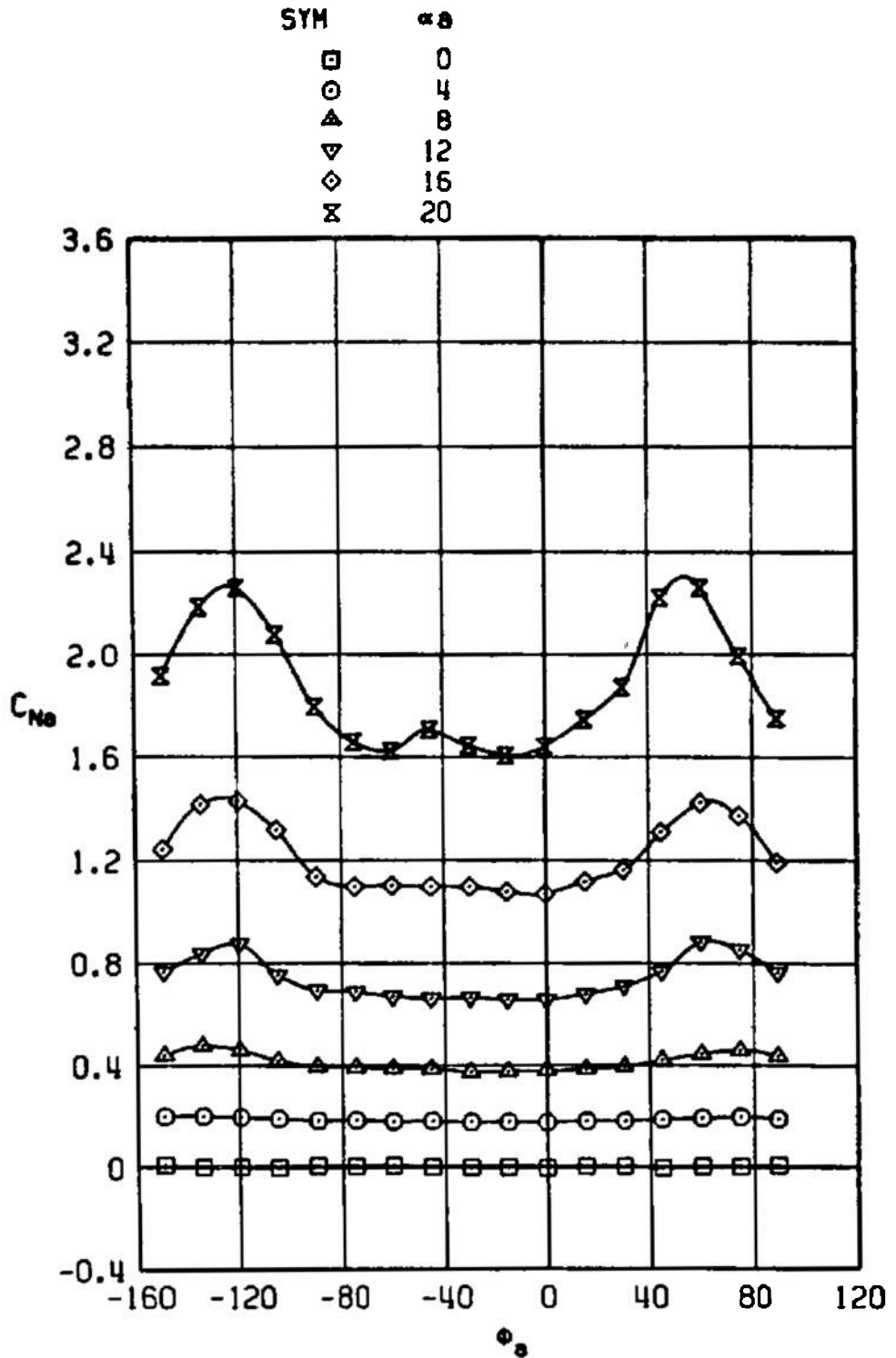


b.  $M_\infty = 0.80$   
 Figure 14. Continued.

SYM	$\alpha$
□	0
○	4
△	8
▽	12
◇	16
×	20



c.  $M_\infty = 0.95$   
 Figure 14. Continued.



d.  $M_\infty = 1.10$   
Figure 14. Concluded.

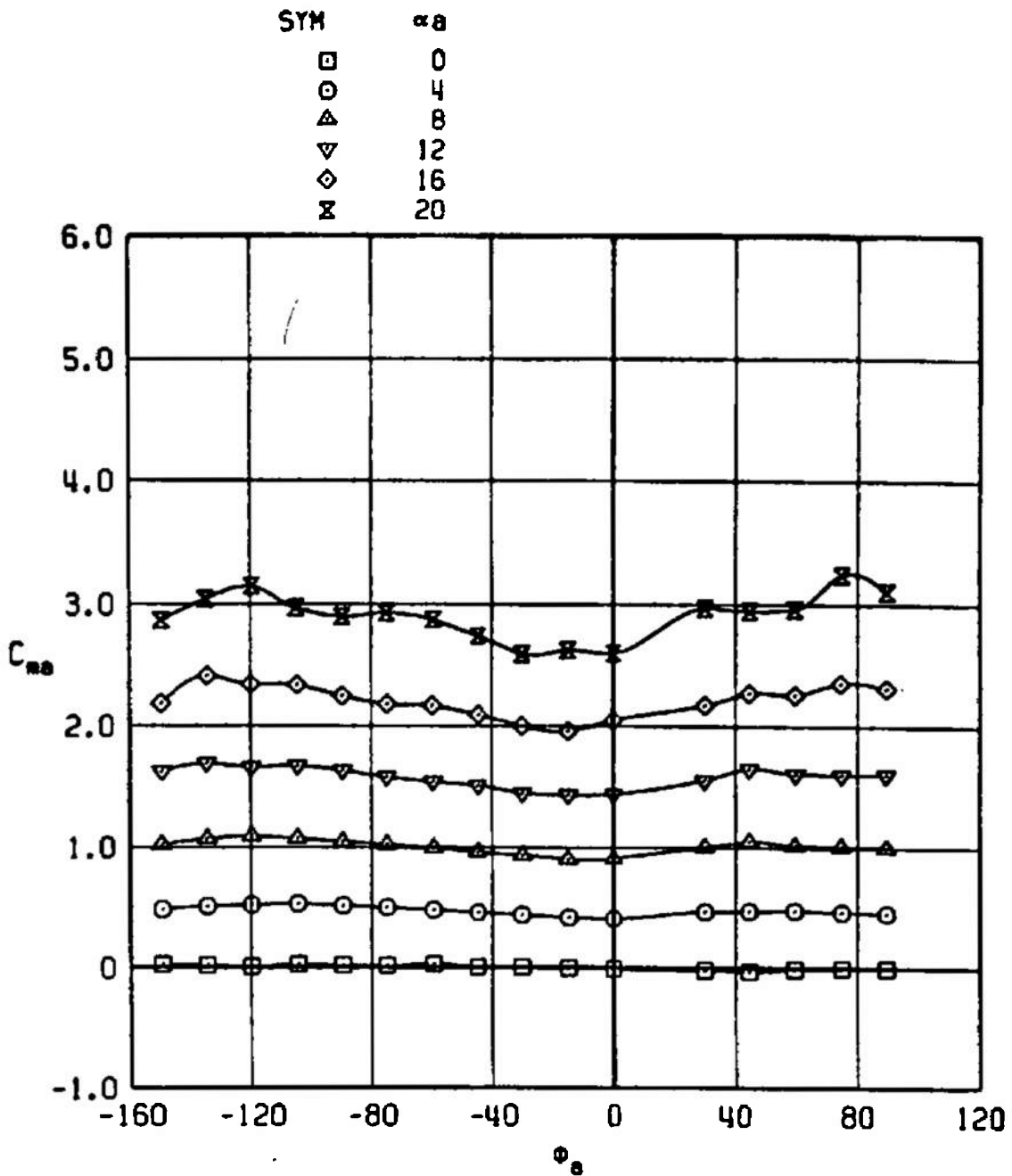
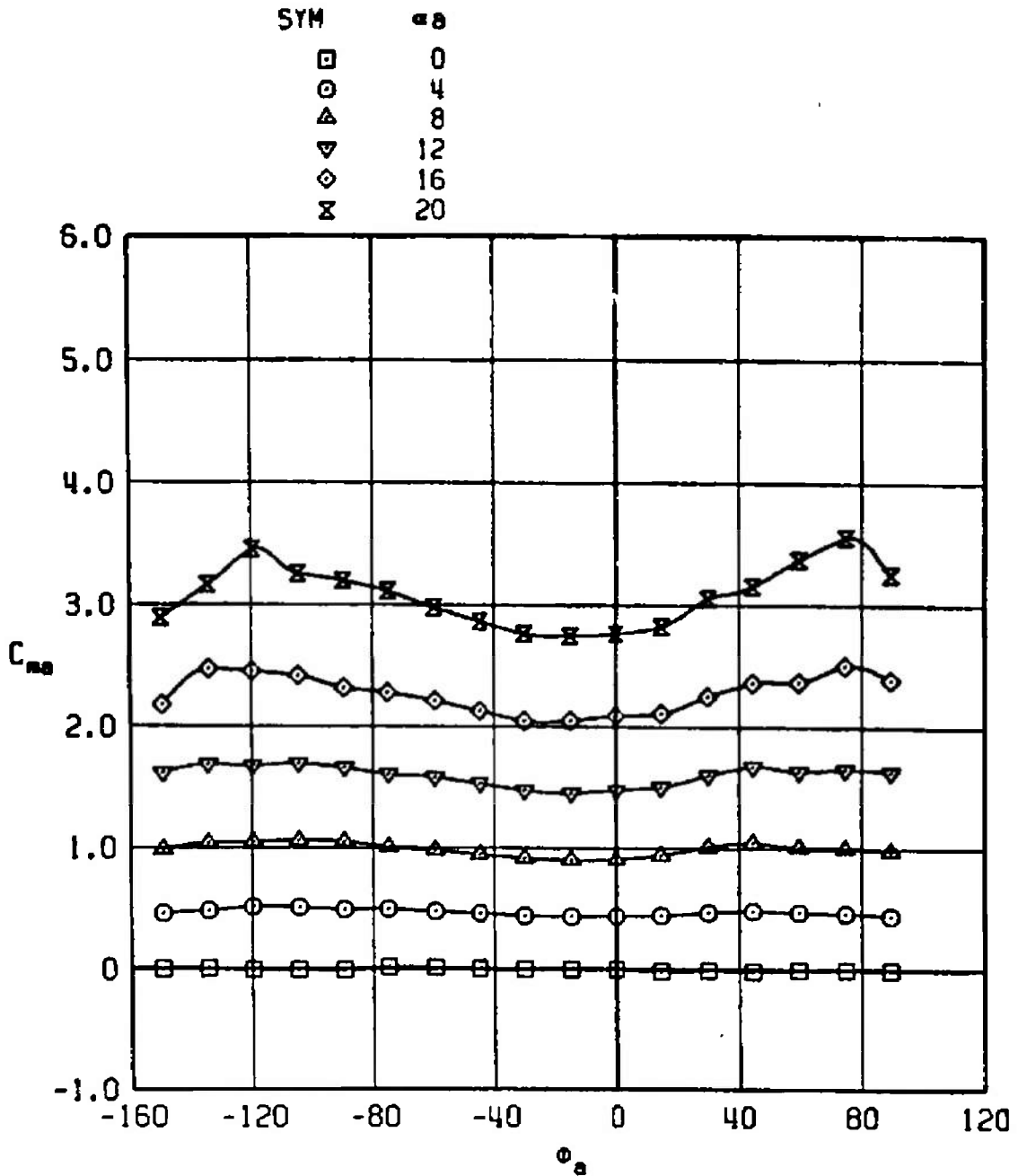
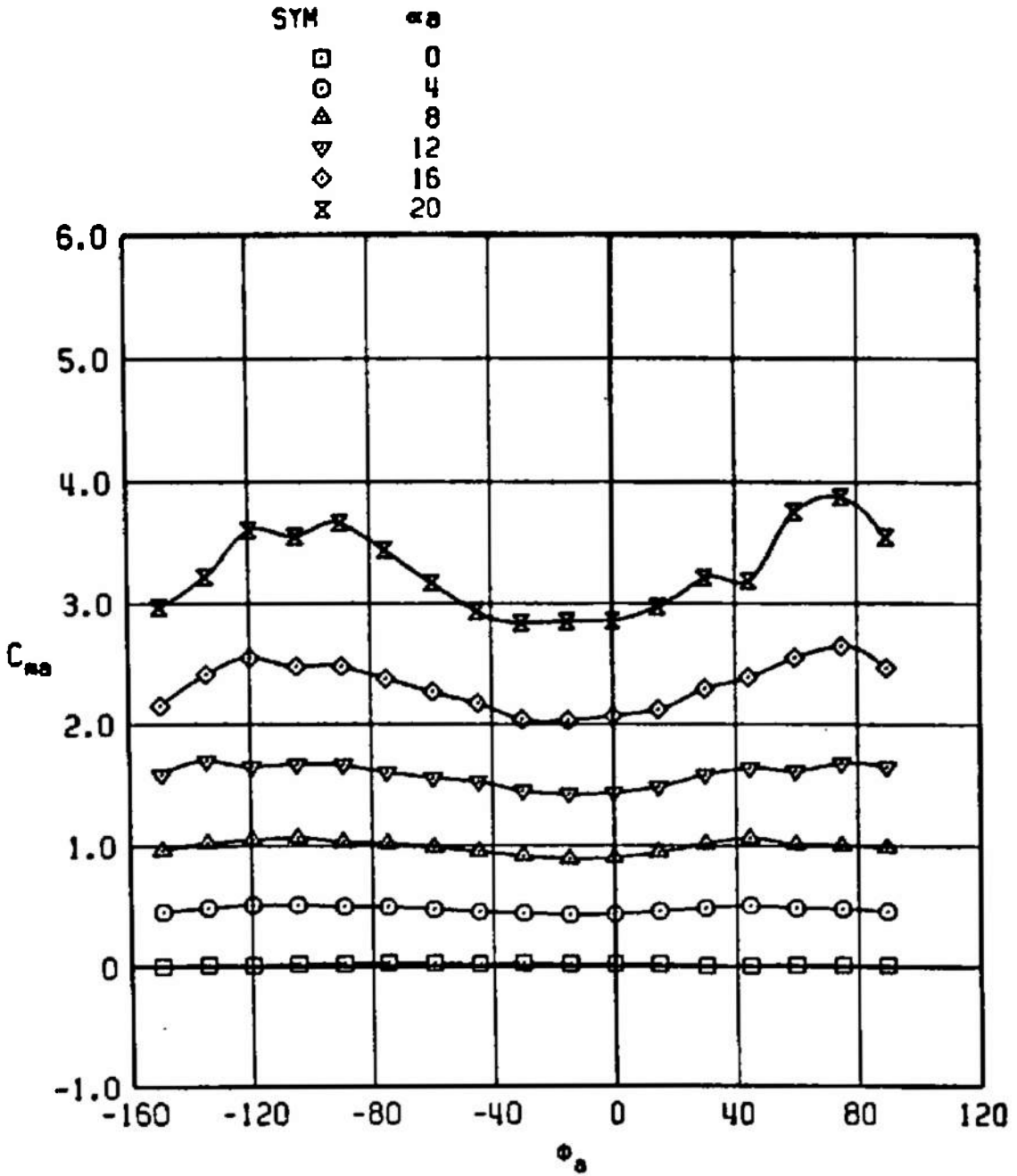


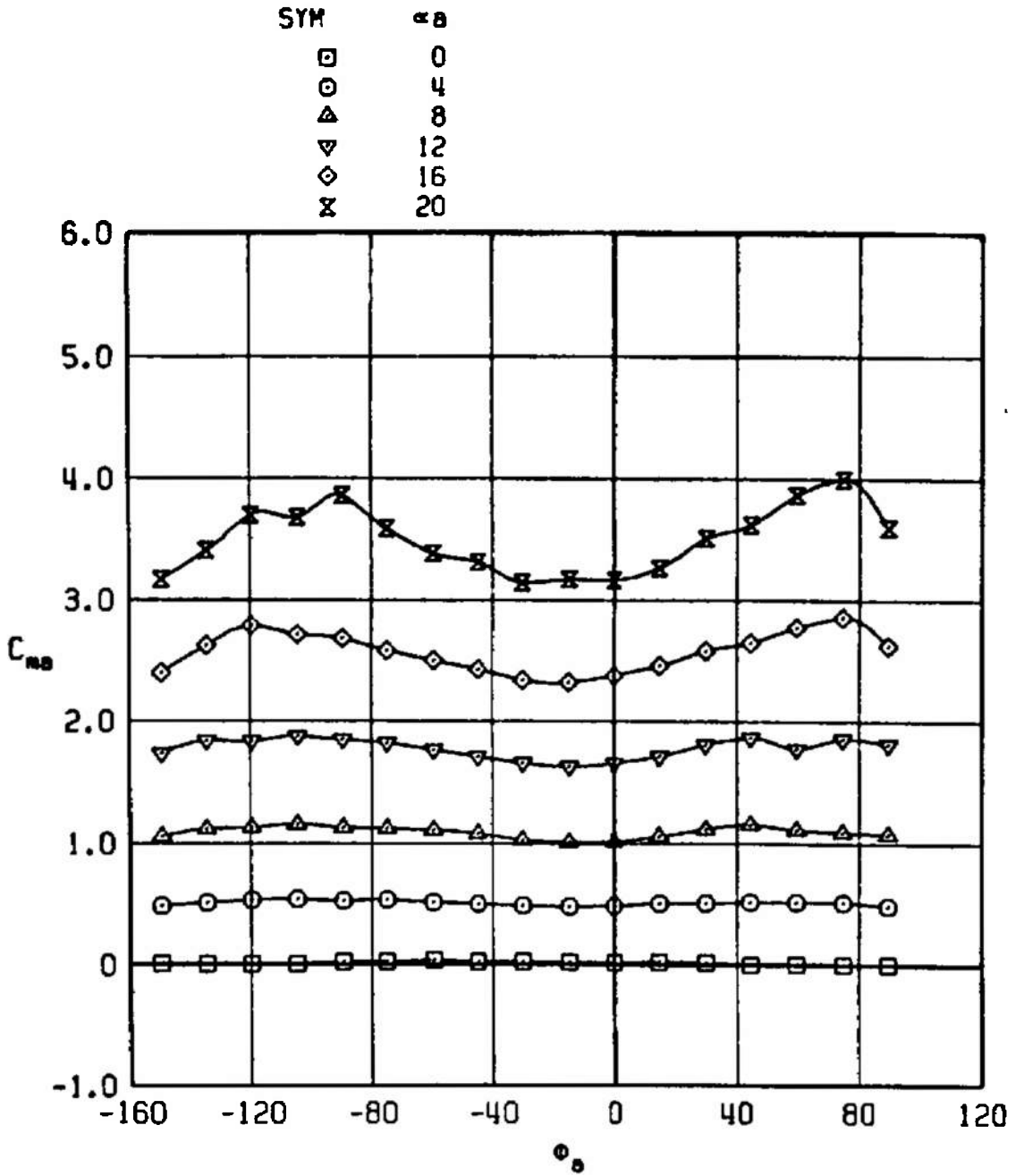
Figure 15. Variation of the missile pitching-moment coefficient with model roll angle.



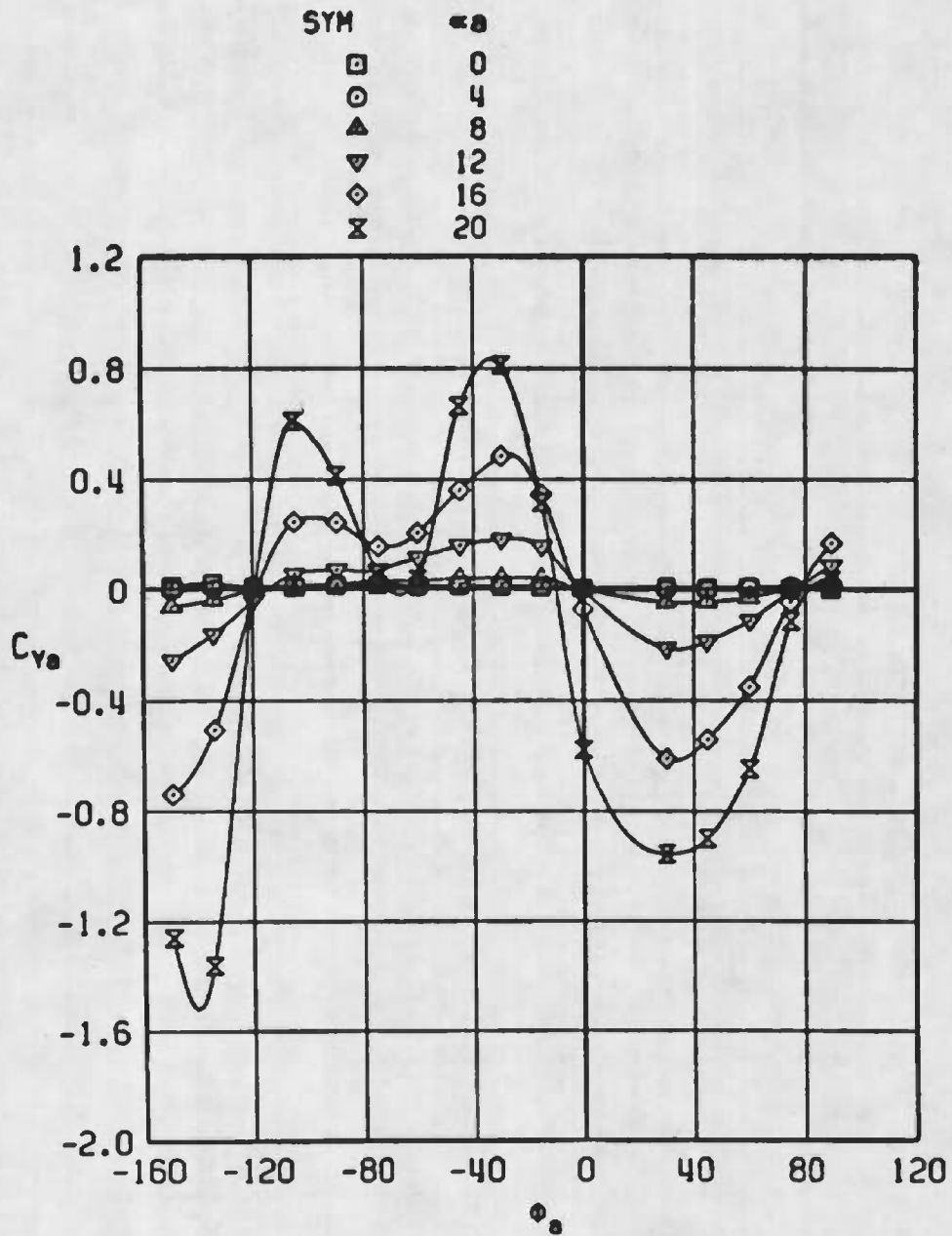
b.  $M_\infty = 0.80$   
 Figure 15. Continued.



c.  $M_\infty = 0.95$   
 .Figure 15. Continued.

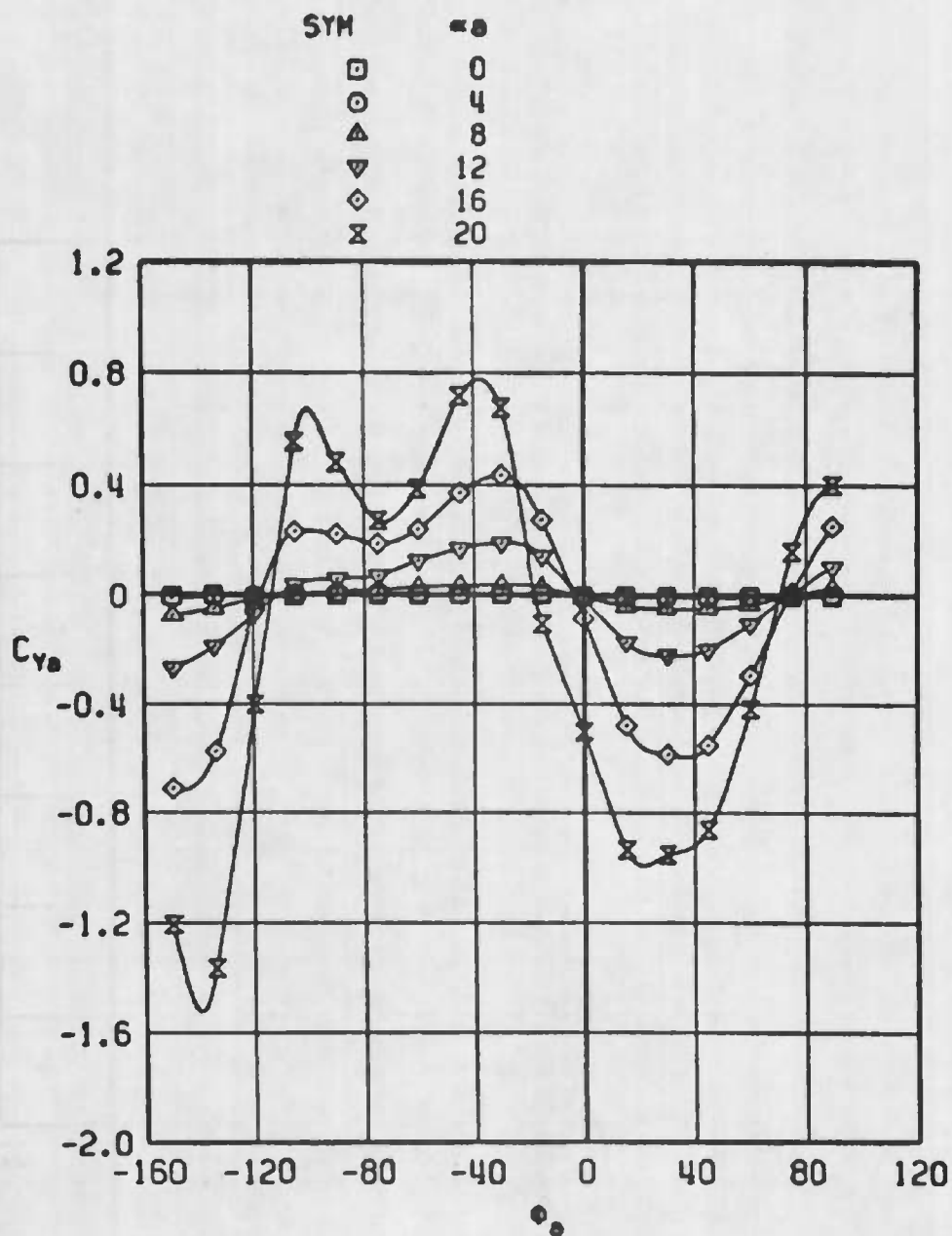


d.  $M_\infty = 1.10$   
 Figure 15. Concluded.

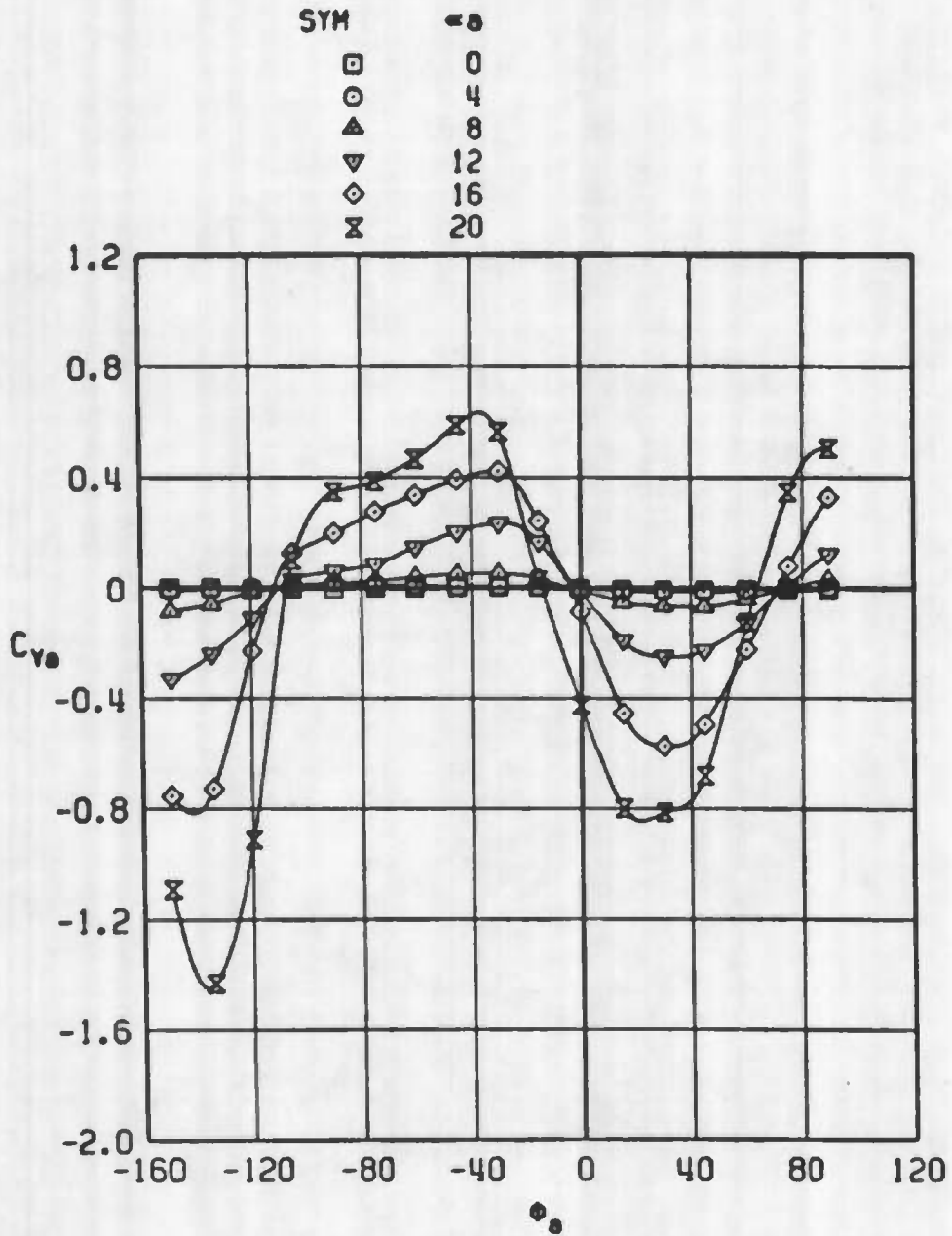


a.  $M_\infty = 0.50$

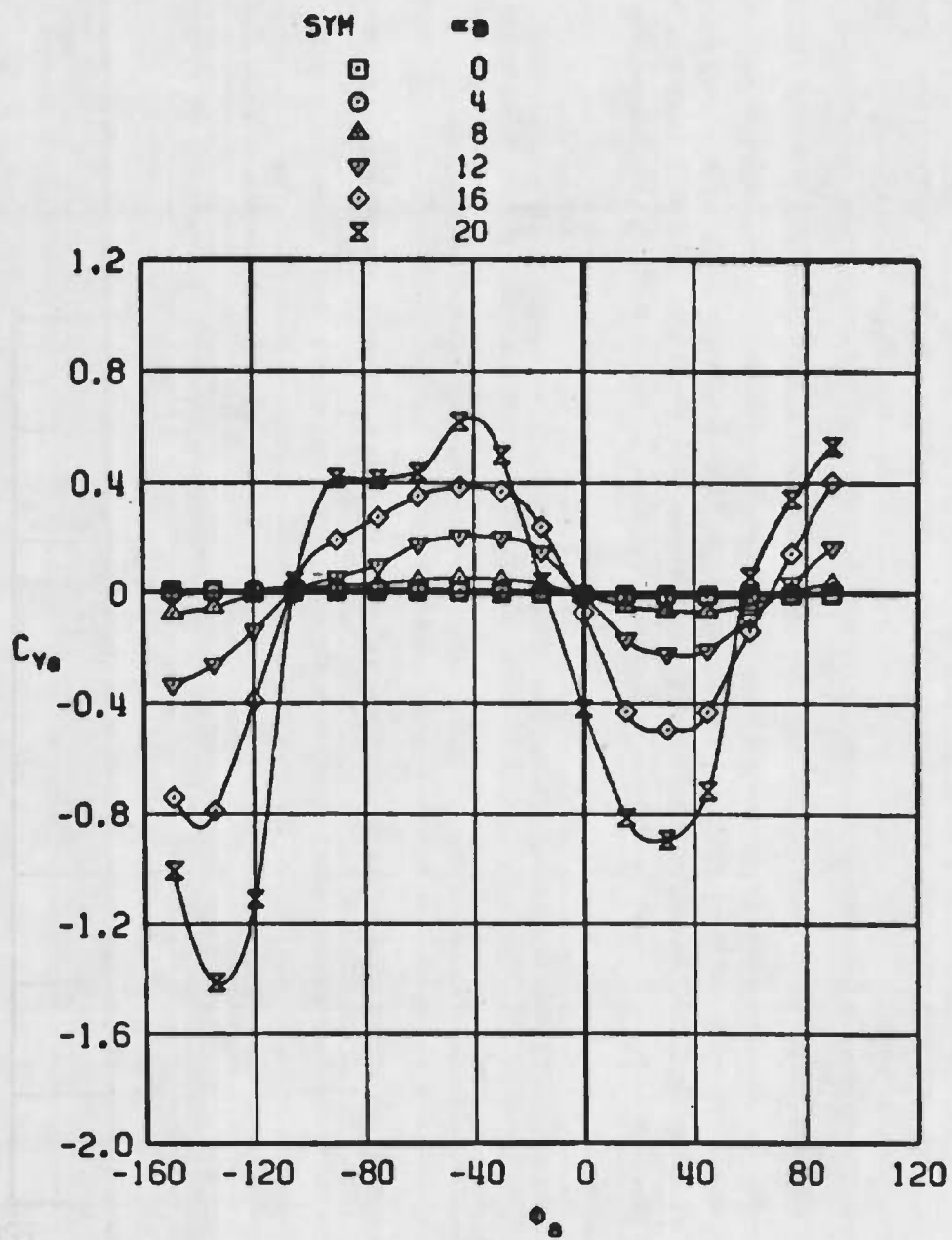
Figure 16. Variation of the missile side-force coefficient with model roll angle.



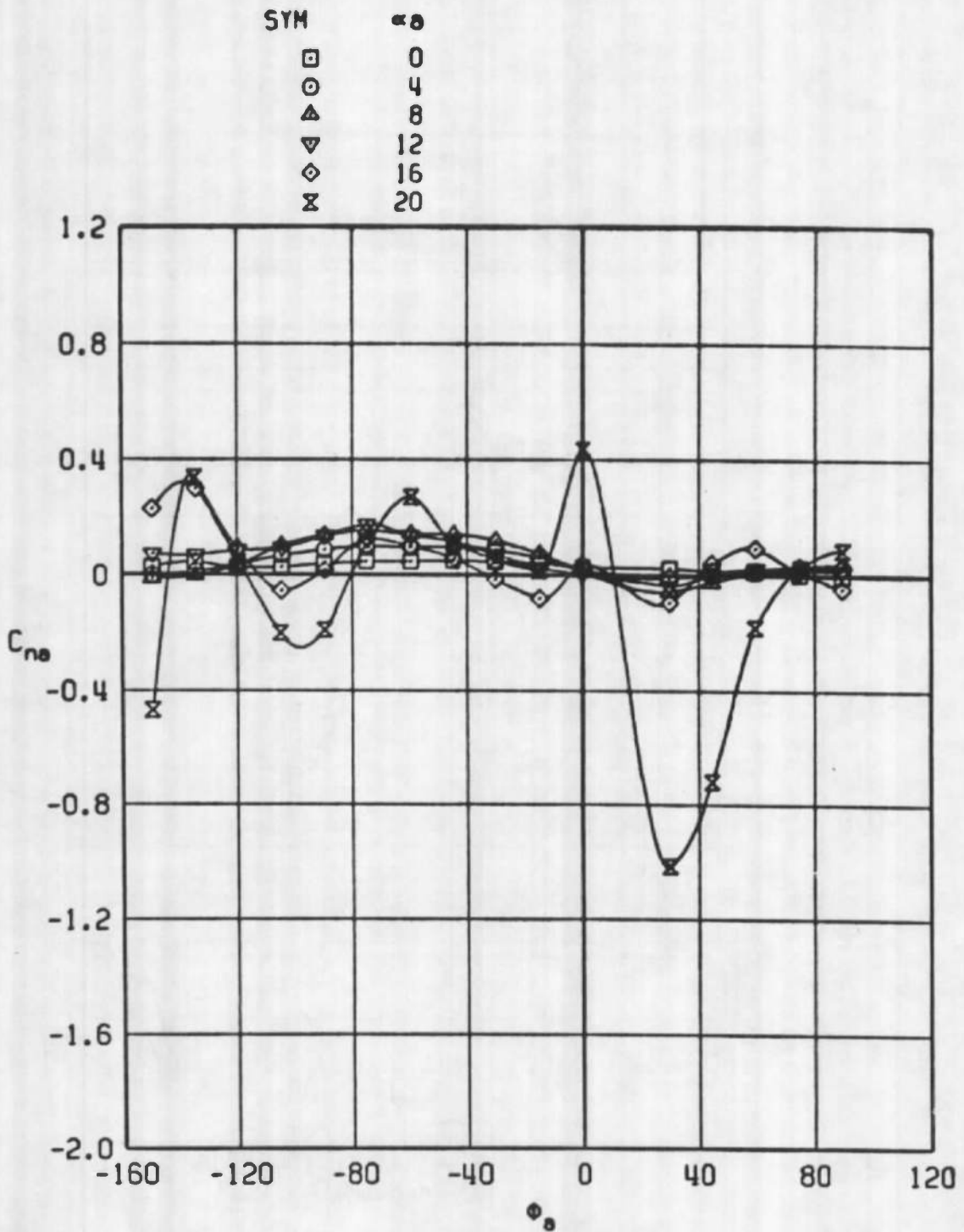
b.  $M_\infty = 0.80$   
 Figure 16. Continued.



c.  $M_\infty = 0.95$   
 Figure 16. Continued.

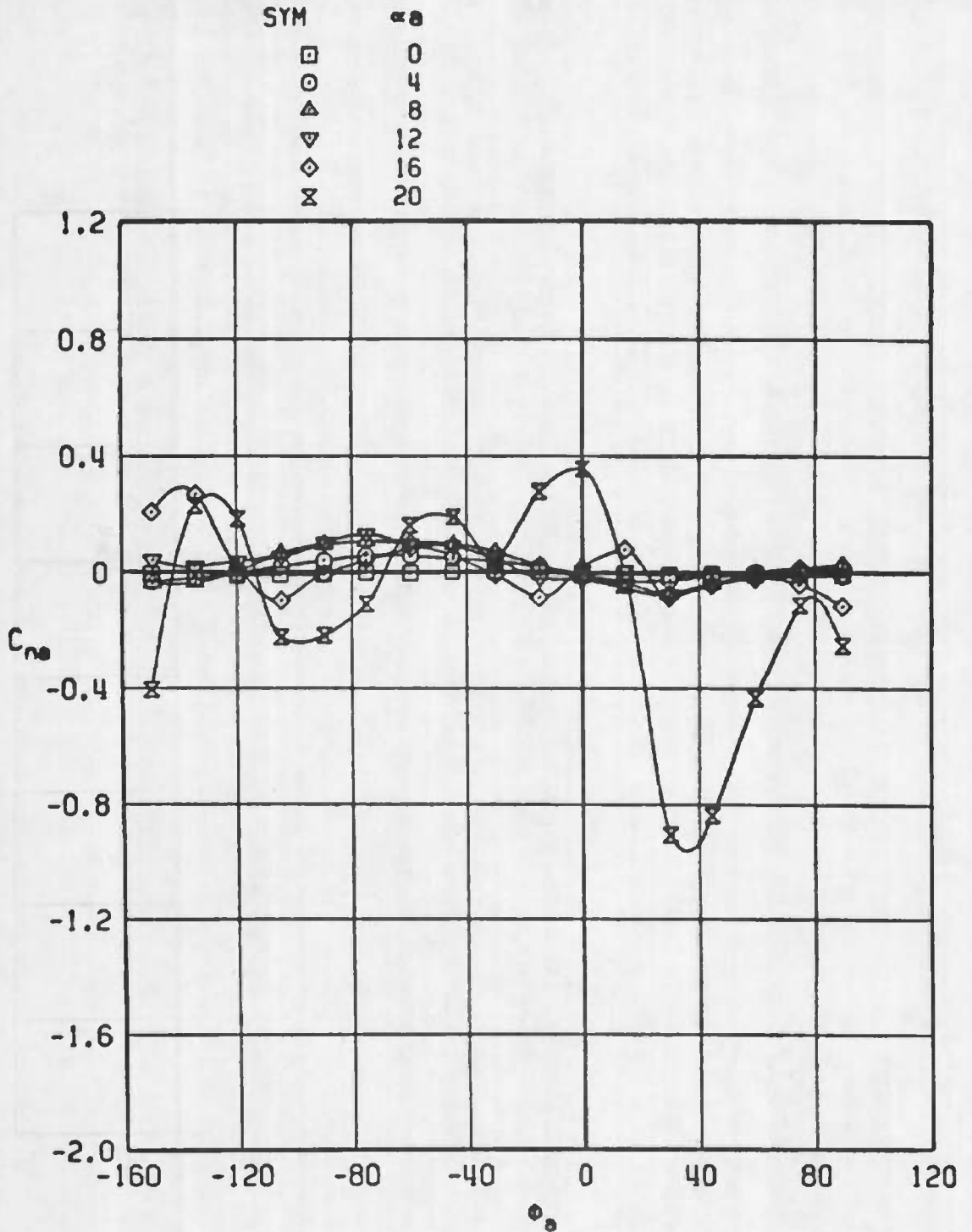


d.  $M_\infty = 1.10$   
 Figure 16. Concluded.

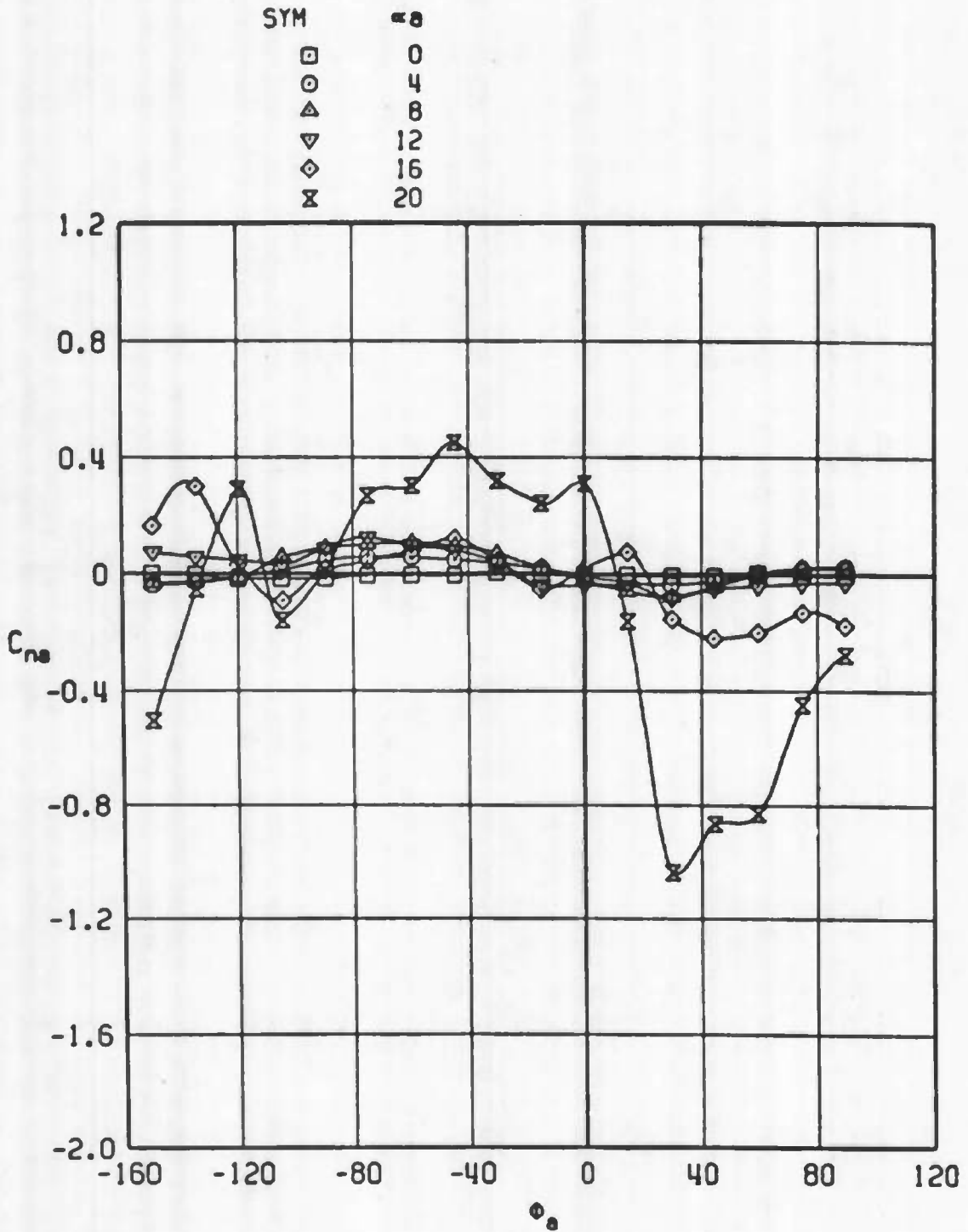


a.  $M_\infty = 0.50$

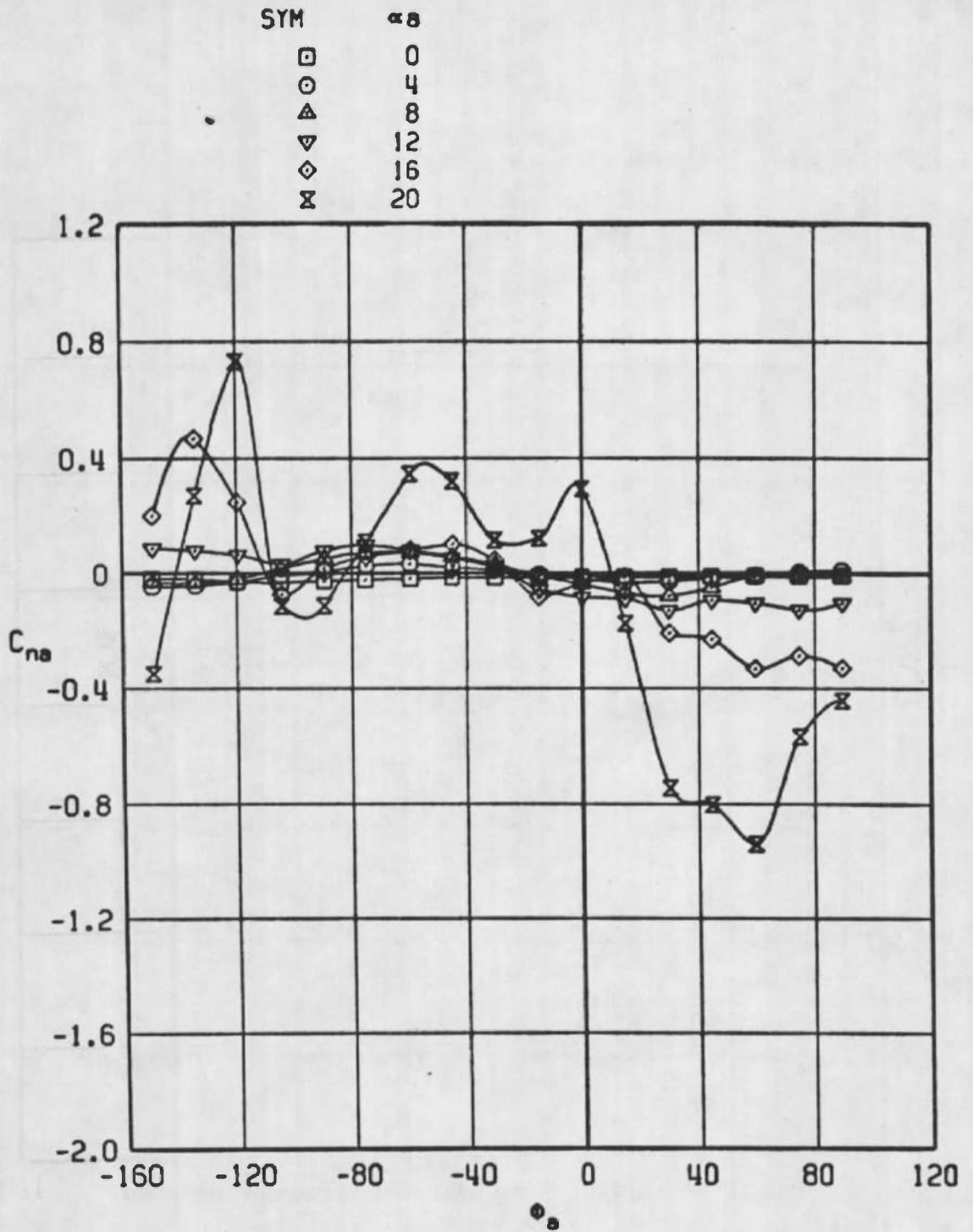
Figure 17. Variation of the missile yawing-moment coefficient with model roll angle.



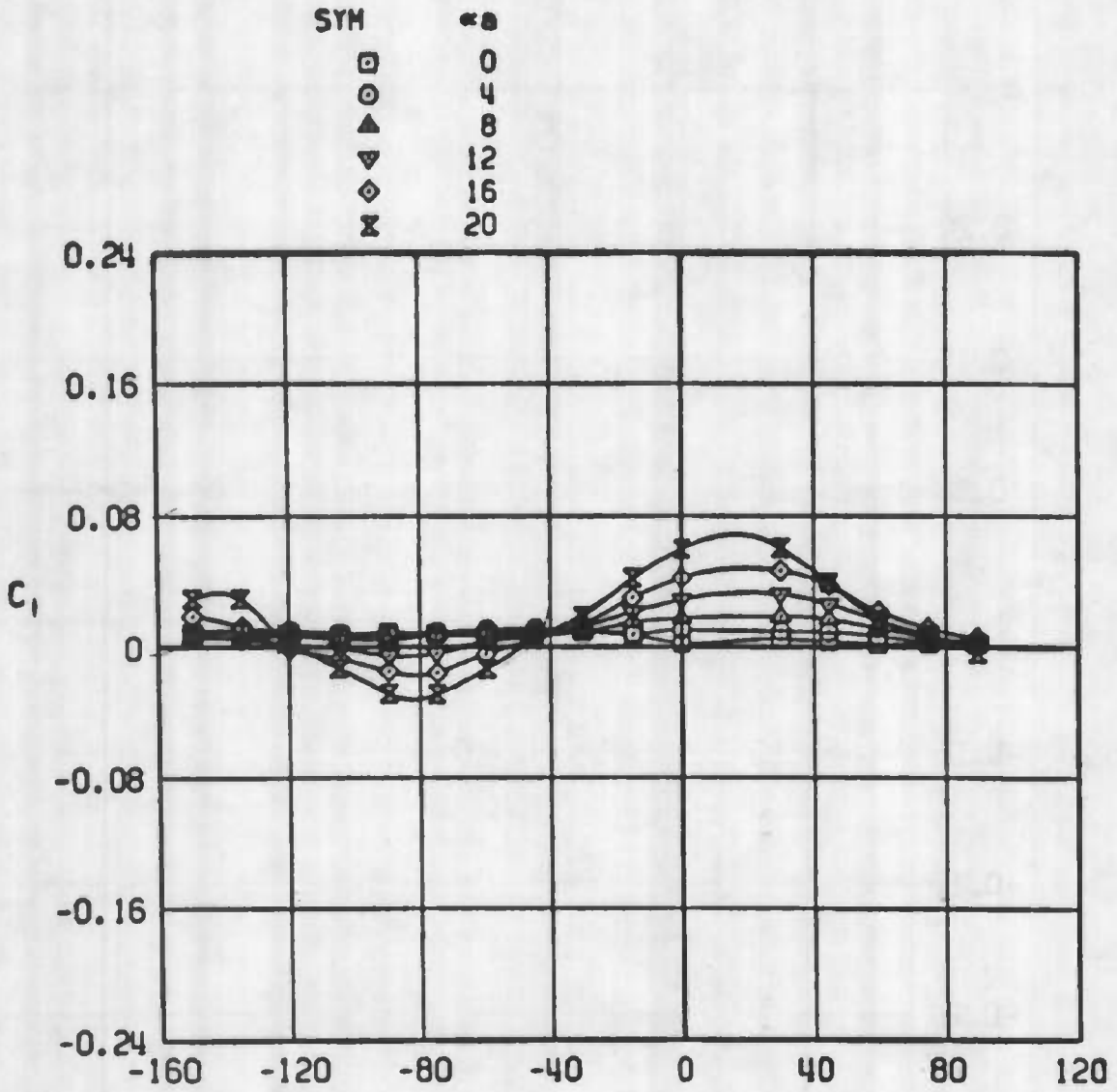
b.  $M_\infty = 0.80$   
 Figure 17. Continued.



c.  $M_\infty = 0.95$   
 Figure 17. Continued.

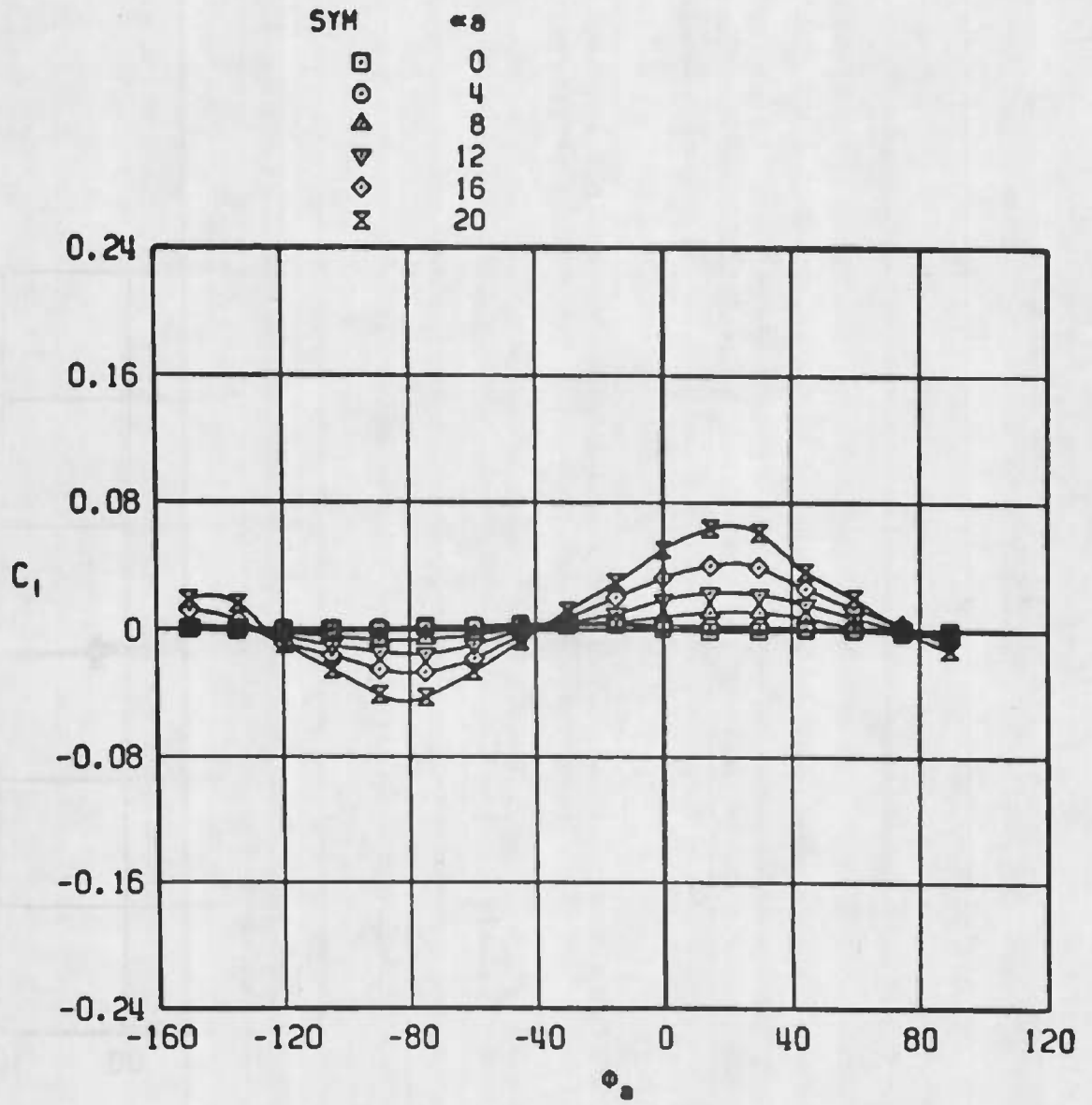


d.  $M_\infty = 1.10$   
 Figure 17. Concluded.

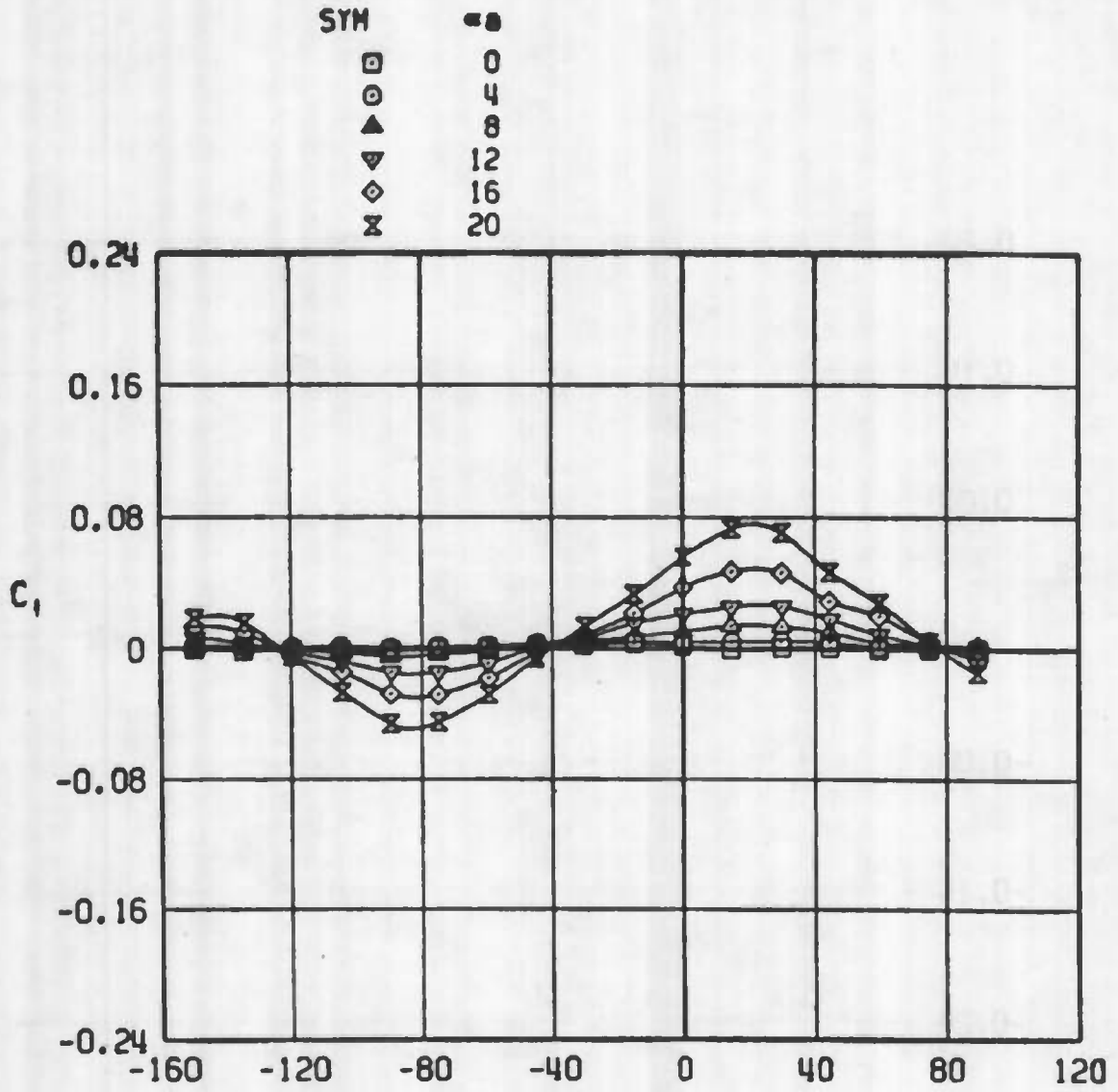


a.  $M_\infty = 0.50$

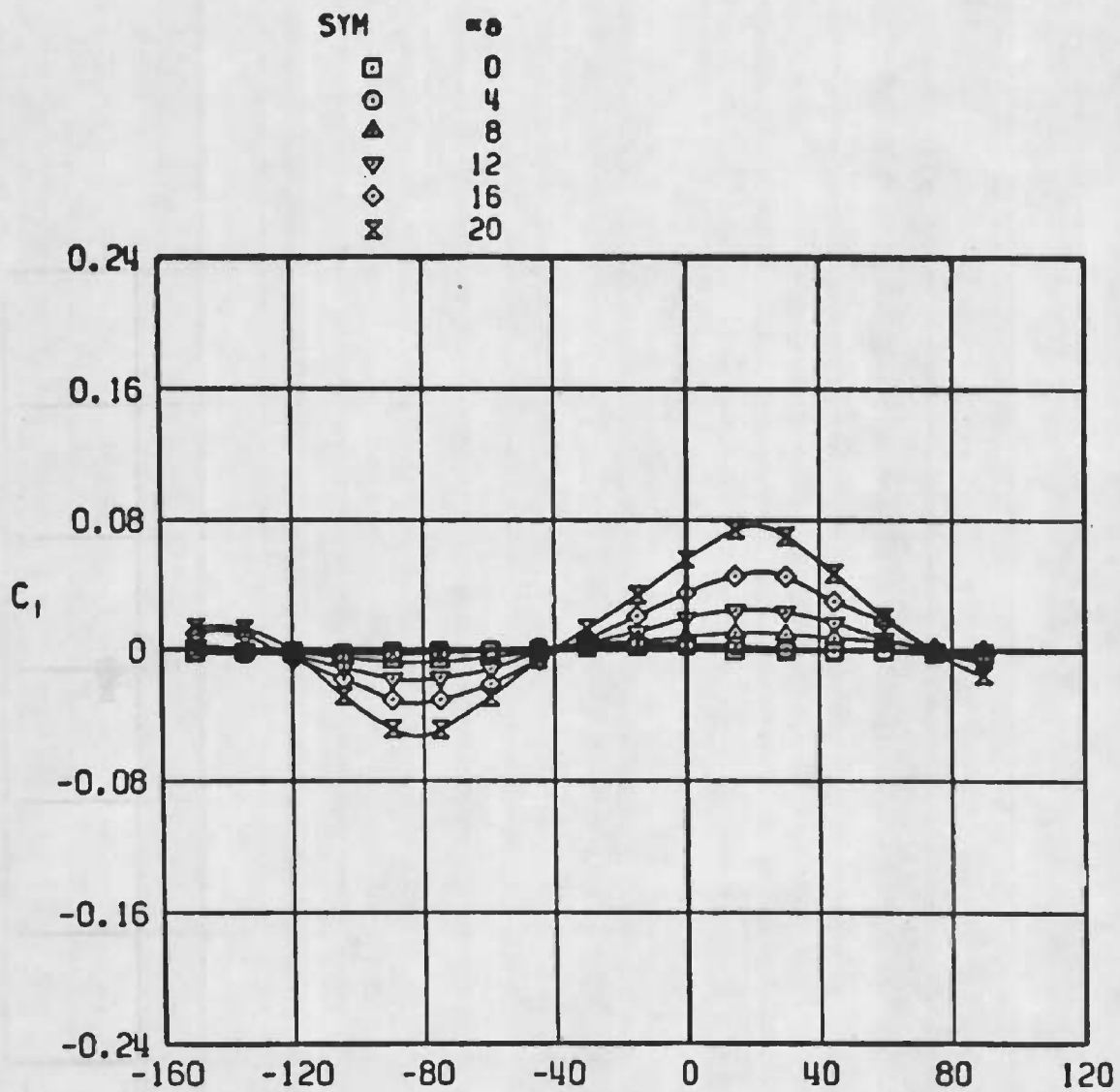
Figure 18. Variation of the missile rolling-moment coefficient with model roll angle.



b.  $M_\infty = 0.80$   
 Figure 18. Continued.



c.  $M_\infty = 0.95$   
 Figure 18. Continued.



d.  $M_\infty = 1.10$   
 Figure 18. Concluded.

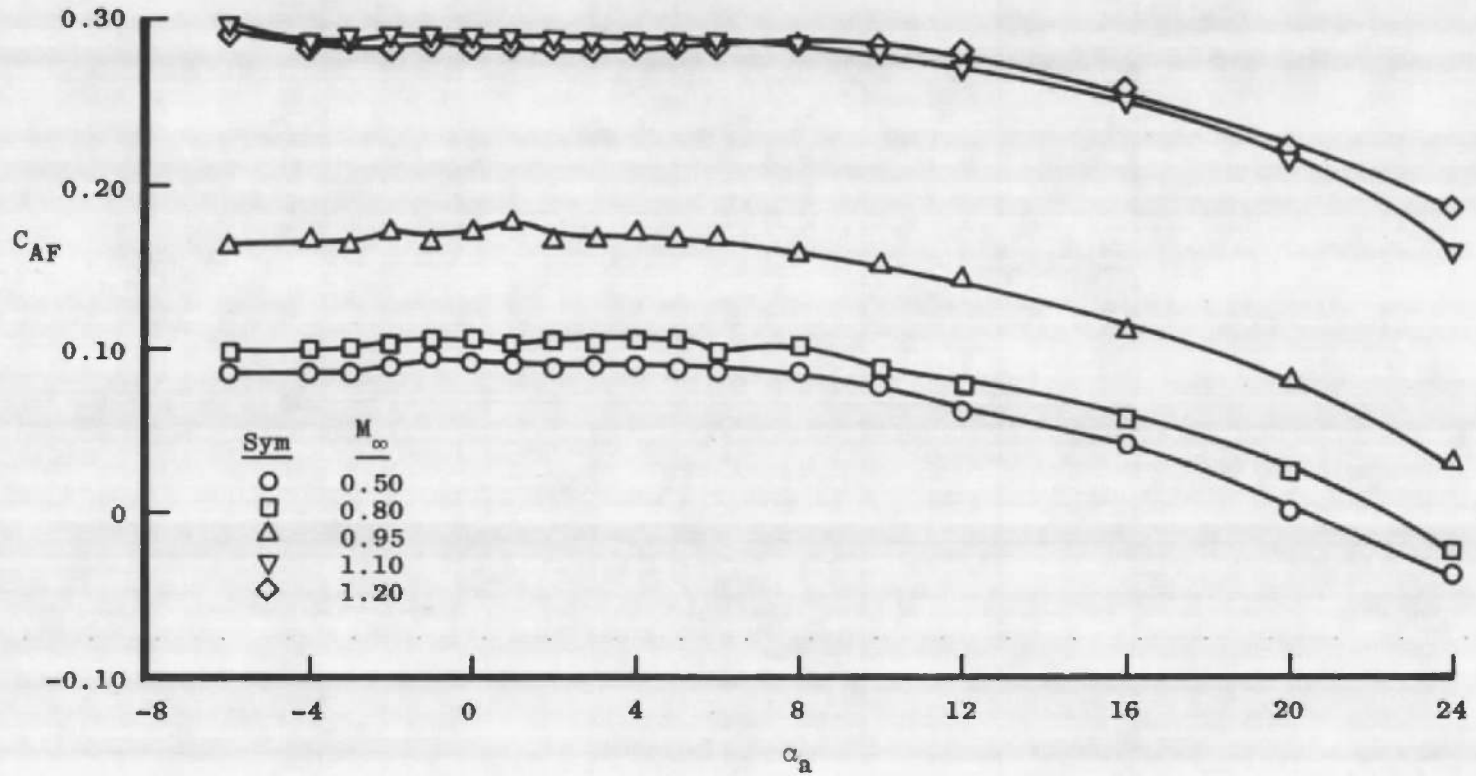


Figure 19. Variation of the missile forebody-axial-force coefficient with angle of attack and Mach number,  $\phi_a = 0$ .

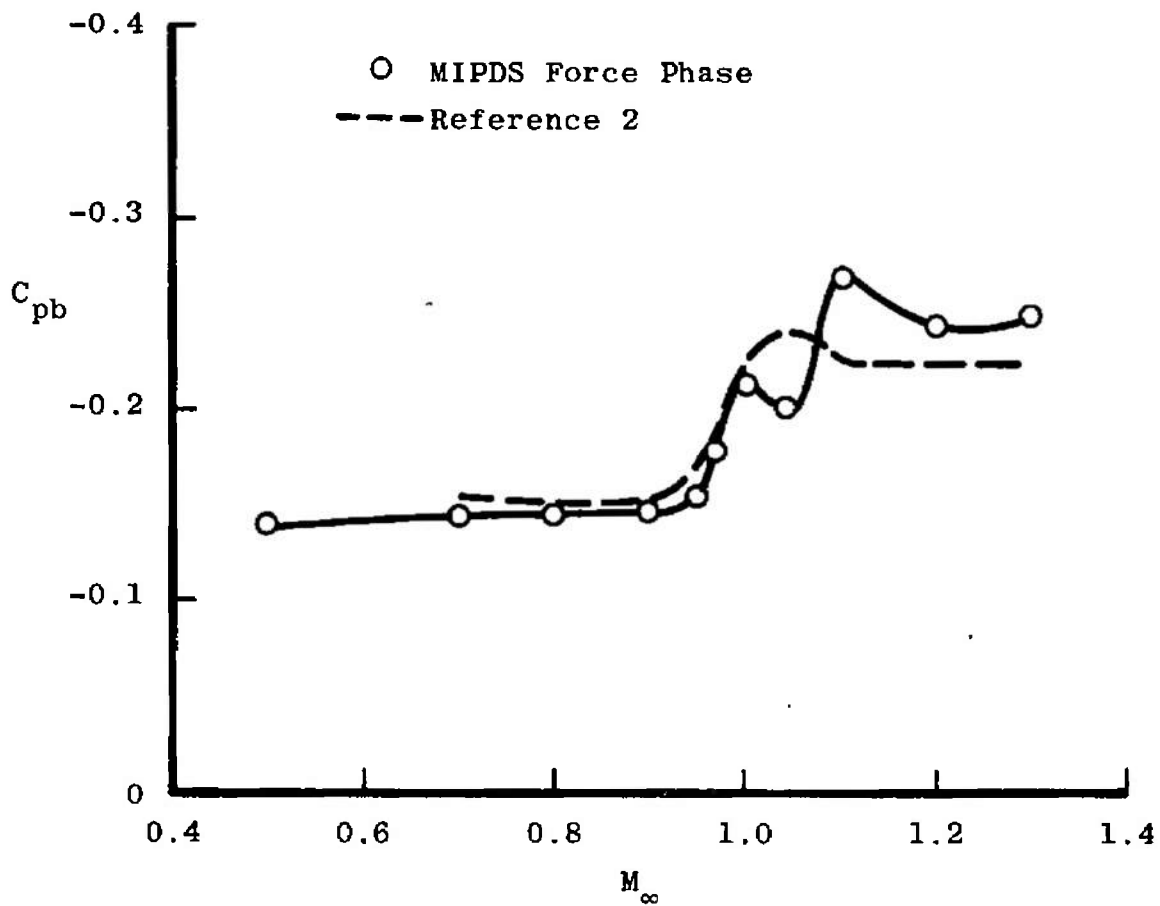
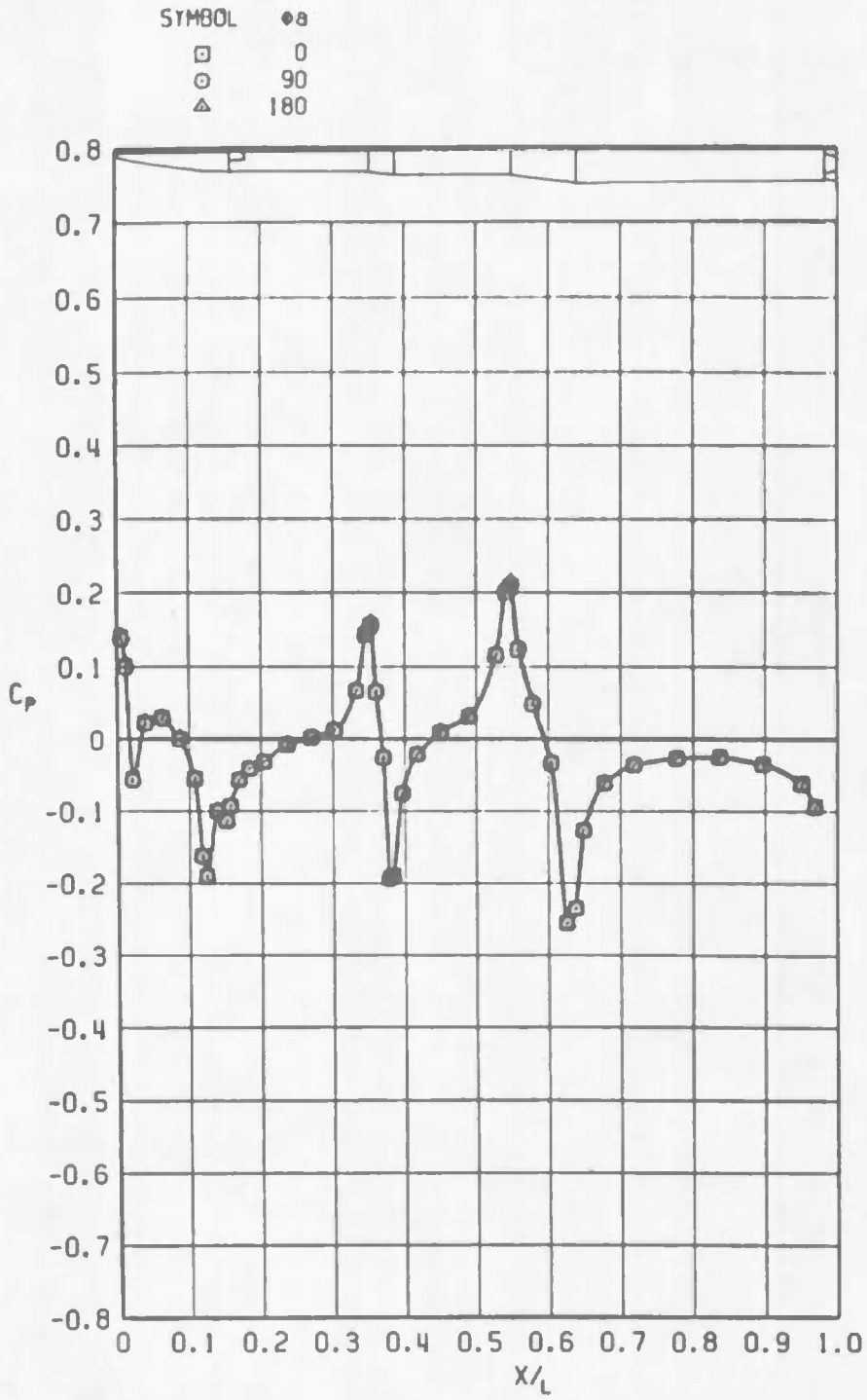
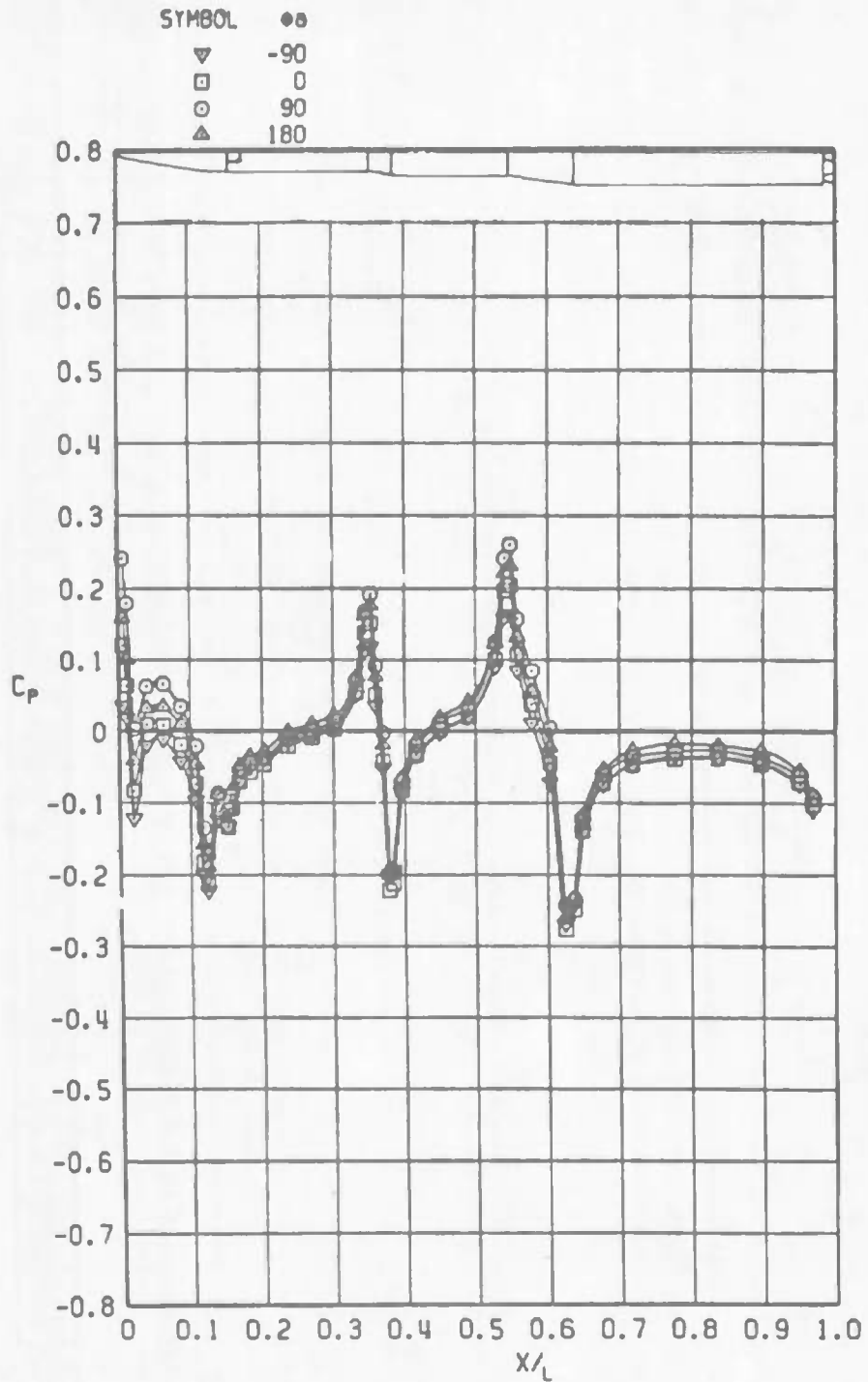


Figure 20. Comparison of free-flight and test model base pressure coefficients.

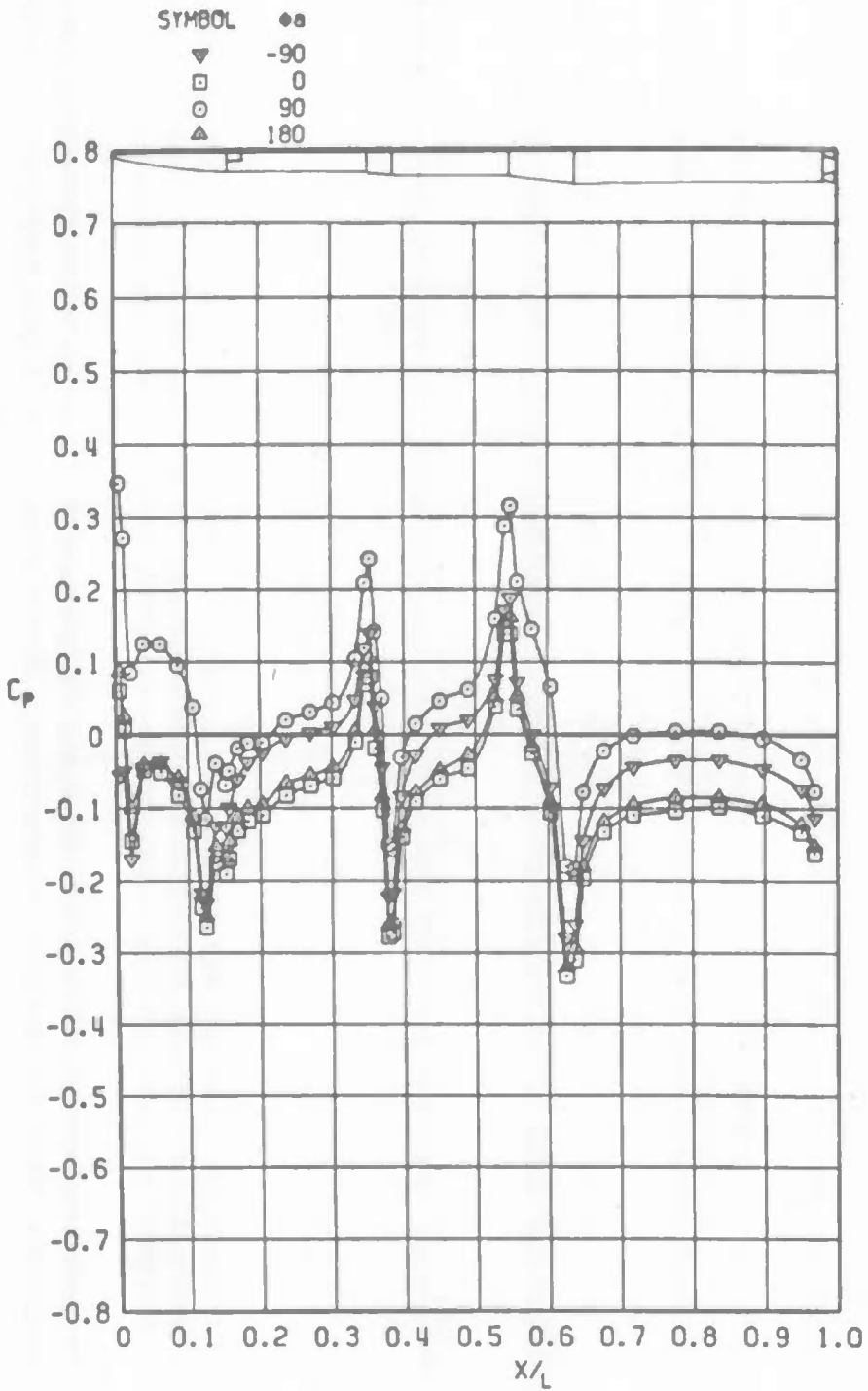


a.  $\alpha_a = 0$

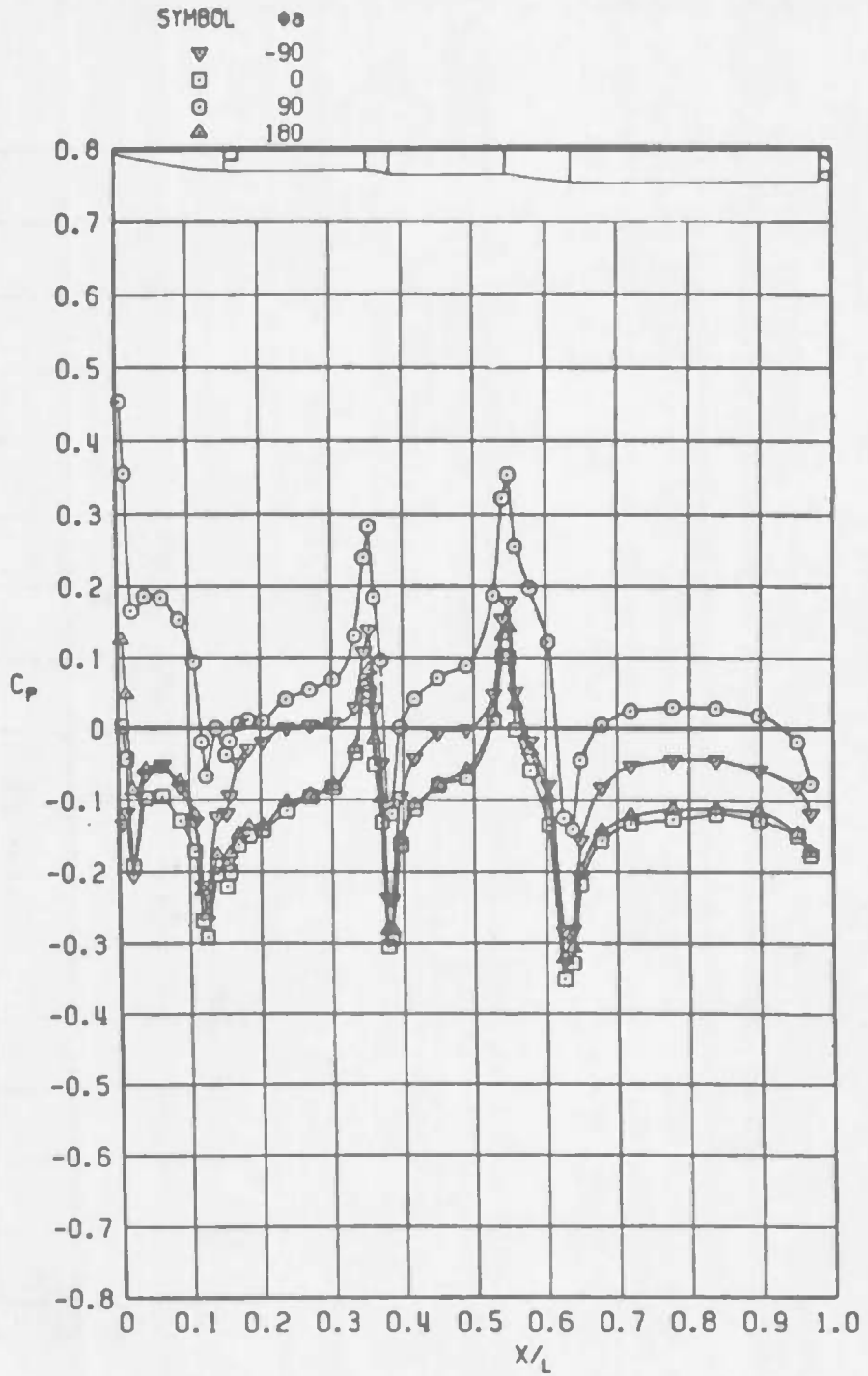
Figure 21. Missile pressure distributions,  $M_\infty = 0.5$ .



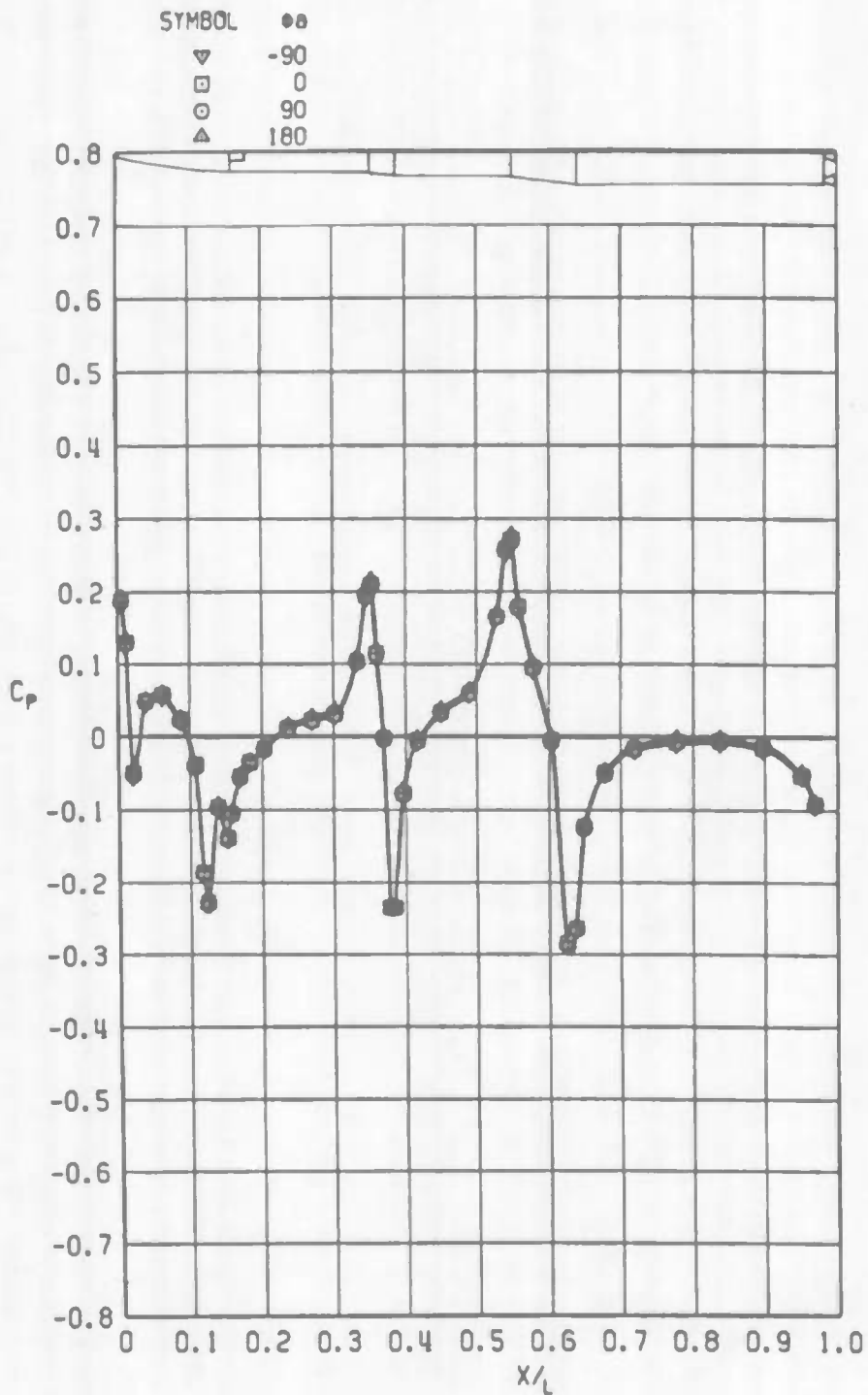
b.  $\alpha_a = 4$  deg  
Figure 21. Continued.



c.  $\alpha_0 = 8$  deg  
 Figure 21. Continued.

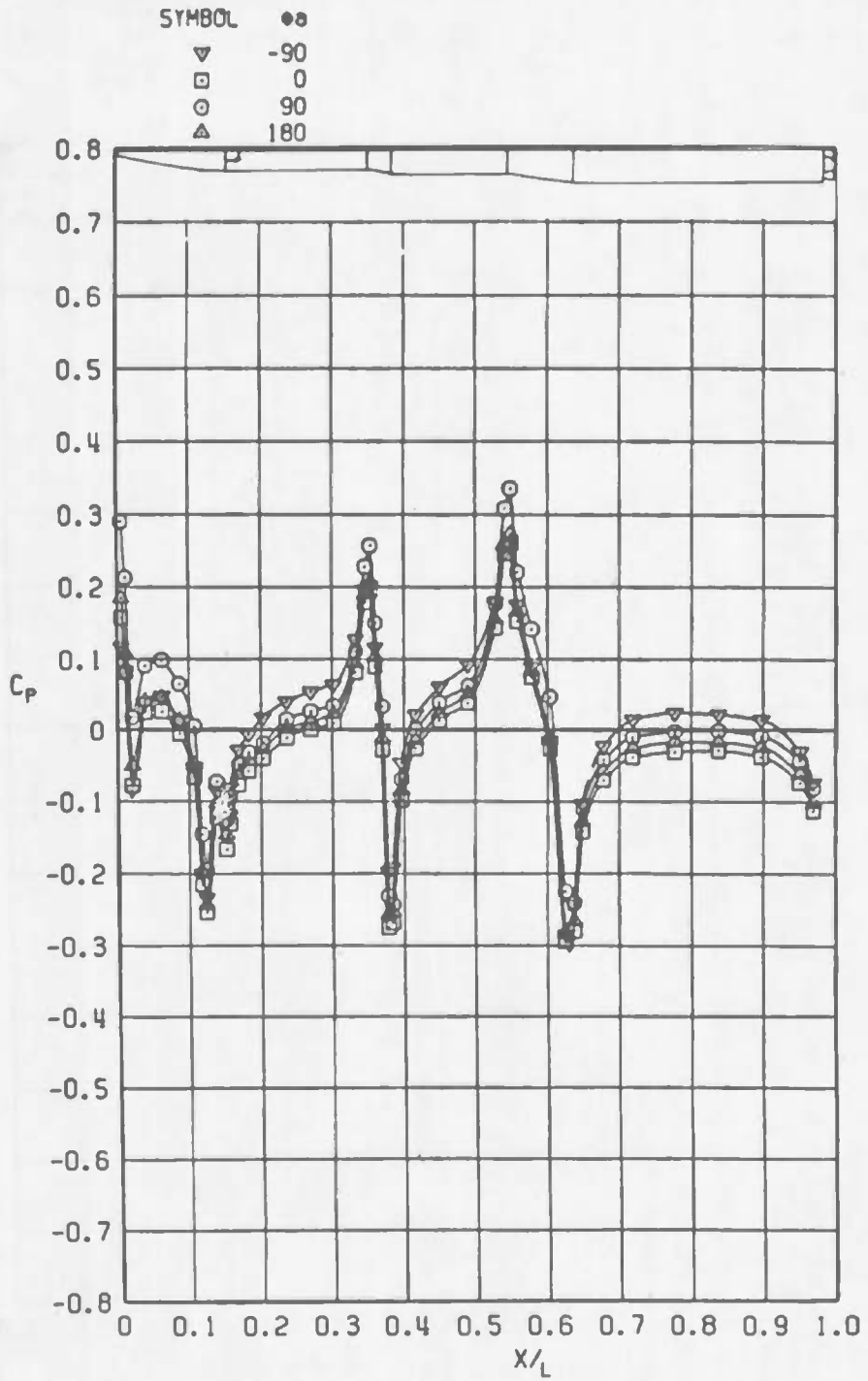


d.  $\alpha_n = 12$  deg  
 Figure 21. Concluded.

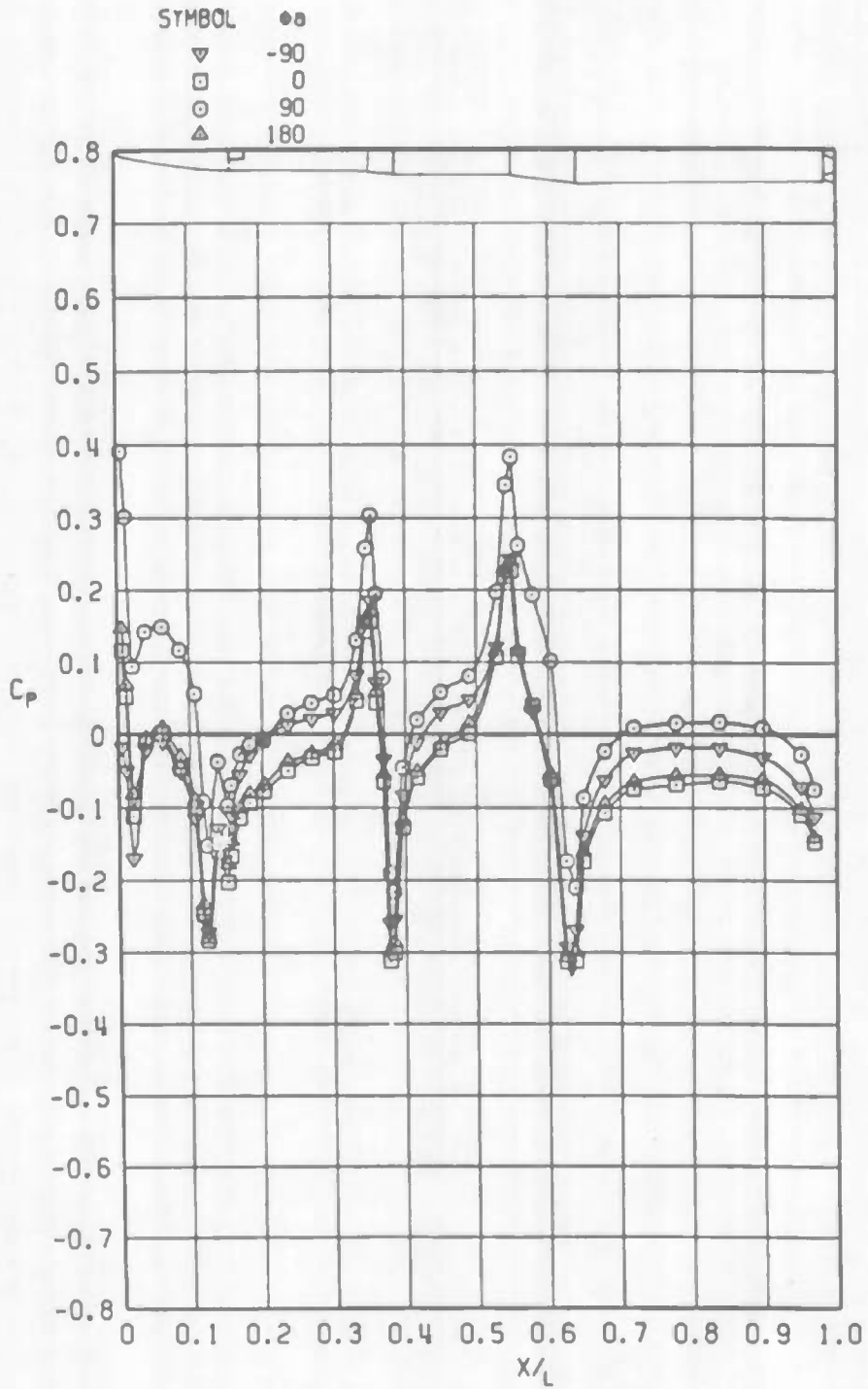


a.  $\alpha_a = 0$

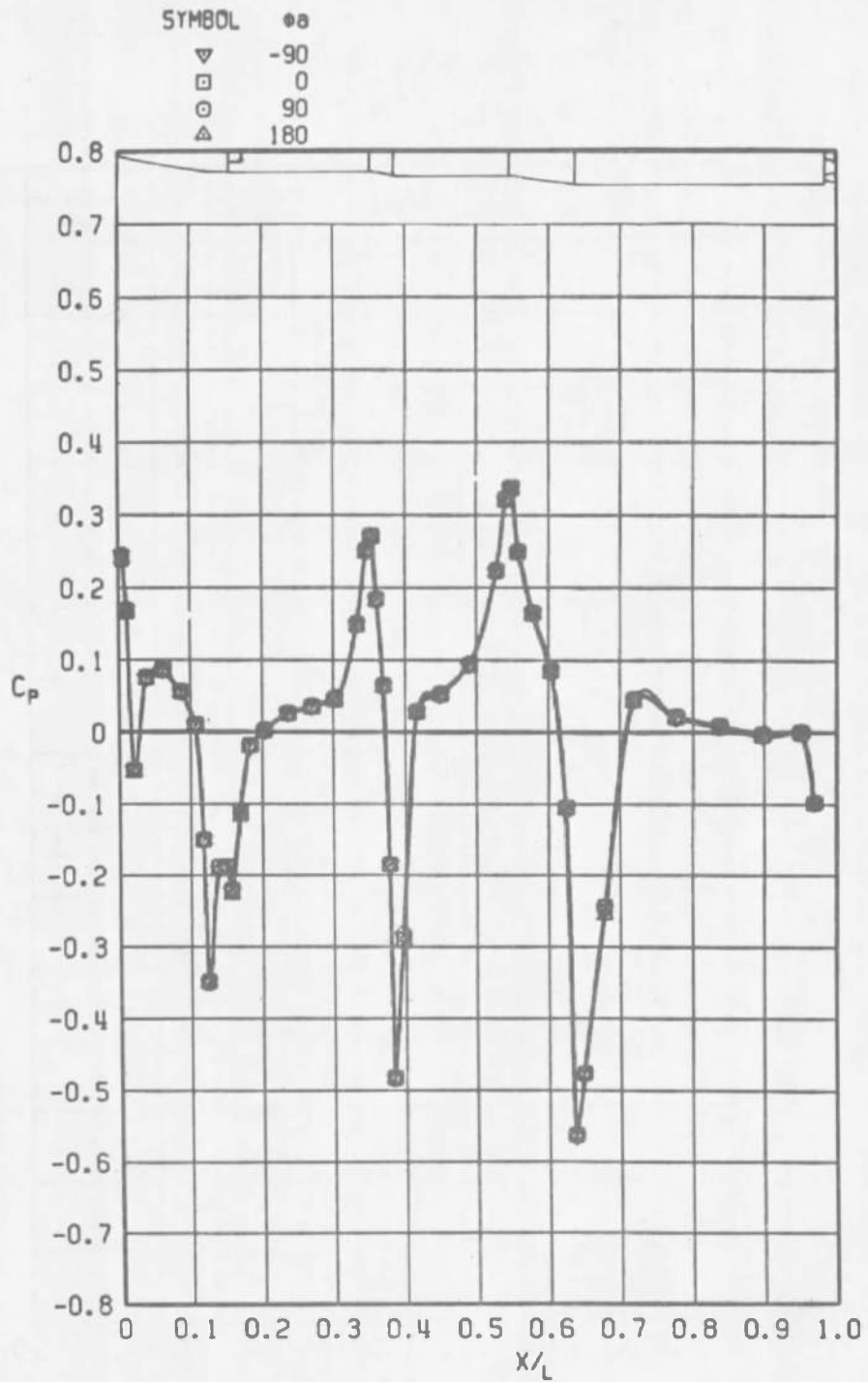
Figure 22. Missile pressure distributions,  $M_\infty = 0.8$ .



b.  $\alpha_a = 4$  deg  
 Figure 22. Continued.

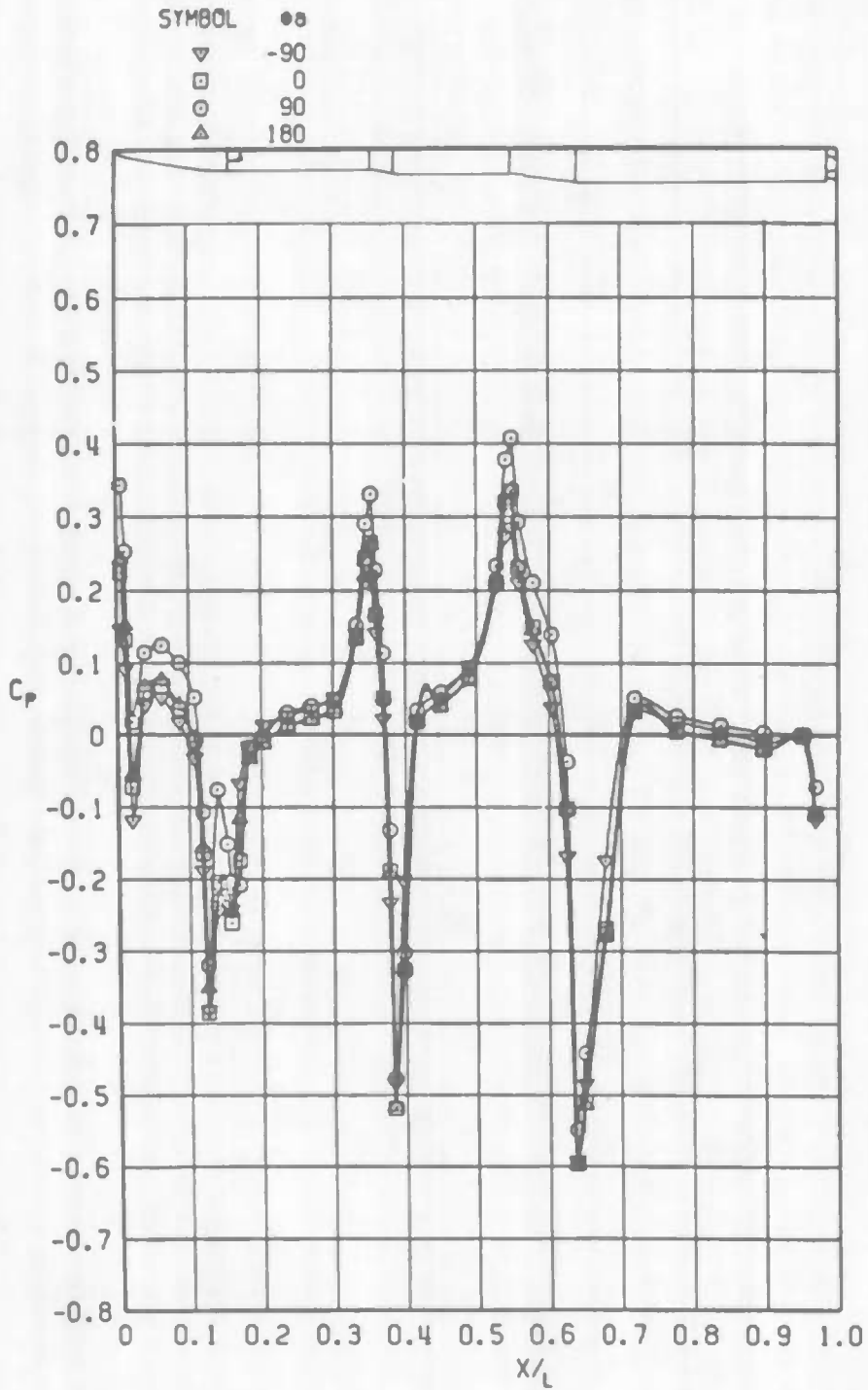


c.  $\alpha_0 = 8$  deg  
 Figure 22. Concluded.

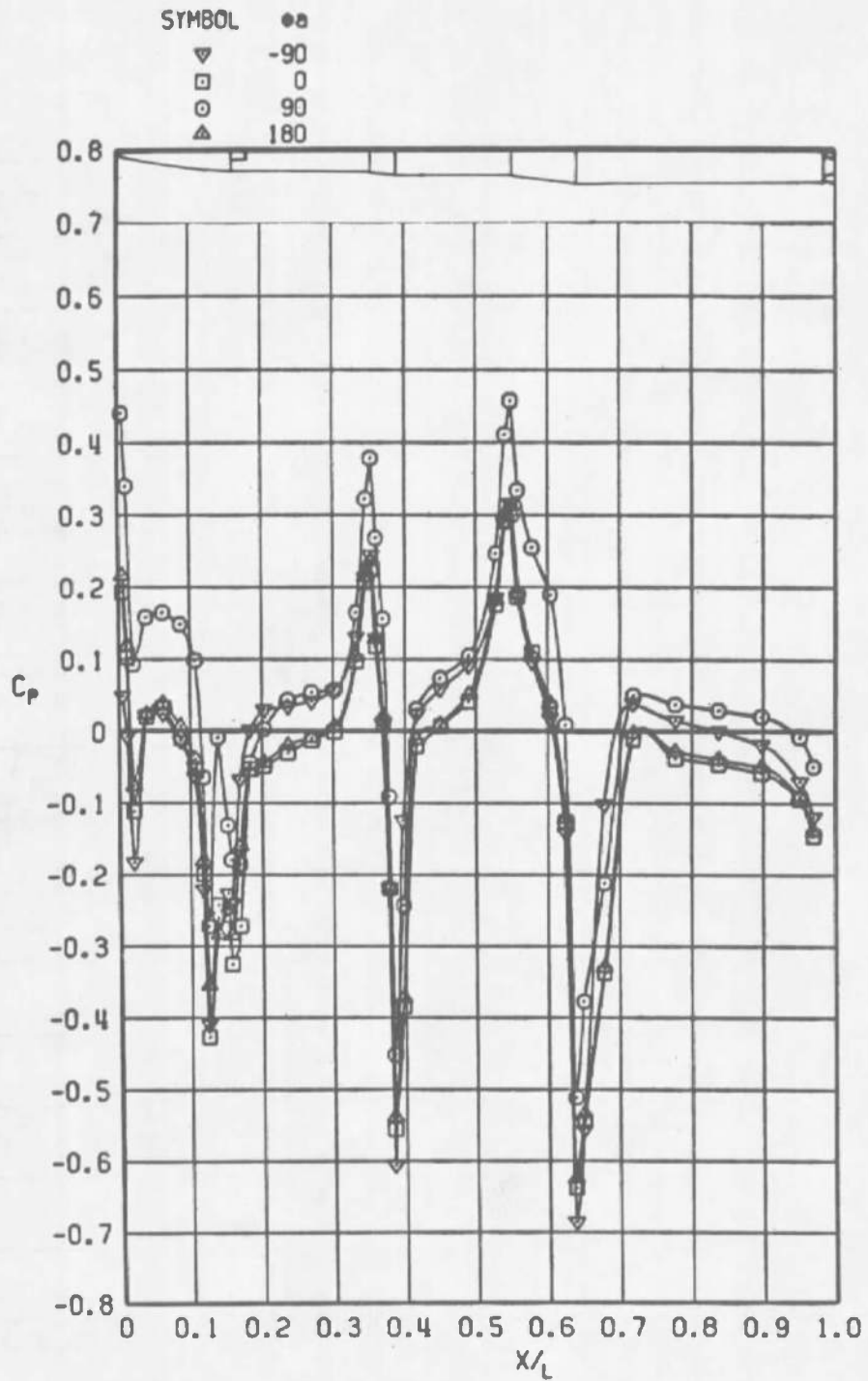


a.  $\alpha_0 = 0$

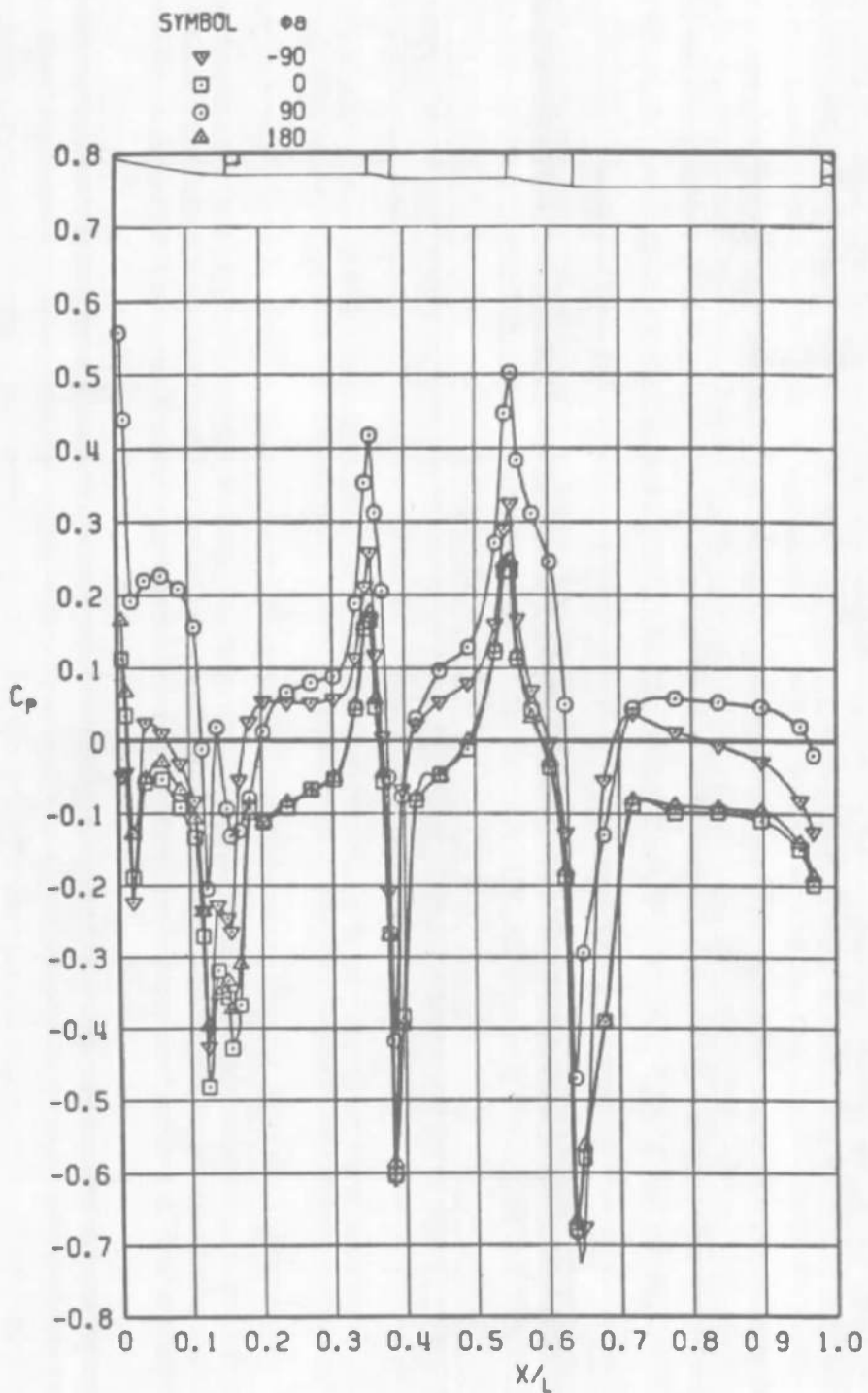
Figure 23. Missile pressure distributions,  $M_\infty = 0.95$ .



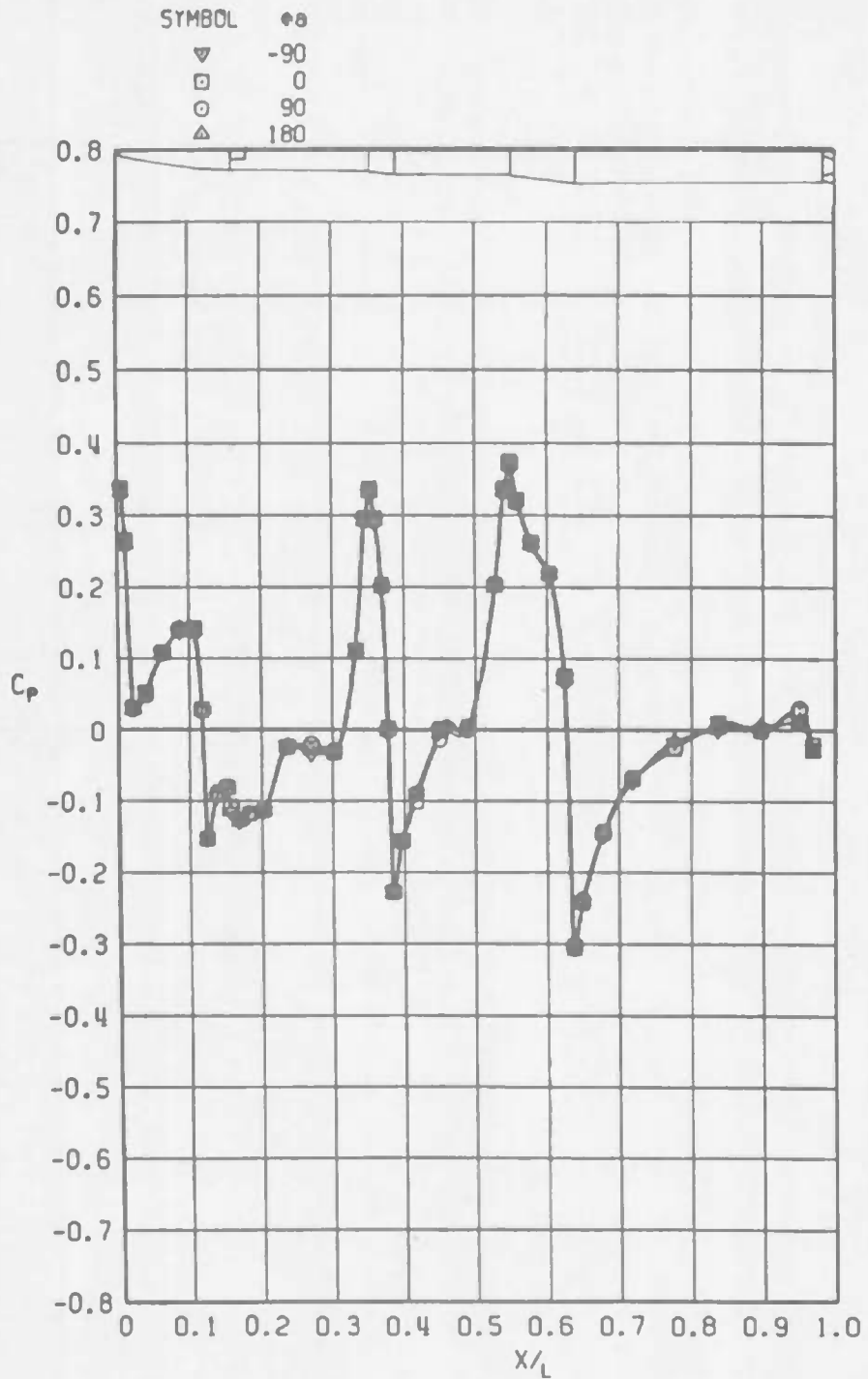
b.  $\alpha_n = 4$  deg  
 Figure 23. Continued.



c.  $\alpha_a = 8$  deg  
 Figure 23. Continued.

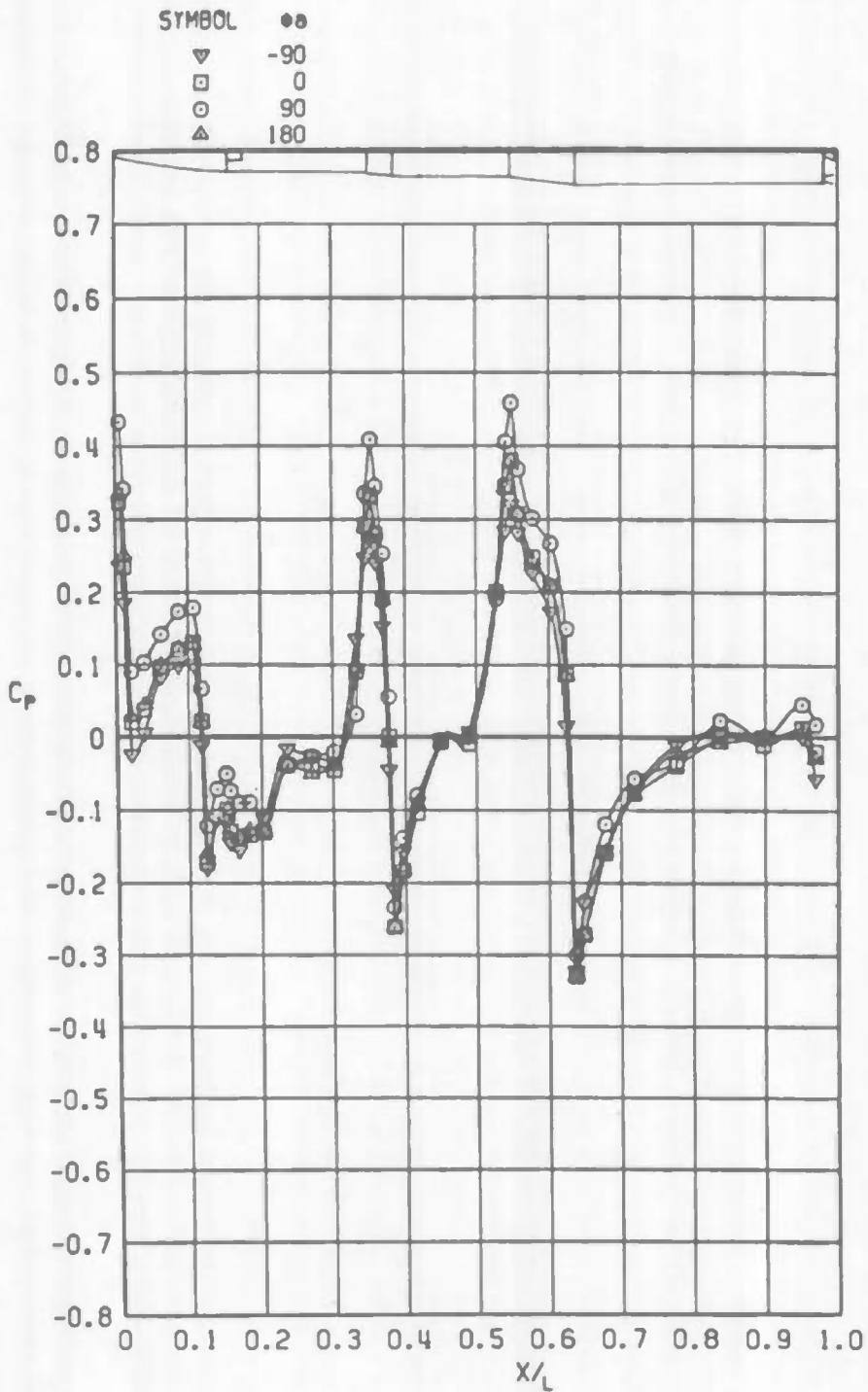


d.  $\alpha_a = 12$  deg  
 Figure 23. Concluded.

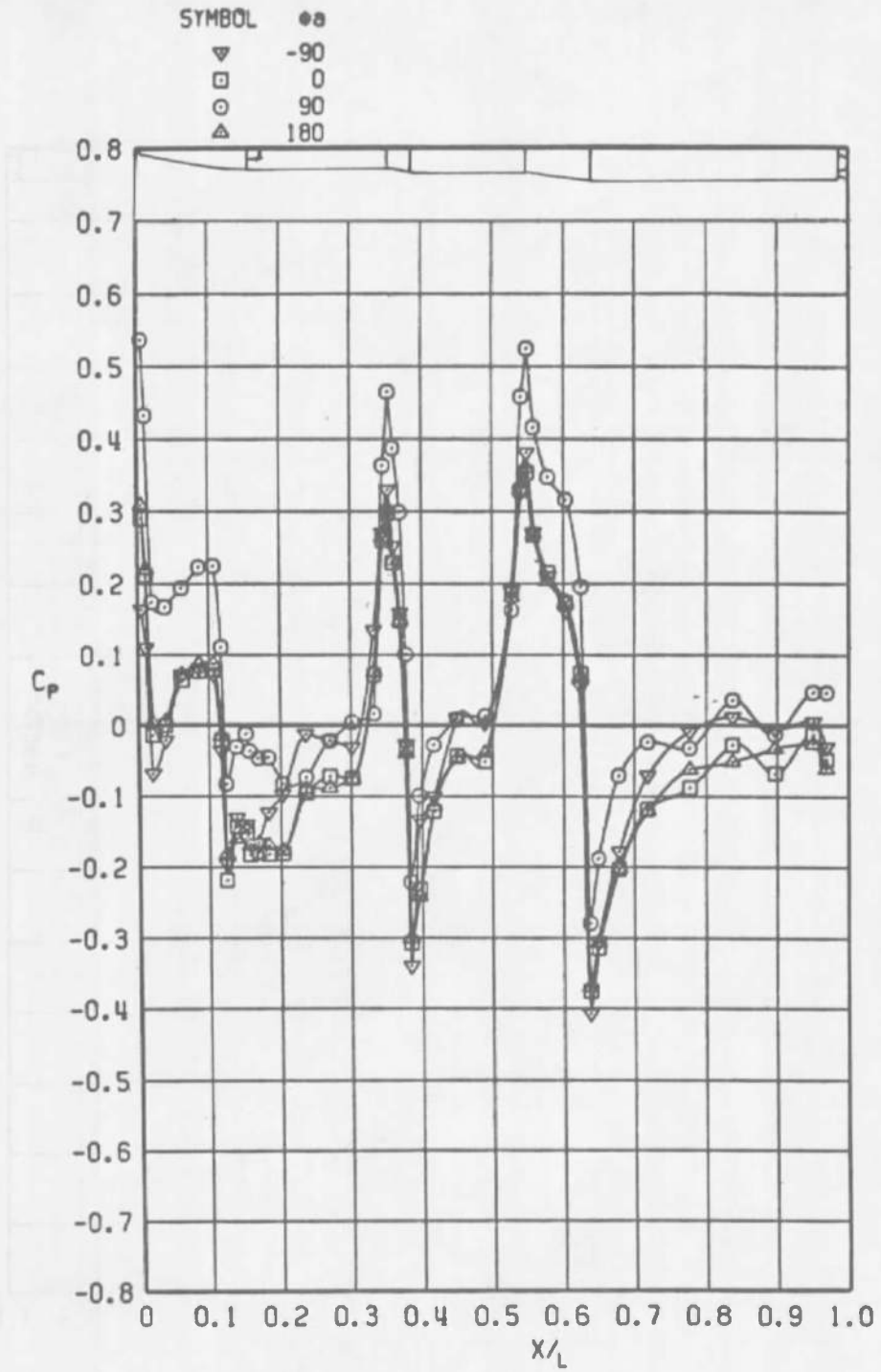


a.  $\alpha_a = 0$

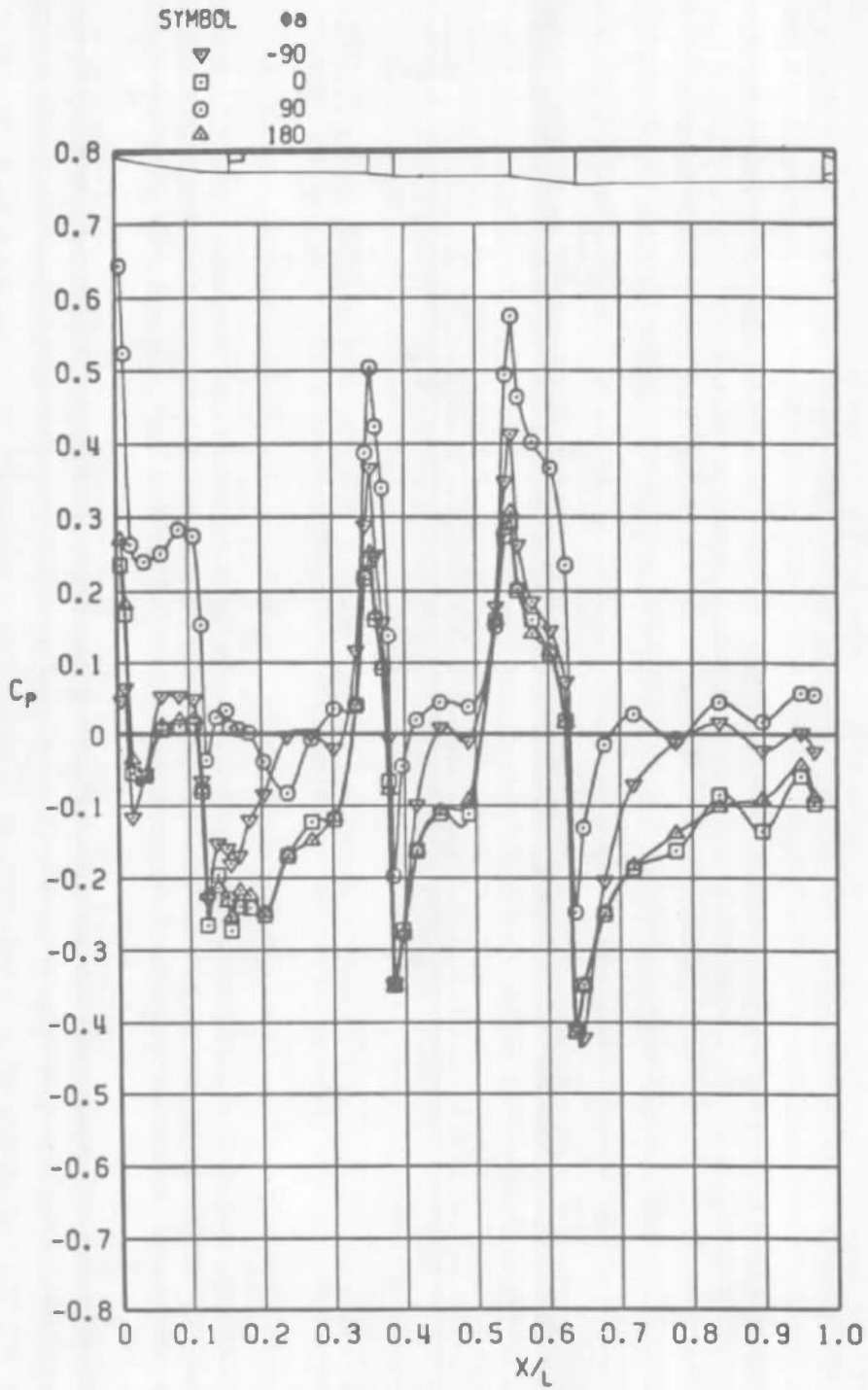
Figure 24. Missile pressure distributions,  $M_\infty = 1.1$ .



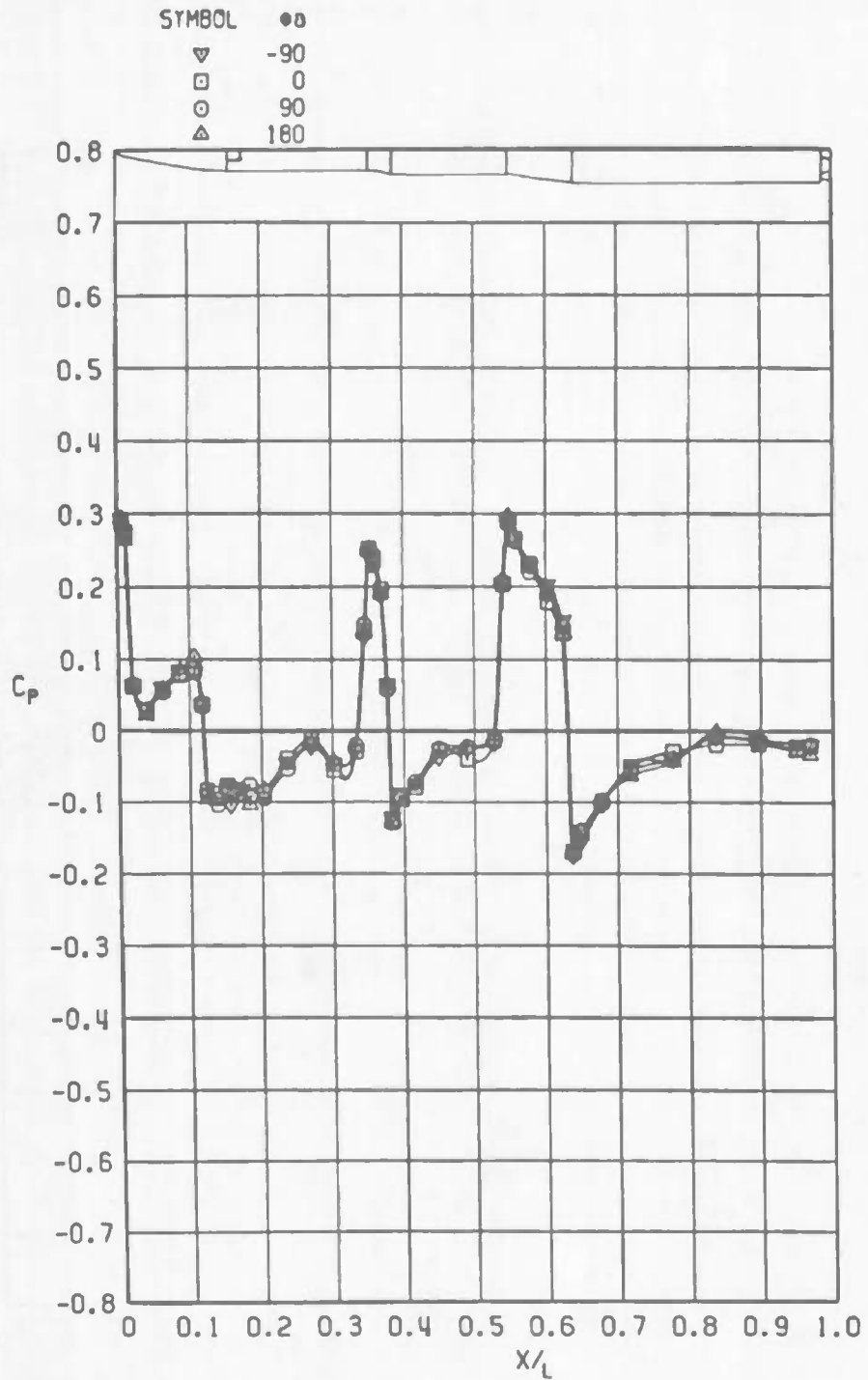
b.  $\alpha_a = 4$  deg  
 Figure 24. Continued.



c.  $\alpha_a = 8$  deg  
 Figure 24. Continued.

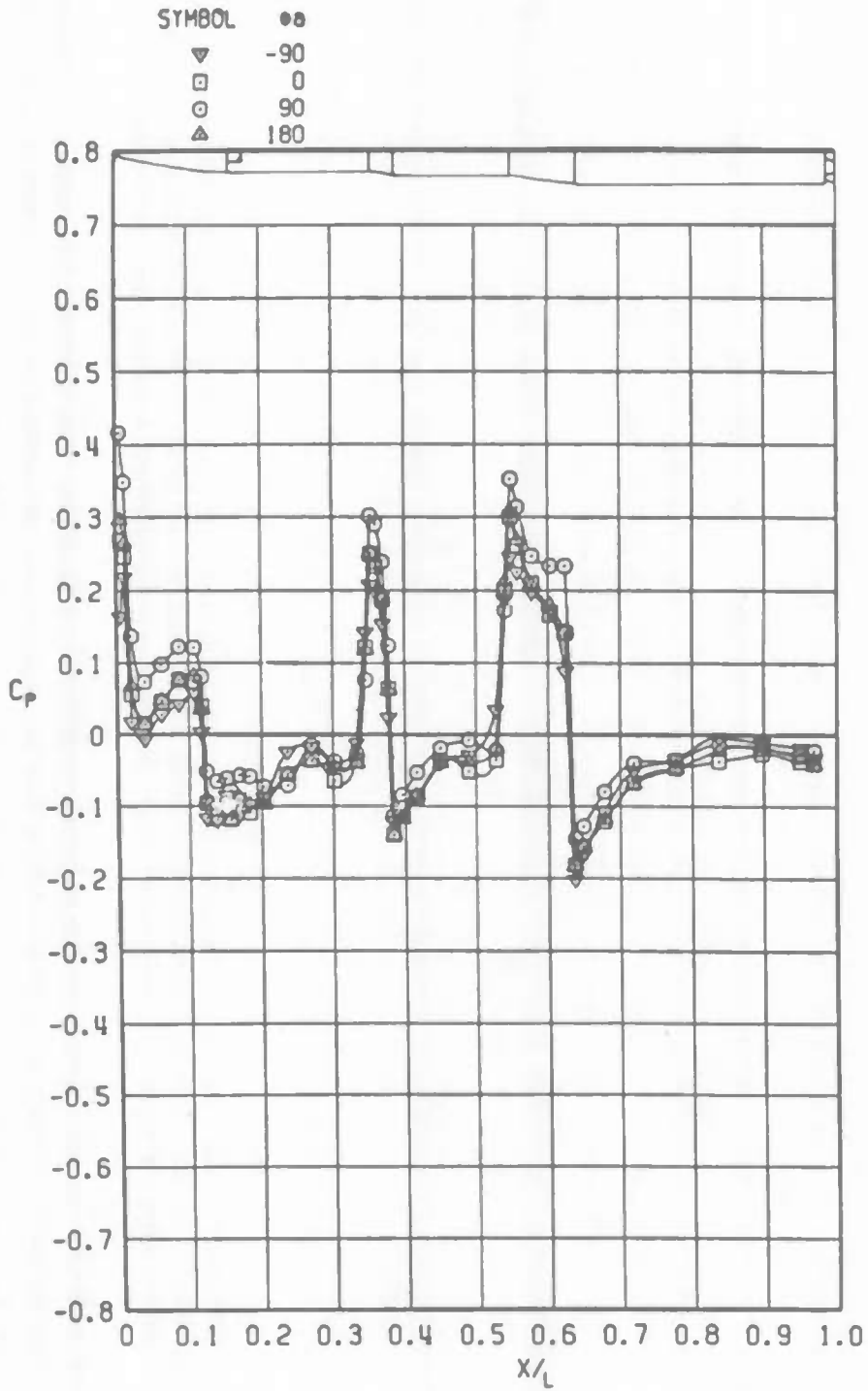


d.  $\alpha_2 = 12$  deg  
 Figure 24. Concluded.

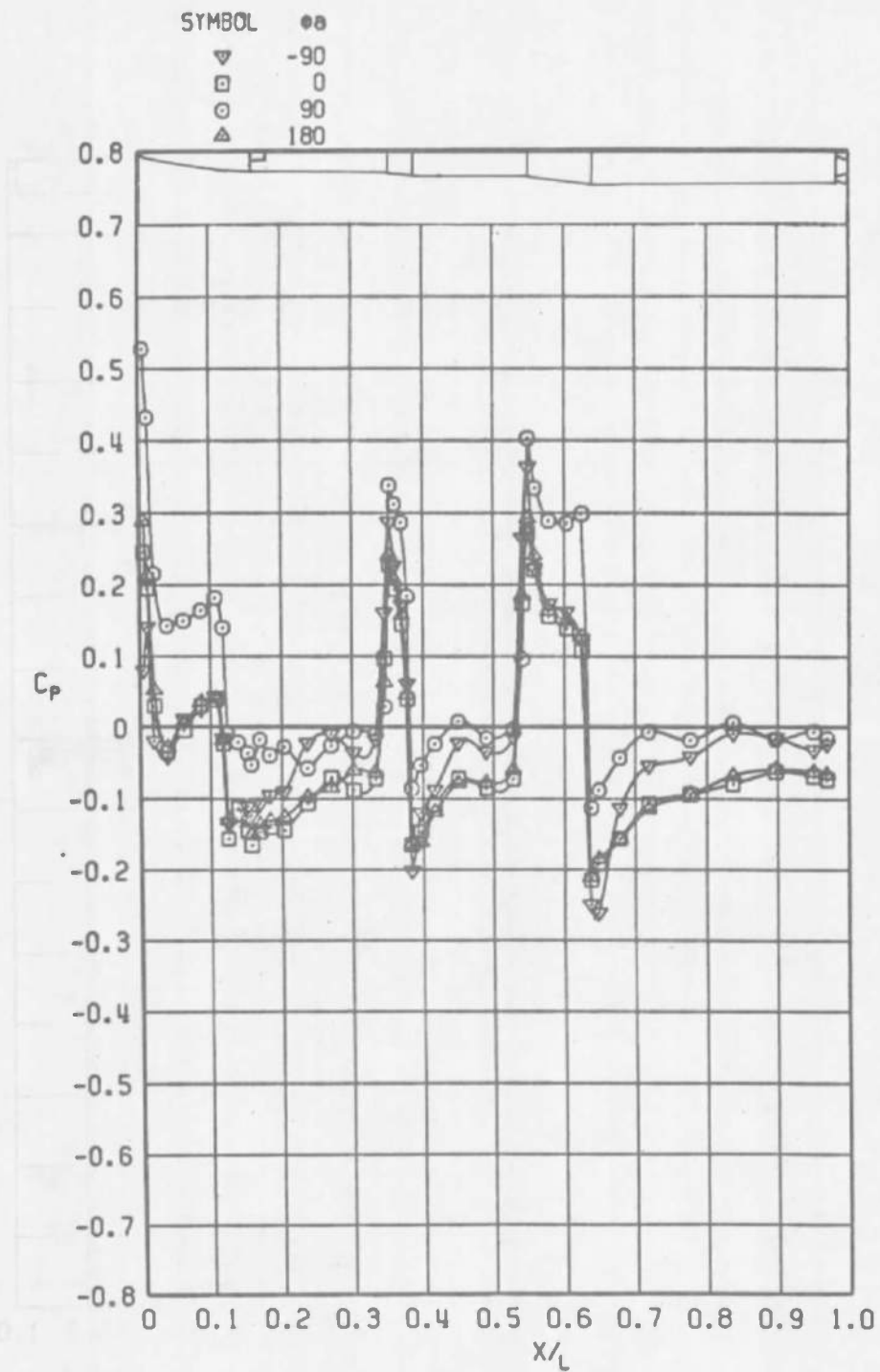


a.  $\alpha_a = 0$

Figure 25. Missile pressure distributions,  $M_\infty = 1.3$ .



b.  $\alpha_a = 4$  deg  
 Figure 25. Continued.



c.  $\alpha_0 = 8^\circ$   
Figure 25. Concluded.

Table 1. Model Surface Pressure Orifices

Missile Station	Model Station	Length Ratio	Angle Orientation, deg									
			90	105	120	135	150	159	165	180	270	
66.00	3.960	0.005	1									
70.00	4.200	0.011	2									
77.00	4.620	0.020	3									
90.00	5.400	0.038	4									
108.00	6.480	0.062	5									
126.00	7.560	0.086	6	---	---	---	---	---	---	---		82
141.00	8.460	0.107	7									
148.64	8.918	0.117	8									
152.64	9.158	0.123	9									
164.00	9.840	0.138	10	46	50	56	60	---	68	72		83
173.42	10.405	0.151	11	---	---	---	---	---	---	73	---	---
175.421	10.525	0.153	---	---	---	---	---	66	---	---	---	---
177.42	10.645	0.156	12	---	---	---	---	---	---	74	---	---
187.00	11.220	0.169	13	47	51	57	61	67	69	75		84
197.00	11.820	0.183	14	---	---	---	---	---	---	76	---	---
201.05	12.063	0.188	---	---	---	---	---	---	---	77	---	---
212.00	12.720	0.203	15	48	52	58	62	---	70	78		85
236.00	14.160	0.236	16	49	53	59	63	---	71	79		86
261.42	15.685	0.270	17	---	---	---	---	---	---	---		87
285.00	17.100	0.302	18									
308.00	18.480	0.333	19									
317.20	19.032	0.346	20									
322.83	19.370	0.353	21									
328.00	19.680	0.360	22									
335.00	20.100	0.370	23	---	54	---	64	---	---	80		88

Table 1. Concluded

Missile Station	Model Station	Length Ratio	Angle Orientation, deg								
			90	105	120	135	150	159	165	180	270
341.24	20.474	0.378	24								
345.24	20.714	0.384	25								
354.00	21.240	0.396	26								
370.00	22.200	0.417	27	---	---	---	---	---	---	---	89
394.00	23.640	0.450	28								
424.00	25.440	0.490	29								
452.00	27.120	0.528	30								
461.40	27.684	0.541	31								
467.00	28.020	0.549	32								
474.00	28.440	0.558	33								
489.50	29.370	0.579	34								
508.00	30.480	0.604	35	---	55	---	-65	---	---	81	90
523.56	31.414	0.625	36								
531.73	31.904	0.637	37								
541.17	32.470	0.649	38								
562.17	33.730	0.678	39								
592.17	35.530	0.719	40	---	---	---	---	---	---	---	91
636.17	38.170	0.778	41								
680.17	40.810	0.838	42								
724.17	43.450	0.898	43								
764.00	45.840	0.951	44								
778.00	46.680	0.970	45								
784.20	47.052	0.979	Base Pressures - $C_{p92}$ through $C_{p95}$								

Table 2. Summary of Nominal Test Conditions

$M_\infty$	Pt, psfa	$p_\infty$ , psfa	$q_\infty$ , psf	Re x 10 <sup>-6</sup> /ft
0.50	2,950	2,500	430	4.0
0.70*	2,380	1,700	580	↓
0.80	2,200	1,450	650	
0.90	2,080	1,230	700	
0.95	2,050	1,150	725	
1.00	2,020	1,060	750	
1.05	2,000	990	765	
1.10	1,980	930	780	
1.20	1,960	815	815	
1.30	1,950	710	840	

\*Force phase only

Table 3. Summary of Pressure Data Uncertainty

$M_\infty$	$\Delta q_\infty$	$\Delta C_p$
0.50	±5.14	±0.0147
0.80	±3.86	±0.0111
0.95	±2.89	±0.0091
1.10	±3.14	±0.0080
1.13	±3.36	±0.0070

**Table 4. Summary of Force Data Uncertainty****a. Main Balance**

$M_\infty$	$\Delta C_{Na}$	$\Delta C_{ma}$	$\Delta C_{ya}$	$\Delta C_{na}$	$\Delta C_A$	$\Delta C_L$
0.50	$\pm 0.034$	$\pm 0.049$	$\pm 0.016$	$\pm 0.023$	$\pm 0.016$	$\pm 0.017$
0.80	$\pm 0.023$	$\pm 0.033$	$\pm 0.011$	$\pm 0.016$	$\pm 0.011$	$\pm 0.012$
0.95	$\pm 0.021$	$\pm 0.029$	$\pm 0.010$	$\pm 0.014$	$\pm 0.010$	$\pm 0.010$
1.10	$\pm 0.019$	$\pm 0.026$	$\pm 0.009$	$\pm 0.013$	$\pm 0.009$	$\pm 0.010$
1.13	$\pm 0.018$	$\pm 0.025$	$\pm 0.008$	$\pm 0.012$	$\pm 0.008$	$\pm 0.009$

**b. Nose Balance**

$M_\infty$	$\Delta C_{Nan}$	$\Delta C_{man}$	$\Delta C_{yan}$	$\Delta C_{nan}$	$\Delta C_{An}$	$\Delta C_{Ln}$
0.50	$\pm 0.011$	$\pm 0.006$	$\pm 0.008$	$\pm 0.004$	$\pm 0.005$	$\pm 0.002$
0.80	$\pm 0.008$	$\pm 0.004$	$\pm 0.005$	$\pm 0.002$	$\pm 0.004$	$\pm 0.002$
0.95	$\pm 0.007$	$\pm 0.003$	$\pm 0.005$	$\pm 0.002$	$\pm 0.003$	$\pm 0.002$
1.10	$\pm 0.006$	$\pm 0.003$	$\pm 0.004$	$\pm 0.002$	$\pm 0.003$	$\pm 0.001$
1.30	$\pm 0.006$	$\pm 0.003$	$\pm 0.004$	$\pm 0.002$	$\pm 0.003$	$\pm 0.001$

## NOMENCLATURE

$A_b$	Missile base area, 0.0479 ft <sup>2</sup>
$A_{cav}$	Main balance cavity area, 0.0369 ft <sup>2</sup>
$A_{cavn}$	Nose balance cavity area, 0.0276 ft <sup>2</sup>
$C_{A,bn}$	Base axial-force coefficient for the missile $\frac{(p_\infty - \bar{p}_b)A_b + (p_\infty - \bar{p}_{cav})A_{cav}}{q_\infty S}$
$C_{A,b}$	Base axial-force coefficient for the nose section $\frac{(p_\infty - \bar{p}_{cavn})A_{cavn}}{q_\infty S}$
$C_{AF}$	Missile forebody axial-force coefficient, (total measured axial force/ $q_\infty S$ ) - $C_{A,b}$
$C_{AFn}$	Nose forebody axial-force coefficient, (total measured nose axial force/ $q_\infty S$ ) - $C_{A,bn}$
$C_\ell$	Missile rolling-moment coefficient, referenced to model centerline, rolling moment/ $q_\infty Sd$
$C_{\ell n}$	Nose rolling-moment coefficient, referenced to model centerline, nose rolling moment/ $q_\infty Sd$
$C_{ma}$	Missile pitching-moment coefficient, referenced to MS 34.074 and model centerline, pitching moment/ $q_\infty Sd$
$C_{man}$	Nose pitching-moment coefficient, referenced to MS 10.525 and model centerline, nose pitching moment/ $q_\infty Sd$
$C_{Na}$	Missile normal-force coefficient, normal force/ $q_\infty S$
$C_{Nan}$	Nose normal-force coefficient, nose normal force/ $q_\infty S$

$C_{na}$	Missile yawing-moment coefficient, referenced to MS 34.074 and model centerline, yawing moment/ $q_{\infty} S d$
$C_{nan}$	Nose yawing-moment coefficient, referenced to MS 10.525 and model centerline, nose yawing moment/ $q_{\infty} S d$
$C_p$	Pressure coefficient, (model pressure - $p_{\infty}$ )/ $q_{\infty}$
$C_{pb}$	Missile base pressure coefficient, (base pressure - $p_{\infty}$ )/ $q_{\infty}$
$C_{ya}$	Missile side-force coefficient, side-force/ $q_{\infty} S$
$C_{yan}$	Nose side-force coefficient, nose side force/ $q_{\infty} S$
$d$	Model reference diameter, 3.942 in.
MS	Model station, in.
$M_{\infty}$	Free-stream Mach number
$\bar{p}_b$	Average base pressure, psfa
$\bar{p}_{cav}$	Average main balance cavity pressure, psfa
$\bar{p}_{cavn}$	Average nose balance cavity pressure, psfa
$p_t$	Free-stream total pressure, psfa
$p_{\infty}$	Free-stream static pressure, psfa
$q_{\infty}$	Free-stream dynamic pressure, psf
Re	Free-stream unit Reynolds number, millions per foot
$S$	Model reference area, 0.0848 ft <sup>2</sup>
$\alpha_a$	Total or complex angle of attack, deg

$\phi_a$  Model roll angle, see Fig. 2; positive clockwise looking upstream, deg

Note: All force and moment coefficients are presented in the aeroballistic axes system.